



This is to certify that the

dissertation entitled

SHAPE OPTIMIZATION OF PLATE STRUCTURES  
USING HOMOGENIZATION WITH APPLICATIONS  
IN MECHANICAL DESIGN

presented by

CIRO ANGEL SOTO

has been accepted towards fulfillment  
of the requirements for

Ph.D. degree in MECHANICAL ENGINEERING

1/10/93 A. DIAZ  
Major professor

2/21/1994

Date \_\_\_\_\_





3 1293 01025 6471

**LIBRARY**  
**Michigan State**  
**University**

**PLACE IN RETURN BOX to remove this checkout from your record.**  
**TO AVOID FINES return on or before date due.**

DATE DUE	DATE DUE	DATE DUE
5/10/96		
SEP 25 1996		
<del>271.1</del> NOV 28 2000		
<del>508.01</del> JUL 20 2001		

MSU is An Affirmative Action/Equal Opportunity Institution

c:\circ\date\due.pm3-p.1

SHAPE OPTIMIZATION OF PLATE STRUCTURES  
USING HOMOGENIZATION WITH APPLICATIONS  
IN MECHANICAL DESIGN

By

Ciro Angel Soto

A DISSERTATION

Submitted to  
Michigan State University  
in partial fulfillment of the requirements  
for the degree of

DOCTOR OF PHILOSOPHY

Department of Mechanical Engineering

1993

## ABSTRACT

### SHAPE OPTIMIZATION OF PLATE STRUCTURES USING HOMOGENIZATION WITH APPLICATIONS IN MECHANICAL DESIGN

By

Ciro Angel Soto

This work is about the problem of computing the stiffest topology and shape of Mindlin plates subject to several independent loading conditions. A structural shape is identified here with a distribution of ribs symmetrically located above and below a core of fixed geometry. Small scale close ribs are used to build microscopically ribbed plates, and to expand the space of designs in order to guarantee attainability of the optimum. Homogenization techniques are used to compute effective stiffness of such plates and to establish a relation between the density of ribs and the plate stiffness, a fundamental piece of information for shape optimization algorithms based on homogenization techniques. Effective properties are derived for two micro structures. The first micro structure is made up by *two orthogonal* layers of ribs, and the second one is built from a finite number of layers of ribs arranged in *arbitrary* directions. The effective properties of multi-layer material plates are expressed using only four variables or '*moments*'. A new formulation of the layout optimization problem, using these variables is presented. This formulation splits the optimization problem in two subproblems, one where the optimum distribution of material used to build the ribs is computed, and another subproblem where the optimum moments are computed for prescribed amounts of material and strain fields. Numerical experiments and example problems with applications from the automotive industry are included.

To Nazaret, who sacrificed her time for me.

To Alberto Mata, who never forgot our friendship.

## ACKNOWLEDGMENTS

Special thanks to my advisor Professor Alejandro Díaz for all his help, support and advice. I learned many things on the art of research from you.

Thanks to the members of my committee, Professors Noboru Kikuchi, Alan Haddow, Thomas Pence and Charles MacClure, for expending their time in correcting this document.

Thanks to Professor Robert Lipton whose ideas are spread throughout this dissertation.

Thanks to Professor Martin Bendsøe for his suggestions during the investigation. Thanks also to Professor Klaus Schittkowski for letting me use his nonlinear programming solver.

This work would have been very difficult to do without the computational programs Monique™ from RTB Corporation, and HyperMesh™ from Altair Engineering. Thanks for letting me use them.

I will never forget my cheese sandwich lunches with Matthew Brach and Taner Önsay sharing thoughts about how to solve the world's problems. Thanks for those moments.

Thanks to Faramarz Farahanchi and Muqqafat Soomar for their kind company. Also thanks to Neil Whitbeck for sharing with us his chalkboard thoughts on philosophy.

Very special thanks to my friends Ricardo Palma and Ender Parra for their invaluable help. This effort is also yours.



## PREFACE

When I began my doctoral studies I thought that getting a doctoral degree was going to be an enjoyable and pleasant experience. I thought that I would get the degree and would go back to work to have an easier life. The end has come and from the evaluation of these years I would say that they were hard years for me and my family. However, difficult times also teach, and I learned a lot. I learned that there are much more important things than to live to work. I learned that our life style must be changed to a simpler life where people can talk and share pleasant moments instead of fighting for a better position in their jobs or for making more money. I learned that our desires to have more in order to satisfy our appetites can be replaced by turning to ourselves and finding out what we want to be, instead of accepting what society forces us to be. I learned that there are many people that die every day for not having the piece of bread that we throw in the garbage. I learned that my scientific research is not helpful to any of those hungry people who want a hope in their life; and I learned that when we scientists neglect the welfare of others in our attempts to satisfy our egos by reaching new stages of complex thinking and inventing sophisticated theories, we betray the human race. I am happy of having learned all these things. Now I want to transform my knowledge and use all my energy to help any human being that needs me.

C.S.



## TABLE OF CONTENTS

LIST OF TABLES .....	viii
LIST OF FIGURES .....	ix
CHAPTER 1 INTRODUCTION	
1.1 Introduction .....	1
1.2 Historical Review.....	3
1.3 Outline .....	9
CHAPTER 2 HOMOGENIZED PROPERTIES OF RANK-2 MINDLIN PLATES	
2.1 Homogenization of the Mindlin Plate Equation .....	12
2.1.1 Background .....	12
2.1.2 Mindlin Plate Model.....	18
2.1.3 Derivation of Effective Properties .....	20
2.1.4 Results Using Layered Materials .....	22
2.2 Comparison With Other Models For Ribbed Plates .....	29
2.2.1 Comparison of Effective Properties in Bending .....	30
2.2.2 Comparison Based on the Mean Compliance of a Simply Supported Plate .....	38
CHAPTER 3 HOMOGENIZED PROPERTIES OF RANK-L MINDLIN PLATES - MOMENT REPRESENTATION	
3.1 Effective Properties for Rank-L Material Plates.....	44
3.1.1 Set up of the Mindlin Plate Equations.....	44
3.1.2 Computation of Homogenized Stiffness Properties.....	46
3.2 Moment Representation of the Homogenized Properties .....	57
3.2.1 Moment Representation of Bending Stiffness .....	61
3.2.2 Moment Representation of Shear Stiffness.....	62

3.2.3	Moment Representation of Membrane Stiffness.....	62
3.2.4	Feasible Set in the Moment Space.....	63
3.2.5	Determination of the Micro Structure Geometry.....	64
CHAPTER 4 FORMULATION AND IMPLEMENTATION OF THE LAYOUT OPTIMIZATION PROBLEM		
4.1	Hierarchical Moment Formulation of the Stiffness Maximization Problem.....	70
4.1.1	Optimization Problem Statement.....	70
4.1.2	The Local Problem.....	72
4.1.3	Equilibrium Equations.....	73
4.1.4	The Global Problem.....	74
4.2	Numerical Implementation of the Optimization Problem.....	75
4.2.1	Solution of the Equilibrium Equation.....	75
4.2.2	Solution of Optimization Problems.....	76
4.2.3	Convergence Criteria.....	78
4.2.4	Algorithm Implementation.....	79
CHAPTER 5 EXAMPLES		
5.1	Comparison with Previous Work.....	82
5.2	Comparison of Micro Structure Models.....	87
5.2.1	Uniform Transverse Load.....	87
5.2.2	Point Loads on the Diagonals.....	91
5.3	Parametric Study.....	95
5.3.1	Influence of the Thickness Ratio $r=h_2/h_1$ .....	95
5.3.2	Influence of the Amount of Material $V_{max}$ .....	99
5.3.3	Comparison of Cross Sections.....	102
5.4	Industrial Examples.....	105
5.4.1	A Car Hood.....	105
5.4.2	A Car Door.....	110
CONCLUDING REMARKS.....		113
APPENDIX.....		117
LIST OF REFERENCES.....		119

## LIST OF TABLES

<u>Table</u>		<u>Page</u>
2.1	Summary of homogenized properties of one-family, ribbed plates.....	35
3.1	Effective stiffness for rank-L material plates.....	58



## LIST OF FIGURES

<u>Figure</u>	<u>Page</u>
1.1 Problem statement.....	2
1.2 Michell truss (Michell, (1904)).....	3
1.3 Plate with properties varying in one direction. ....	6
1.4 Layered material configuration. ....	8
1.5 Square cell geometry used in (Bendsøe and Kikuchi, (1988)). ....	9
1.6 A layered material plate with three layers in arbitrary orientation.....	10
2.1 Two-scale concept of microscopically periodic materials. ....	13
2.2 Layered materials.....	14
2.3 Large scale geometry of the plate.....	15
2.4 Small scale domain.....	15
2.5 Graphical description of the homogenization procedure.....	16
2.6 Assembly strategies for the weak plate.....	17
2.7 Basic cell in a plate made using a rank-1 material. ....	23
2.8 Basic cell of a plate made of rank-2 material.....	27
2.9 Geometry of plate cross section. ....	29
2.10 Laminated plate model.....	32
2.11 Effect of rib width on material properties.....	36
2.12 Effect of rib height on material properties. ....	37
2.13 Effect of rib width on mean compliance.....	40
2.14 Effect of rib height on mean compliance.....	42
3.1 Rank-L layer plate ( $L=3$ in this picture). ....	44
3.2 Basic cell for a rank-1 material plate. ....	49
5.1 Gray scale to identify the cross section of the plate in the optimum shapes....	81
5.2. Typical histogram for optimality condition.....	82
5.3. Example 1: geometry and loads. ....	84

5.4	Example 1:	optimum shapes with rank-2 materials. ....	84
5.5	Example 1:	Cheng and Olhoff (1981) result for the pinned plate.....	85
5.6	Example 1:	Cheng and Olhoff (1981) result for the clamped plate.....	85
5.7	Example 1:	iteration histories. ....	86
5.8	Example 1:	optimality condition ratio histograms. ....	86
5.9	Example 2:	geometry and loads. ....	88
5.10	Example 2:	optimum shapes. ....	88
5.11	Example 2:	distribution of one-layer materials in the plate. ....	89
5.12	Example 2:	distribution of two-layer materials in the plate.....	89
5.13	Example 2:	distribution of three-layer materials using the rank-L micro structure. ....	90
5.14	Example 2:	iteration histories. ....	90
5.15	Example 2:	optimality condition ratio histograms. ....	91
5.16	Example 2:	geometry and loads. ....	92
5.18	Example 2:	distribution of one-layer materials in the plate. ....	93
5.19	Example 2:	distribution of two-layer materials in the plate. ....	93
5.20	Example 2:	distribution of three-layer materials using the rank-L micro structure. ....	94
5.21	Example 2:	iteration histories. ....	94
5.22	Example 2:	optimality condition ratio histograms. ....	95
5.23	Example 3:	geometry and loads. ....	96
5.24	Example 3:	optimum shapes. ....	97
5.25	Example 3:	iteration histories. ....	97
5.26	Example 3:	optimality condition ratio histograms. ....	98
5.28	Example 3:	optimum shapes. ....	100
5.29	Example 3:	iteration histories. ....	100
5.30	Example 3:	optimality condition ratio histograms. ....	101
5.31	Example 3:	geometry and loads. ....	102
5.32	Example 3:	optimum shapes. ....	103
5.33	Example 3:	iteration histories. ....	104
5.34	Example 3:	optimality condition ratio histograms. ....	104
5.35	Example 4:	geometry and loads. ....	106
5.36	Example 4:	optimum shapes. ....	107
5.37	Example 4:	iteration histories. ....	108

<u>Figure</u>		<u>Page</u>
5.38	Example 4: interpretation of the optimum shape of the car hood. ....	108
5.39	Example 4: optimum shape obtained using the rank-L micro structure. ....	109
5.40	Example 4: iteration histories. ....	109
5.41	Example 4: optimality condition ratio histograms. ....	110
5.42	Example 5: geometry and loads. ....	111
5.44	Example 5: iteration histories. ....	112
5.45	Example 5: optimality condition ratio histograms. ....	112

# CHAPTER 1

## INTRODUCTION

### 1.1 Introduction

A natural way to improve structural designs is to optimize the use of material for prescribed load conditions so that the ‘performance’ of the system is maximized while the amount of material is controlled. In this case, ‘performance’ can be measured in several ways. When applied loads are static, it is convenient to characterize a given design by its flexibility or compliance. This measure is convenient from the mathematical view point and appropriate from the engineering perspective. Mathematically, shape optimization problems formulated in terms of the mean compliance are easier to solve. From the engineering viewpoint, compliance is one of the most popular ways to distinguish between designs simply because it is a measure of the relation between the excitation and response of the structural system, i.e., forces and displacements.

This dissertation deals with structural shape optimization under static loads. Specifically, it is concerned with the computation of the optimum layout and shape of plate structures that minimize the mean compliance of the structure. This problem can be stated in the following way: *given* a plate of uniform thickness occupying the domain  $\Omega_0 \times (-h_1, h_1)$  (Figure 1.1), and *given* the loading and displacement boundary conditions, *find* the distribution (layout) of ribs ( $\Omega_R$  in Figure 1.1) that minimizes the mean compliance (external work) of the structure. An isoperimetric constraint that prescribes an upper limit on the amount of material used to build  $\Omega_R$  is consider in the formulation. This problem may be written in a compact form as

$$\begin{aligned} & \underset{\Omega_0}{\text{minimize}} \quad C(u), \\ & \int_{\Omega_0} \rho d\Omega \leq V_{\max} \end{aligned} \tag{1.1.1}$$

State Equations

where  $\rho$  is the area density of ribs on  $\Omega_0$ , and  $V_{max}$  is a prescribed area fraction of the plate domain  $\Omega_0$  that will be covered by the ribbed domain  $\Omega_R$ , i.e.,  $V_{max} = \Omega_R / \Omega_0$ , and  $u$  is the state variable (i.e., displacements). The thickness of the ribbed domain is fixed to a prescribed value  $2h_2$ .

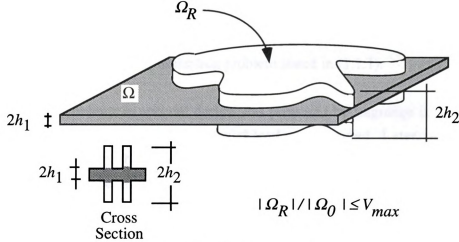


Figure 1.1.1. Problem statement.

It is important to distinguish this problem from the sizing and boundary variation problems. In sizing and boundary variation problems the layout (topology) of the structure is known *a priori* (e.g., the number of holes in a plate), and the sizes of the plate cross section and/or the position of the boundary of the domain are considered as design variables. In the problem stated in equation (1.1.1) the topology (layout) of  $\Omega_R$  is unknown (e.g., the number and shape of holes in the plate are unknown). Hence, the problem is more general and its solution is more difficult to find.

Structural sizing optimization has had limited success because it starts from a fixed topology that may not be optimum for the problem. New approaches that overcome this limitation consider the use of composite materials with micro voids to obtain the optimum shape. The introduction of these materials expands the space of possible designs allowing alternatives other than a single isotropic material to be allocated at a given point in the domain. The presence of microscopically composite materials call for homogenization techniques to compute *average* material properties that will be used in the solution algorithm. Using composite materials with micro voids the shape optimization problem can



be transformed into a problem of optimization of material distribution where the solid material volume fraction is the design variable. A more detailed description of this method will be given in the following chapters.

## 1.2 Historical Review

In this brief historical review two main fields of research will be reviewed: structural shape optimization and homogenization of composite materials. Both fields will be discussed in relation to the solution of the optimization problem stated in (1.1.1).

One of the first problems in optimal design was proposed by Lagrange in 1770 when the optimal shape of a column subject to an axial load was obtained. Later, in 1856, the first topology optimization problem was solved by Saint-Venant, who found the stiffest cross section of a prismatic beam subject to torsion -- the annular cross section. Another well-known layout optimization problem was solved by Michell in (1904), who found the optimum shape of trusses for minimum weight working with a continuum medium (Figure 1.2).

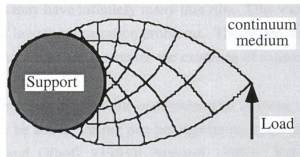


Figure 1.2. Michell truss (Michell, (1904)).

In the late 60's, Prager and Taylor (1968) proposed an optimality criteria method to compute optimal shapes of structures. The method consisted of two main steps. The first one was the derivation of necessary conditions for optimality using, for example, Kuhn-Tucker conditions. These conditions led to a differential equation of the form:

$$\frac{\text{Strain Energy Density}}{\text{Unit Stiffness Density}} = \text{constant} \quad (1.1.2)$$

In a second step, equation (1.1.2) was integrated to compute the optimal distribution of elastic stiffness on the structure. When equation (1.1.2) cannot be integrated, an iterative algorithm is built to solve the problem where condition (1.1.2) is used at each iteration step to verify the optimality of the proposed solution. This approach is the basis of the algorithm that is used in the present research to find the optimum layout and shape of structures.

During the 70's, problems of optimum design of trusses and grillages were studied extensively (Pedersen, (1970); Prager and Rozvany, (1977)). In 1973 Zienkiewicz and Campbell wrote what appears to be the first paper on boundary variations using finite element methods. They used the nodal coordinates of the discretized boundary as design variables. Many researchers made important contributions using boundary variation techniques during the 70's, among them Tvergaard, (1975); Kristensen and Madsen, (1976); Dems and Mroz, (1978); Rousselet and Haug, (1980). These techniques are now popular in commercial software to solve optimal design problems where the topology of the structure is known. Also in the 70's the problem of optimal thickness of plates to maximize the plate stiffness for a given amount of material was treated by several researchers (Armand, (1974); Olhoff, (1975); Lurie and Cherkaev, (1976)), who found that optimum shapes may have infinitely many thin ribs. This was the beginning of a new era in the solution of layout optimization problems. Thereafter, composite materials were considered as a way to model and guarantee the existence of solutions.

In the early 80's researchers reached the conclusion that in some cases optimum layout of structures could only be attained using non homogeneous anisotropic materials (Olhoff, *et al*, (1980); Cheng and Olhoff, (1981); Armand, (1982); Kohn and Strang, (1982); Bendsøe, (1982a)). They stated that problems of optimum layout of ribs on plates required that composite materials be used to obtain the *rapidly varying thickness* solutions observed earlier. The physical reason for this is that at each point of the domain the use of an anisotropic material allows one to arrange the material more effectively compared to a simple isotropic material. In other words, the use of an anisotropic materials expands the space of solutions. In particular, if we build the plate with a microscopically porous material whose porosity is potentially different at each point in the plate (i.e., a non homogeneous plate) we are allowing the possibility of creation of holes (using high porosity) or solid regions (using low porosity) at any location of the plate. Therefore, the topology of the plate is not prescribed but automatically generated as a result of the optimization process.



The problem of computing effective properties, and their bounds, in composites has been addressed since the time of Maxwell, who in 1873 was studying the effective conductivity in composite materials. A microscopic non homogeneous composite material is characterized by a change of properties in two scales. These materials have properties that depend on two coordinates in different scales, a large scale coordinate, labeled  $x$  here, and a small scale, labeled  $y = \frac{x}{\varepsilon}$ , where  $\varepsilon$  is a very small parameter that characterizes the order of magnitude of the composite mixture. For instance, the elastic tensor of a composite material microscopically mixed is  $E(x, y) = E(x, \frac{x}{\varepsilon})$ . In this work we will use a subset of non homogeneous composite materials called *pseudo-periodic*. The properties of these materials are such that  $E(x, y) = E(x, y + p)$ , where  $p$  is the period in the small scale. After applying a homogenization technique the *homogenized* (also called *average* or *effective*) properties  $\bar{E}(x)$  are computed, and the dependency on  $y$  is eliminated. Notice that these properties still depend on the large scale coordinate  $x$ .

In 1889 Voigt found an upper bound ( $E_V$ ) for effective mechanical properties ( $\bar{E}$ ) in composites, given by

$$E_V(x) = \frac{1}{\|Y\|} \int_Y E(x, y) dY, \quad \text{for fixed } x \quad (1.1.3)$$

$E(x, y)$  is the mechanical property at location  $x$ , and  $Y$  is the small scale domain where the properties change as a function of the coordinate  $y$ . A lower bound was found in 1906 by Reuss, given by

$$E_R(x) = \left[ \frac{1}{\|\Omega\|} \int_Y \frac{1}{E(x, y)} dY \right]^{-1}, \quad \text{for fixed } x. \quad (1.1.4)$$

These bounds are known in the literature as “elemental bounds” and are such that any physically meaningful effective properties must satisfy the inequality  $E_R \leq \bar{E} \leq E_V$ . In 1963 Hashin and Shtrikman found optimal lower ( $E_{HS}^L$ ) and upper ( $E_{HS}^U$ ) bounds in mechanical properties of composites. Optimal bounds are those bounds that cannot be improved with the only information of volume fractions and individual properties of the

components. Hashin-Shtrikman bounds satisfy  $E_R \leq E_{HS}^L \leq \bar{E} \leq E_{HS}^U \leq E_V$ . These bounds were found using physical arguments and variational principles.

From the mathematical viewpoint, a boundary value problem where composite materials are used may be described by a partial differential equation with coefficients changing rapidly in the domain. In 1973, De Giorgi and Spagnolo introduced the theory of G-convergence a theory that provided the mathematical basis for the proofs of existence of *average* or *effective* operators in boundary value problems governed by partial differential equations with rapidly varying coefficients. In 1976 Babuska introduced the term *homogenization* to denote the process of computation of effective properties. Duvaut (1976) computed the effective bending stiffness of Kirchhoff plates with material properties changing in one direction (Figure 1.3) based on G-convergence theory. Due to the Kirchhoff assumption (i.e., no transverse shear deformation), this set of homogenized properties did not include stiffness in the direction of the transverse shear. In 1978, Bensoussan, Lions and Papanicolaou published the book "Asymptotic Analysis for Periodic Structures" where they presented a systematic approach to compute effective coefficients in BVP's with rapidly varying coefficients. This is the approach used in this research to treat the Mindlin plate equations.

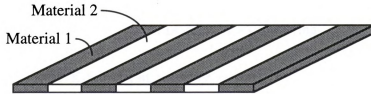


Figure 1.3. Plate with properties varying in one direction.

Since 1980, mathematicians have become more involved not only in the field of homogenization and the computation of optimal bounds, but also in the layout optimization problem. In 1980, Banichuk, and independently Cea (1980), discussed the layout optimization problem for a wide variety of problems, including plates, from a theoretical viewpoint. One of the pioneers in layout optimization in plate structures using homogenization techniques was Bendsøe (1982a, 1982b) who used the results of Duvaut (1976) for Kirchhoff plates to compute homogenized bending stiffness for plates with ribs in one direction. He also computed homogenized bending stiffness for plates with ribs in two orthogonal directions using a method he called "smear out".



Bourgeat and Tapiéro (1983) proved the existence of homogenized coefficients for the Mindlin equations, and Lewinski and Telega (1988) derived the homogenized bending and transverse shear stiffness of Mindlin plates with properties varying in one direction. Kohn and Vogelius (1984) introduced a more general homogenized Kirchhoff plate model where the ratio between the variation of the thickness and the mean plate thickness was considered as a variable. This work clarified aspects of the behavior of rapidly varying thickness plates and will be discussed later in Chapter 1. In 1986 Kohn and Strang published a series of three papers (1986a,b,c) where they studied the relations between optimal design and homogenization using variational calculus and convex analysis.

Francfort and Murat (1986) found optimal bounds for layered materials (Figure 1.4) using G-convergence theory. Layered materials are built from two isotropic materials mixed at microscopic scale. The way layering materials are constructed is explained in more detail in the body of this document. There were some important conclusions in the work of Francfort and Murat: *i)* The strongest (and the weakest) material in two- and three-dimensional elasticity can be built using the layering scheme, i.e., Hashin-Shtrikman bounds are attained with layered materials. *ii)* Homogenized properties of composite materials built with layers in more than one direction can be computed analytically. These conclusions had important consequences on the development of layout optimization problems using homogenization. Layered materials are also called *rank- $n$*  layered materials, where  $n$  indicates the number of directions of layering.

In 1988 Bendsøe and Kikuchi put together previous research and solved the layout optimization problem (1.1.1) in plane elasticity. They used homogenization techniques and an optimality criterion approach and solved the state equation using finite element methods. The composite material that they used was a microscopically porous material modeled using a square cell with a rectangular hole in it (Figure 1.5). Since porous rank-1 layered materials have no stiffness for in-plane shear deformations, Bendsøe and Kikuchi might have considered this as a potential problem in the use of layered materials and decided to use the square cell instead. Recent investigations (Allaire and Kohn, (1993)) have shown that non optimal micro structures, such as those modeled with the square cell, give optimum designs that make less use of composite materials in comparison with designs obtained using optimum micro structures, such as those modeled with layered materials.

The microscopic cell introduced by Bendsøe and Kikuchi (1988) was parameterized with two variables  $a$  and  $b$  (Figure 1.5). The global orientation of the material axes at each point

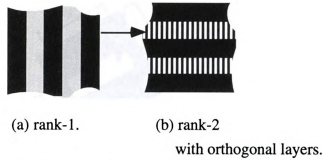


Figure 1.4. Layered material configuration.

of the domain,  $\Theta$  in Figure 1.5, is considered as a third variable in the problem. This results in a total of three design variables at each location of the domain. In 1989 Pedersen showed that the optimal orientation of the material axes,  $\Theta$ , in two-dimensional elasticity problems for a single load case coincided with the axes of principal strains. This simplified the algorithm to find the optimum orientation of the material axes in such particular case, and provided a clue for more complicated cases, e.g., multiple load cases and plate problems.

In 1991 Díaz and Belding applied the Bendsøe-Kikuchi approach to compute optimum layouts of trusses. Suzuki and Kikuchi (1991b) used the homogenized stiffness properties computed in two-dimensional elasticity to build a plate model based on classical laminate theory. By 1992 the approach of Bendsøe and Kikuchi was well known and researchers became actively involved in the extension of this method to other problems, such as multiple load case problems (Díaz and Bendsøe, (1992)), and maximization of natural frequencies (Díaz and Kikuchi, (1992)). An extensive review of the Bendsøe-Kikuchi approach is available in (Bendsøe, *et al.* (1992)).

Recently, Lipton (1993a) proposed a new representation of effective properties of Kirchhoff plates. He derived a four-variable representation for layering material plates with an arbitrary but finite number of layers oriented in any direction (see Figure 1.6 for a case of three layers). He called this the “moment representation” since it was based on moments of a probability measure. This compact formulation allows one to work with mixtures of a more general geometry, including multiple layers in arbitrary orientations. This representation works very well with a new formulation of the optimization problem introduced by Jog, Haber and Bendsøe (1992). Working in



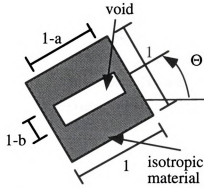


Figure 1.5. Square cell geometry used in (Bendsøe and Kikuchi, (1988)).

two-dimensional elasticity and a single load case, they carried out analytical optimization over the widths and orientation of the layers in rank-2 layered materials (Figure 1.4 (b)) for a given amount of material and a given field of strains. This allowed them to pose the layout optimization problem using composite materials that align themselves to have the optimum orientation and optimum relative layer widths for the given strain field and amount of material. They called these materials “self-optimizing materials”. In this new formulation the original optimization problem is split into two hierarchically related problems: one *local* optimization problem where the stiffest arrangement of ribs is found for a given set of strains and a certain amount of material, and a *global* optimization problem where they solve for the best distribution of material in the plate domain.

### 1.3 Outline

The work is organized as follows:

In Chapter 2 the derivation of the homogenized stiffness properties of Mindlin plates using materials layered in two orthogonal directions (Figure 1.4 (b)) is presented. This had been done in part by (Lewinski and Telega, (1988)) using layers in only one direction. Here we present the application of asymptotic expansions to the Mindlin equations to plates with layers in two orthogonal directions and study the derived formulas in the context of shape optimization. An extensive comparison of models of effective properties of plates is also included in this chapter.

In Chapter 3 a “moment representation” of the stiffness properties of Mindlin plates is derived. Following the work done by Lipton (1993a) in Kirchhoff plates, effective stiffness formulas for layered material Mindlin plates with  $L$  layers of ribs are derived for bending and shear deformations. These formulas are expressed in terms of only four variables. This is the first time this representation is derived and implemented for Mindlin plates.

In Chapter 4 we present a formulation and implementation of the mean compliance minimization problem that makes use of the results of Chapters 2 and 3. We focus our attention on a new formulation called here the *hierarchical moment formulation*. This new formulation splits the optimization problem in two: one problem where the optimum distribution of material is computed, and another where the optimum micro structure is computed for a given amount of material and strain fields.

In Chapter 5 example problems are solved using the different micro structure models developed and discussed in previous chapters. The examples include a comparison with previous results of Cheng and Olhoff (1981); a comparison between the rank-2 (Chapter 2) and rank-L (Chapter 3) micro structures; a parametric study of variables involved in the optimization problem; and two example problems that show the applicability of the approach to mechanical design problems with applications in industry.

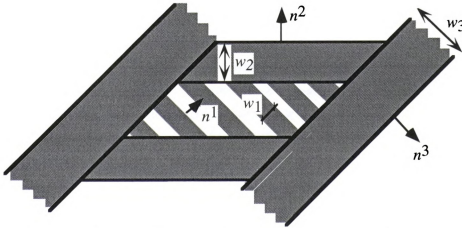


Figure 1.6. A layered material plate with three layers in arbitrary orientation.

## CHAPTER 2

### HOMOGENIZED PROPERTIES OF RANK-2 MINDLIN PLATES

#### 2.1 Homogenization of the Mindlin Plate Equation

##### 2.1.1 Background

The problem of homogenization in composite materials deals with the computation of homogenized elastic properties (also called *effective* or *average* properties) of a mixture of two or more materials. When the mixture is periodic and occurs at a scale of order  $\epsilon$ , which is small compared to the scale of the body, the material is called “microscopically periodic” or “periodic in a small scale”. Figure 2.1 shows this two-scale concept in a generic three-dimensional body. These materials have properties that depend on two coordinates in different scales, a large scale coordinate, labeled  $x$  here, and a small scale, labeled  $y = \frac{x}{\epsilon}$ . For instance, the elastic tensor of a composite material microscopically mixed is  $E_{ijkl}(x, y) = E_{ijkl}(x, \frac{x}{\epsilon})$ . The periodicity of the material is present when the properties satisfy  $E_{ijkl}(x, y) = E_{ijkl}(x, y + p)$ , where  $p$  is the period in the small scale. When the periodicity is a function of  $x$ , the material is called pseudo-periodic. Any function that measures mechanical behavior of a body made of such materials, e.g., deformation or stress, also depends on both coordinates  $x$  and  $y$ . After applying a homogenization technique the homogenized properties  $\bar{E}_{ijkl}(x)$  are computed, and the dependency on  $y$  is eliminated. Homogenization techniques for periodic materials have been used very successfully to obtain effective properties of a variety of mixtures of materials in different geometric arrangements (e.g., Duvaut (1976), Bourgat (1977), Guedes and Kikuchi (1990)). These properties can be used to determine the large scale behavior of a body made of such materials using standard procedures (e.g., finite element methods) without a detailed knowledge of the small scale behavior. This feature makes homogenization methods very attractive in shape optimization problems where the shape of the body is represented as a material property (e.g., Bendsøe (1989)).

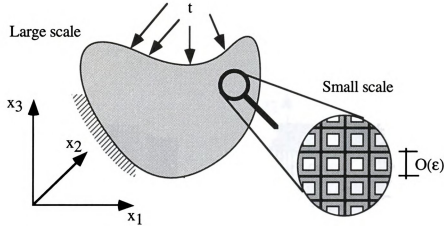


Figure 2.1. Two-scale concept of microscopically periodic materials.

### Microscopically Periodic Materials

Microscopically periodic materials are characterized by a *basic cell* that is repeated periodically in the domain occupied by the material. It is advantageous to use the simplest geometry capable of generating a reasonable complete set of stiffness properties for the small scale mixture of the materials involved. Layered materials characterized by a *rank-n* cell are particularly useful in shape optimization since their homogenized properties can be expressed in an explicit form.

Given two materials with properties  $E^+$  and  $E^-$ , respectively, a rank-1 material is built stacking alternatively  $E^+$  and  $E^-$  in a single direction, as illustrated by Figure 2.2 (a). A rank-2 material is made by stacking one of the two basic materials, say  $E^+$ , and the rank-1 material in a different direction (not necessarily orthogonal to the first one) as shown in Figure 2.2 (b). The process may be continued to build a rank-n material stacking  $E^+$  and rank-(n-1) layers in different directions.

In layout and shape optimization problems we need to work with materials with  $E^- = 0$  in order to produce holes in the domain. This case is not considered in the G-convergence theory (Allaire and Kohn, (1993)). The reason is that positive definiteness of the stiffness tensor is a basic assumption in the computation of effective properties. It is then necessary to work with non degenerate materials to perform homogenization techniques. Therefore, a “hole” is represented by a very weak material with  $E^- \neq 0$ , one in which  $E^+/E^- \gg 1$ . This technique is referred to as “regularization” in the literature. Once the optimum topology is obtained, a second step is required, i.e., the limit as  $E^- \rightarrow 0$  needs to be

taken. In practice, the limit process is not performed and optimum topologies with  $E^+/E^- \gg 1$  are considered as final results. In this context  $E^+$  is called the strong material and  $E^-$  the weak material.

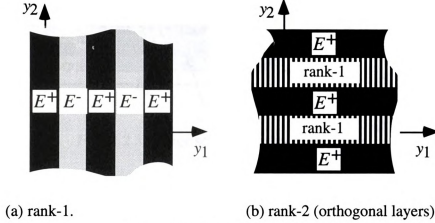


Figure 2.2. Layered materials.

### Notation and Definitions

#### Large Scale

The notation used here was strongly influenced by the work of Guedes (1990).

As shown in Figure 1.1, the domain occupied by the plate is denoted by  $\Omega$ , a bounded open set in  $\mathbb{R}^3$ . In this derivation we assume that  $\Omega$  is the parallelepiped  $\Omega = (0, L_x) \times (0, L_y) \times (-h_2, h_2)$ , as shown in Figure 2.3. It is made up by three plies arranged symmetrically about the neutral plane  $\Omega_0 \subset \mathbb{R}^2$ . The three plies are labeled the *core ply*  $\Omega^{cp} = \Omega_0 \times [-h_1, h_1]$ , and the two *external plies*  $\Omega^{ep} = \Omega_0 \times (\pm h_2, \pm h_1)$ . Each ply may be made of a microscopically periodic material, provided that the symmetry of the plate about  $\Omega_0$  is preserved.

The coordinate system for any point in  $\Omega$  is denoted by  $\mathbf{x} = (x_1, x_2, x_3) = (x, y, z)$ . The material properties of each ply do not change with the thickness direction  $z$ . It is convenient to introduce a system of coordinates for points in  $\Omega_0 \subset \mathbb{R}^2$ , denoted by  $x = (x_1, x_2) = (x, y)$ . The boundary of  $\Omega_0$ , denoted by  $\Gamma$ , is divided into two parts,  $\Gamma^d$  where displacements are prescribed, and  $\Gamma^t$  where tractions are applied. They are such that  $\Gamma^d \cap \Gamma^t = \emptyset$ . It is also assumed that  $\Gamma$  satisfies Lipschitz conditions (smoothness).



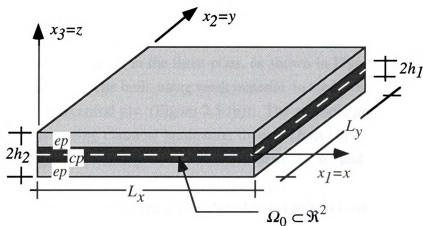


Figure 2.3. Large scale geometry of the plate

### Small Scale

A basic cell is defined as the open set  $Y \times (-h_2, h_2)$ ,  $Y = (0, 1) \times \mathbb{R}$ , as shown in Figure 2.4. A microscopically  $Y$ -periodic plate is built repeating periodically  $Y \times (-h_2, h_2)$  in  $\Omega_0$ , which means that periodicity is not present in the thickness direction. The system of coordinates for any point in the small domain is  $\mathfrak{Y} = \{y_1, y_2, y_3\} = \{x_1/\varepsilon, x_2/\varepsilon, x_3\}$ . The system of coordinates for any point in  $Y$  is labeled here  $y = \{y_1, y_2\} = \{x_1/\varepsilon, x_2/\varepsilon\}$ .

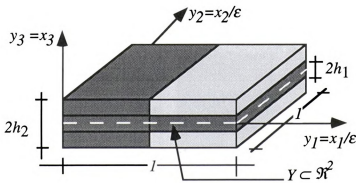


Figure 2.4. Small scale domain.

### Graphical Illustration of the Homogenization Procedure

We present here a graphical description of the construction of the basic cell used in homogenization of a ribbed plate. To simplify the exposition we use a rank-1 material to build a plate with ribs along only one direction.



We start with two different isotropic materials, a strong one,  $E^+$ , and a weak one,  $E^-$ , which are used to build two plates made by three plies. We label *strong plate* the one built using the strong material in the three plies, as shown in Figure 2.5 (a). Similarly, we label *weak plate*, the plate built using weak material in the lower and upper plies and strong material in the central ply (Figure 2.5 (b)). The stiffness properties of these two plates are computed using classical lamination theory (Jones (1975)), which yields the reduced stiffness matrix of each plate as a function of  $h_1$ ,  $h_2$ ,  $E^+$  and  $E^-$ .

A small scale cell is built by cutting a very thin slice (of order  $\epsilon$ ) from the strong and weak plates and placing the slices next to each other, as illustrated in Figure 2.5 (c). The result is a basic cell whose thickness is large ( $2h_2$ ) in comparison with the other two dimensions. The strong plate slice represents the ribs and the weak plate slice models the gap between the ribs. This cell is repeated in the domain  $\Omega_0 \subset \mathbb{R}^2$  to build a large

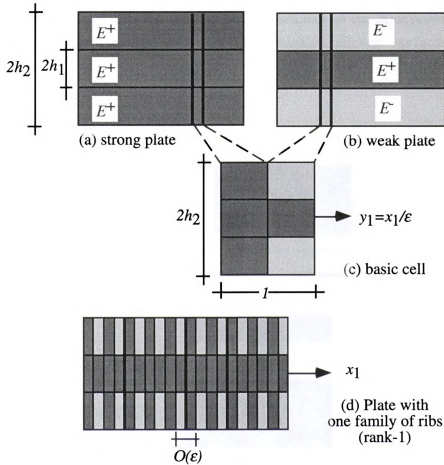


Figure 2.5. Graphical description of the homogenization procedure.

scale plate of dimensions  $L_x \times L_y \times 2h_2$ , as shown in Figure 2.5 (d). The stiffness properties of this plate change rapidly in a small scale.

In order to build a plate made of a rank-2 material one combines a thin slice of the strong plate (Figure 2.5 (a)) with a thin slice of the plate made of rank-1 material. This stacking process is made in a second direction, e.g.,  $x_2$ . The resulting plate has two families of ribs, one running in the  $x_1$  direction and the other in the  $x_2$  direction.

A similar procedure may be followed to build plates with different cross section. Depending on the type of material used in each ply of the weak plate it is possible to build plates with internal ribs (honeycomb) or perforated plates. Figure 2.6 shows three possible arrangements for symmetric plates. Since the assembly of the weak plate is performed *before* the homogenization procedure, the homogenized formulas developed here also work for honeycomb and perforated plates. The honeycomb configuration is particularly attractive not only because it is stiffer compared to a ribbed plate of the same weight, but also because the flat top and bottom surfaces of the honeycomb plate are often more suitable for industrial uses than the corrugated, uneven surfaces of ribbed plates.




RIBBED		rank-2 isotropic rank-2
HONEYCOMB		isotropic rank-2 isotropic
PERFORATED		rank-2 rank-2 rank-2

Figure 2.6. Assembly strategies for the weak plate.

### 2.1.2 Mindlin Plate Model

The derivation of effective properties for the ribbed plate is based on Mindlin's plate model. It begins here with the presentation of the equilibrium statement for such plate in a form that is particularly suitable to carry out the homogenization process, described in the next section.

The strain energy in a symmetric plate including in-plane, bending and shear deformations is given by the expression

$$U = \frac{1}{2} \int_{\Omega_0} \varepsilon^t(u) M \varepsilon(u) + \kappa^t(u) B \kappa(u) + \gamma^t(u) S \gamma(u) d\Omega \quad (2.1.1)$$

where

$$u = \{v_x, v_y, v_z, \theta_x, \theta_y\}^t \quad \text{is the displacement vector,}$$

$$\varepsilon = \left\{ \frac{\partial v_x}{\partial x}, \frac{\partial v_y}{\partial y}, \frac{\partial v_x}{\partial y} + \frac{\partial v_y}{\partial x} \right\}^t \quad \text{is the in-plane strain vector,}$$

$$\kappa = \left\{ -\frac{\partial \theta_y}{\partial x}, \frac{\partial \theta_x}{\partial y}, \frac{\partial \theta_x}{\partial x} - \frac{\partial \theta_y}{\partial y} \right\}^t \quad \text{is the curvature vector,}$$

$$\gamma = \left\{ \theta_y + \frac{\partial v_z}{\partial x}, -\theta_x + \frac{\partial v_z}{\partial y} \right\}^t \quad \text{is the transverse shear deformation vector,}$$

$$v_x, v_y, v_z \quad \text{are the displacements of the neutral plane in the } x, y \text{ and } z \text{ directions, respectively and}$$

$$\theta_x \text{ and } \theta_y \quad \text{are the rotations about the } x \text{ and } y \text{ axes using the right hand convention.}$$

The matrices  $M$ ,  $B$  and  $S$  are the stiffness matrices for membrane, bending and transverse shear deformations, respectively.  $M$  and  $B$  can be defined as  $M \equiv D_0$  and  $B \equiv D_2$ , where  $D_j$  ( $j=0$  or  $2$ ) are computed using

$$D_j = D_j^{cp} \int_{-h_0}^{h_0} z^j dz + 2[D_j]^{ep} \int_{h_0}^{h_1} z^j dz \quad (\text{no sum over } j), \quad j=0 \text{ or } 2. \quad (2.1.2a)$$

while the transverse shear stiffness matrix is computed as

$$S = 2h_1 \begin{bmatrix} \bar{D}_{44} & 0 \\ 0 & \bar{D}_{55} \end{bmatrix}^{cp} + 2(h_2 - h_1) \begin{bmatrix} \bar{D}_{44} & 0 \\ 0 & \bar{D}_{55} \end{bmatrix}^{ep} \quad (2.1.2b)$$

The superscripts 'cp' and 'ep' refer to core and external plies, respectively. Because of their dependence on the ply thicknesses, entries in  $D_0$ ,  $D_2$ , and  $S$  will vary rapidly in regions of rapid thickness variations.

The matrices  $D_j^{cp}$  and  $D_j^{ep}$  in (2.1.2a) are of the form

$$D_j = \begin{bmatrix} \bar{D}_{11} & \bar{D}_{12} & \bar{D}_{16} \\ & \bar{D}_{22} & \bar{D}_{26} \\ \text{sym} & & \bar{D}_{66} \end{bmatrix} \quad (2.1.2c)$$

Matrices  $D_0$ ,  $D_2$  and  $S$ , reflect the plane stress assumption ( $\sigma_z = 0$ ), i.e.,

$$\bar{D}_{ij} = D_{ij} - \frac{1}{D_{33}} D_{i3} D_{3j} \quad (i, j \neq 3, \quad i, j = 1, \dots, 6) \quad (2.1.2d)$$

The entries  $D_{ij}$  in (2.1.2d) are the stiffness coefficients of an orthotropic material.

It is convenient to organize material properties into a set of matrices  $W^{k\ell}$  of dimension (5x3) such that the strain energy  $U$  in (2.1.1) may be expressed as the sum

$$U = \frac{1}{2} \sum_{i,k=1}^5 \sum_{j,\ell=1}^3 \int_{\Omega_0} W_{ij}^{k\ell} \partial_\ell u_k \partial_j u_i d\Omega \quad (2.1.3a)$$

where

$$\{\partial_i\} = \left\{ \frac{\partial}{\partial x}, \frac{\partial}{\partial y}, 1 \right\} \quad (2.1.3b)$$

are operators in the macroscopic coordinates  $\{x, y, z\}$ . Explicit formulas for the matrices  $W^{k\ell}$  appear in the Appendix. The notation convention in (2.1.3b) is unusual, particularly the definition of  $\partial_3$ , but it is very convenient for the derivation of the finite element model. With this notation we may write equilibrium equations for the plate in the following form:

### Equilibrium Equations with Rapidly Varying Coefficients

Let  $u = \{v_x, v_y, v_z, \theta_x, \theta_y\}^t$  and  $\hat{u} = \{\delta v_x, \delta v_y, \delta v_z, \delta \theta_x, \delta \theta_y\}^t$ . The equilibrium solution  $u^\varepsilon \in V^\ell$  is such that

$$\sum_{i,k=1}^5 \sum_{j,\ell=1}^3 \int_{\Omega_0} W_{ij}^{k\ell} \partial_\ell u_k^\varepsilon \partial_j \hat{u}_i d\Omega = \sum_{i=1}^5 \left\{ \int_{\Omega_0} f_i^\varepsilon \hat{u}_i d\Omega + \int_{\Gamma^t} t_i \hat{u}_i d\Gamma^t \right\}, \quad \forall \hat{u} \in V^\ell \quad (2.1.4a)$$

where  $V^\ell$  is the space of kinematically admissible functions, e.g.,

$$V^\ell = \left\{ \hat{u} \in \left( H^1(\Omega_0) \right)^5 : \hat{u} = 0 \text{ on the boundary } \Gamma^d \right\} \quad (2.1.4b)$$

In (2.1.4),  $f^\varepsilon = \{f_{v_x}, f_{v_y}, f_{v_z}, 0, 0\}^t$  are the body forces (per unit area), and  $t$  is the vector of traction forces on the boundary  $\Gamma^t$ . The superscript  $\varepsilon$  in  $f^\varepsilon$  and  $u^\varepsilon$  denotes the dependency on the parameter  $\varepsilon$ . Assuming  $f^\varepsilon$  and  $t$  are sufficiently smooth, the variational problem (2.1.4) has a unique solution  $u^\varepsilon$ . Due to the variation of  $f^\varepsilon$  and  $W^{k\ell}$  at the microscopic level, the solution depends on  $x$  and  $y$ , that is,  $u^\varepsilon = u^\varepsilon(x, y)$ .

### 2.1.3 Derivation of Effective Properties

We proceed now with the derivation of homogenized plate stiffness properties using the asymptotic expansion technique. Details of this technique are fairly well known and will not be repeated here. A step-by-step description is found in Bensoussan, *et al.* (1978) or Guedes (1990). Following these standard procedures the generalized displacement vector  $u^\varepsilon$  is expressed as

$$u^\varepsilon = u^{(0)}(x, y) + \varepsilon u^{(1)}(x, y) + \varepsilon^2 u^{(2)}(x, y) + \dots \quad (2.1.5a)$$

where the functions  $u^{(j)}(x, y)$ ,  $j=0, 1, \dots, n$ , are  $Y$ -periodic. Equation (2.1.5) is replaced in

(2.1.4) and terms multiplying the same power of  $\varepsilon$  are grouped together. Since  $\varepsilon$  is arbitrary, each group can be set, individually, equal to zero. Then, limits are taken letting  $\varepsilon \rightarrow 0$ , and using the property

$$\text{If } g : \Omega_0 \times Y \rightarrow \mathfrak{R}, \text{ then } \lim_{\varepsilon \rightarrow 0} \int_{\Omega_0} g(x, y) d\Omega = \frac{1}{\|Y\|} \int_{\Omega_0} \int_Y g(x, y) dY d\Omega. \quad (2.1.5b)$$

This process leads to two boundary value problems at different scales. The small scale problem is

$$\sum_{i,p=1}^5 \sum_{j,m=1}^3 \int W_{ij}^{pm} \partial_m^Y \chi_p^{k\ell}(x, y) \partial_j^Y \hat{u}_i(y) dY = \sum_{i=1}^5 \sum_{j=1}^3 \int_Y W_{ij}^{k\ell} \partial_j^Y \hat{u}_i(y) dY, \quad \forall \hat{u} \in V^s, \\ k = 1, \dots, 5 \text{ and } \ell = 1, \dots, 3 \quad (2.1.6a)$$

where the unknown function  $\chi_i^{k\ell}(x, y) \in V^s$  is a Y-periodic “characteristic function” defined on Y for a fixed x.  $V^s$  is the space of Y-periodic functions in the small scale domain Y

$$V^s = \left\{ \hat{u}(y) \in \left( H^1(Y) \right)^5 : \hat{u}(y) \text{ is } Y\text{-periodic} \right\}, \quad (2.1.6b)$$

and the operator  $\partial_i^Y$  is defined as  $\{\partial_i^Y\} = \left\{ \frac{\partial}{\partial y_1}, \frac{\partial}{\partial y_2}, 0 \right\}$ . Notice that the Y-periodicity of the functions in (2.1.6b) takes place of the usual boundary conditions and insures that the problem is well posed.

The problem in the large scale is expressed in terms of the effective properties and does not involve the small-scale coordinate y. Its solution is the unknown displacement  $u^{(0)}(x)$ , a solution to the problem

$$\sum_{i,k=1}^5 \sum_{j,\ell=1}^3 \int \bar{W}_{ij}^{k\ell}(x) \partial_\ell u_k^{(0)}(x) \partial_j \hat{u}_i(x) d\Omega = \sum_{i=1}^5 \left\{ \int_{\Omega_0} f_i(x) \hat{u}_i(x) d\Omega + \int_{\Gamma^t} t_i(x) \hat{u}_i(x) d\Gamma \right\}, \\ \forall \hat{u} \in V^\ell \quad (2.1.7a)$$

where  $\bar{W}_{ij}^{k\ell}(x)$  are the homogenized plate stiffness properties defined by





$$\bar{W}_{ij}^{k\ell} = \frac{1}{\|Y\|} \int_Y (W_{ij}^{k\ell} - \sum_{p=1}^5 \sum_{m=1}^3 W_{ij}^{pm} \partial_m^Y \chi_p^{k\ell}) dY \quad (2.1.7b)$$

and

$$f_i(x) = \frac{1}{\|Y\|} \int_Y f_i^\varepsilon dY \quad (2.1.7c)$$

is the average value of the body force at  $x$ .

In the large scale problem all details of the micro structure are implicit in the homogenized properties  $\bar{W}_{ij}^{k\ell}(x)$ . The *explicit* form of these coefficients becomes available once specific details of the micro structure are prescribed. To compute the homogenized properties using (2.1.7b) one needs first to solve a series of small scale problems (2.1.6) in the small scale domain  $Y$ . Depending on the particular details of the micro structure used, this could be a very difficult procedure. Fortunately, the process is greatly simplified if one uses a layered material for which closed form expressions for  $\partial_m^Y \chi_p^{k\ell}$  (in equations (2.1.6) and (2.1.7b)) are available. This is discussed in the next section. The construction of the homogenized Mindlin plate model with periodically varying stiffness was presented for the first time by Bourgeat and Tapiero (1983). However, they did not make any choice for the geometry of the small scale domain. This choice is made here picking layered materials to build the  $Y$ -periodic Mindlin plate.

#### 2.1.4 Results Using Layered Materials

For simplicity, here and in what follows the discussion will be limited to the computation of *bending* and *transverse shear* components of the homogenized properties  $\bar{W}_{ij}^{k\ell}(x)$ . They correspond to entries in the  $B$  and  $S$  reduced stiffness matrices in the expression for the strain energy in (2.1.1). The *homogenized* version of these matrices will be labeled  $\bar{B}$  and  $\bar{S}$ , respectively. The membrane component can be computed following the same procedure. It is not surprising that they coincide with the effective properties found in plane stress elasticity (Bendsøe, (1989)). Only the final formulas for membrane stiffness will be presented in here.

#### Effective Properties Using a Rank-1 Material

For a plate made of a rank-1 material characterized by the basic cell  $(0,1) \times \mathfrak{R} \times (-h_1, h_1)$  as shown in Figure 2.7, the characteristic functions  $\chi_p^{kl}$  in (2.6) are independent of  $y_2$ .

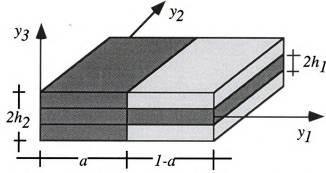


Figure 2.7. Basic cell in a plate made using a rank-1 material.

Entries in matrices  $B$  and  $S$  in (2.1.1) are computed by integration over  $z$  of the material properties in the basic cell, as shown in (2.1.2a) and (2.1.2b). The computation of the homogenized properties follows the procedure in (Bendsøe (1989)). To illustrate this procedure only the derivation of  $\bar{B}(2,2)(x) \equiv \bar{W}_{41}^{41}(x)$  is presented in detail. It is the effective properties associated with  $D_2(2,2)(x,y) \equiv W_{41}^{41}(x,y)$ .

From (2.1.7b), using  $\partial_2^Y \chi_p^{k\ell} = 0$  ( $\chi_p^{k\ell}$  does not depend on  $y_2$ ) and  $\partial_3^Y = 0$ , one obtains

$$\bar{W}_{41}^{41} = \frac{1}{\|Y\|} \int_Y (W_{41}^{41} - W_{41}^{41} \partial_1^Y \chi_4^{41}) dY. \quad (2.1.8)$$

In order to obtain an expression for  $W_{41}^{41} \partial_1^Y \chi_4^{41}$  appropriate indices  $k$  and  $\ell$  and virtual displacement functions  $v$  in the small scale problem (2.1.6) are chosen. In this case, let  $k=4$ ,  $\ell=1$  and  $\hat{u} = \{0, 0, 0, \hat{u}_4(y_1), 0\}^T$ . Then problem (2.1.6) becomes

$$\int_Y W_{41}^{41} \partial_1^Y \chi_1^{41}(x,y) \partial_1^Y \hat{u}_4(y_1) dY = \int_Y W_{41}^{41} \partial_1^Y \hat{u}_4(y_1) dY \quad \text{for a fixed } x \quad (2.1.9)$$

After integration by parts, and since the boundary integrals vanish because of the periodicity of  $\chi^{k\ell}$ , the following equation is obtained

$$\partial_1^Y W_{41}^{41} \partial_1^Y \chi_1^{41}(x,y) = \partial_1^Y W_{41}^{41} \quad (2.1.10)$$

Integrating with respect to  $y_1$  it holds that

$$W_{41}^{41} \partial_1^Y \chi_4^{41} = c_1 + W_{41}^{41} \quad \text{with} \quad c_1 = - \left[ \frac{1}{\|Y\|} \int_Y \frac{1}{W_{41}^{41}(y_1)} dY \right]^{-1} \quad (2.1.11)$$

With this expression for  $W_{41}^{41} \partial_1^Y \chi_4^{41}$  (2.1.8) becomes

$$\bar{W}_{41}^{41} = \frac{1}{\|Y\|} \int_Y c_1 dY = \left[ \int_Y \frac{1}{W_{41}^{41}(y_1)} dY \right]^{-1}. \quad (2.1.12)$$

which is the final result.

The procedure outlined above can be repeated to obtain each entry of the homogenized reduced stiffness matrix. The equations needed for all entries in problem (2.1.6) are

$$\begin{aligned} W_{51}^{51} \partial_1^Y \chi_5^{42} &= c_2 + W_{51}^{42} \quad \text{with} \quad c_2 = - \left[ \frac{1}{\|Y\|} \int_Y \frac{1}{W_{51}^{51}(y_1)} dY \right]^{-1} \left[ \frac{1}{\|Y\|} \int_Y \frac{W_{51}^{42}(y_1)}{W_{51}^{51}(y_1)} dY \right] \\ W_{51}^{51} \partial_1^Y \chi_5^{51} &= c_3 + W_{51}^{51} \quad \text{with} \quad c_3 = - \left[ \frac{1}{\|Y\|} \int_Y \frac{1}{W_{51}^{51}(y_1)} dY \right]^{-1} \\ W_{31}^{31} \partial_1^Y \chi_3^{31} &= c_4 + W_{31}^{31} \quad \text{with} \quad c_4 = - \left[ \frac{1}{\|Y\|} \int_Y \frac{1}{W_{31}^{31}(y_1)} dY \right]^{-1} \end{aligned} \quad (2.1.13)$$

Due to the simple geometry of the rank-1 cell, integrals in (2.1.13) may be simplified considerably. The results can be expressed in a compact and convenient way in terms of the *arithmetic* and *harmonic averages*, defined as follows:

Arithmetic average. For all  $\xi \in [0,1]$ , the *arithmetic average*  $\bar{A}$  of two real numbers  $m_1$  and  $m_2$  is defined here as the function

$$\bar{A}(m_1, m_2, \xi) = \xi m_1 + (1 - \xi) m_2 \quad (2.1.14a)$$

Harmonic average. For all  $\xi \in [0,1]$ , the *harmonic average*  $\underline{A}$  of two positive real numbers  $m_1$  and  $m_2$  is defined here as the function

$$\underline{A}(m_1, m_2, \xi) = \left[ \xi(m_1)^{-1} + (1-\xi)(m_2)^{-1} \right]^{-1} = \frac{m_1 m_2}{\xi m_2 + (1-\xi)m_1} \quad (2.1.14b)$$

For positive  $m_1$  and  $m_2$ ,  $\bar{A} \geq \underline{A}$  and  $\bar{A} = \underline{A}$  if and only if  $m_1 = m_2$ .

The homogenized stiffness properties in bending ( $\bar{B}^{R1}$ ) and shear ( $\bar{S}^{R1}$ ) of a plate made of rank-1 materials may be expressed in compact form using these averages, as follows:

$$\begin{aligned} \bar{B}^{R1}(1,1) &= \underline{A}(B^+(1,1), B^-(1,1), a) \\ \bar{B}^{R1}(1,2) &= \underline{A}(B^+(1,1), B^-(1,1), a) \bar{A}\left(\frac{B^+(1,2)}{B^+(1,1)}, \frac{B^-(1,2)}{B^-(1,1)}, a\right) \\ \bar{B}^{R1}(2,2) &= \bar{A}(B^+(2,2), B^-(2,2), a) - \bar{A}\left(\frac{(B^+(1,2))^2}{B^+(1,1)}, \frac{(B^-(1,2))^2}{B^-(1,1)}, a\right) + \\ &\quad + \bar{A}^2\left(\frac{B^+(1,2)}{B^+(1,1)}, \frac{B^-(1,2)}{B^-(1,1)}, a\right) \underline{A}(B^+(1,1), B^-(1,1), a) \\ \bar{B}^{R1}(3,3) &= \underline{A}(B^+(3,3), B^-(3,3), a) \quad (bending) \\ \bar{S}^{R1}(1,1) &= \underline{A}(S^+(1,1), S^-(1,1), a) \\ \bar{S}^{R1}(2,2) &= \bar{A}(S^+(2,2), S^-(2,2), a) \quad (shear) \end{aligned} \quad (2.1.15a)$$

where the superscript “-” and “+” refer to the weak and strong materials, respectively, and “ $a$ ” is the area fraction of the strong plate (Figure 2.7), i.e., the fraction of the unit cell occupied by the strong material. The superscript “R1” indicates that a rank-1 layered material is assumed.

Equations (2.1.15a) hold for ribbed, honeycomb and perforated plates. In each case the matrices  $B$  and  $S$  must be defined appropriately. Using matrices  $B$  and  $S$  for *ribbed* plates, (2.1.15) yields the following expressions for a ribbed plate with ribs running along only one direction

$$\begin{aligned}
\bar{B}^{R1}(1,1) &= \frac{2}{3} \underline{A}(E_{1111}^+ h_2^3, E_{1111}^+ h_1^3 + E_{1111}^-(h_2^3 - h_1^3), a) \\
\bar{B}^{R1}(1,2) &= \bar{B}^{R1}(2,1) = \frac{2}{3} \underline{A}(E_{1122}^+ h_2^3, E_{1122}^+ h_1^3 + E_{1122}^-(h_2^3 - h_1^3), a) \\
\bar{B}^{R1}(2,2) &= \frac{2}{3} ((1 - \nu^2) \bar{A}(E_{2222}^+ h_2^3, E_{2222}^+ h_1^3 + E_{2222}^-(h_2^3 - h_1^3), a) + \\
&\quad \nu^2 \underline{A}(E_{2222}^+ h_2^3, E_{2222}^+ h_1^3 + E_{2222}^-(h_2^3 - h_1^3), a)) \\
\bar{B}^{R1}(3,3) &= \frac{2}{3} \underline{A}(E_{1212}^+ h_2^3, E_{1212}^+ h_1^3 + E_{1212}^-(h_2^3 - h_1^3), a) \quad (bending)
\end{aligned}$$

$$\begin{aligned}
\bar{S}^{R1}(1,1) &= 2 \underline{A}(E_{1313}^+ h_2, E_{1313}^+ h_1 + E_{1313}^-(h_2 - h_1), a) \\
\bar{S}^{R1}(2,2) &= 2 \bar{A}(E_{2323}^+ h_2, E_{2323}^+ h_1 + E_{2323}^-(h_2 - h_1), a) \quad (shear) \quad (2.1.15b)
\end{aligned}$$

Using matrices  $B$  and  $S$  for honeycomb plates, (2.1.15a) yield the following expressions

$$\begin{aligned}
\bar{B}^{R1}(1,1) &= \frac{2}{3} \underline{A}(E_{1111}^+ h_2^3, E_{1111}^- h_1^3 + E_{1111}^+(h_2^3 - h_1^3), a) \\
\bar{B}^{R1}(1,2) &= \bar{B}^{R1}(2,1) = \frac{2}{3} \underline{A}(E_{1122}^+ h_2^3, E_{1122}^- h_1^3 + E_{1122}^+(h_2^3 - h_1^3), a) \\
\bar{B}^{R1}(2,2) &= \frac{2}{3} ((1 - \nu^2) \bar{A}(E_{2222}^+ h_2^3, E_{2222}^- h_1^3 + E_{2222}^+(h_2^3 - h_1^3), a) + \\
&\quad \nu^2 \underline{A}(E_{2222}^+ h_2^3, E_{2222}^- h_1^3 + E_{2222}^+(h_2^3 - h_1^3), a)) \\
\bar{B}^{R1}(3,3) &= \frac{2}{3} \underline{A}(E_{1212}^+ h_2^3, E_{1212}^- h_1^3 + E_{1212}^+(h_2^3 - h_1^3), a) \quad (bending)
\end{aligned}$$

$$\begin{aligned}
\bar{S}^{R1}(1,1) &= 2 \underline{A}(E_{1313}^+ h_2, E_{1313}^- h_1 + E_{1313}^+(h_2 - h_1), a) \\
\bar{S}^{R1}(2,2) &= 2 \bar{A}(E_{2323}^+ h_2, E_{2323}^- h_1 + E_{2323}^+(h_2 - h_1), a) \quad (shear) \quad (2.1.16)
\end{aligned}$$

Formulas in (2.1.15a) are the same as reported by Lewinski and Telega (1988) and Lewinski (1991).

Formulas for bending stiffness in (2.1.15a) have the same structure of those derived from plane elasticity equations using a rank-1 material (Bendsøe (1989)). These formulas also correspond to the membrane stiffness of ribbed plates,  $\bar{M}^{R1}$ :

$$\bar{M}^{R1}(1,1) = 2 \underline{A}(E_{1111}^+ h_2, E_{1111}^+ h_1 + E_{1111}^-(h_2 - h_1), a)$$



$$\begin{aligned}
\bar{M}^{R1}(1,2) &= 2\bar{A}(E_{1122}^+h_2, E_{1122}^+h_1 + E_{1122}^-(h_2 - h_1), a) \\
\bar{M}^{R1}(2,2) &= 2((1 - v^2)\bar{A}(E_{2222}^+h_2, E_{2222}^+h_1 + E_{2222}^-(h_2 - h_1), a) + \\
&\quad v^2\bar{A}(E_{2222}^+h_2, E_{2222}^+h_1 + E_{2222}^-(h_2 - h_1), a)) \\
\bar{M}^{R1}(3,3) &= 2\bar{A}(E_{1212}^+h_2, E_{1212}^+h_1 + E_{1212}^-(h_2 - h_1), a)
\end{aligned} \tag{2.1.17}$$

### Effective Properties Using a Rank-2 Material

Once the plate made with a rank-1 material is built, one can build a plate using a rank-2 material following the procedure showed in Figure 2.5. The formulas are easily derived using (2.1.15a) and a stacking direction offset of 90 degrees, as shown in Figure 2.8. This micro structure is fully described by two layer widths,  $a$  and  $b$ , and by the global orientation of the micro structure,  $\Theta$ . A model for rank-L ( $L \in \mathbb{N}^+$ ) material plate will be given in next Chapter using a different approach.

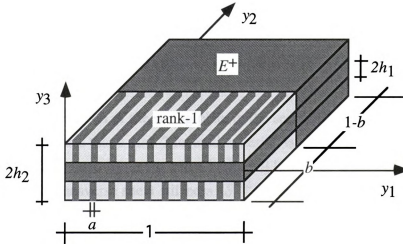


Figure 2.8. Basic cell of a plate made of rank-2 material.

In this case and using the approach of the previous section, we obtain the following results:

$$\begin{aligned}
\bar{M}^{R2}(1,1) &= \bar{A}\left(M^+(1,1), \bar{M}^{R1}(1,1), b\right) - \bar{A}\left(\frac{M^+(1,2)^2}{M^+(2,2)}, \frac{\bar{M}^{R1}(1,2)^2}{\bar{M}^{R1}(2,2)}, b\right) + \\
&\quad \bar{A}^2\left(\frac{M^+(1,2)}{M^+(2,2)}, \frac{\bar{M}^{R1}(1,2)}{\bar{M}^{R1}(2,2)}, b\right) \bar{A}\left(M^+(2,2), \bar{M}^{R1}(2,2), b\right) \\
\bar{M}^{R2}(1,2) &= \bar{M}^{R2}(2,1) = \bar{A}\left(M^+(2,2), \bar{M}^{R1}(2,2), b\right) \bar{A}\left(\frac{M^+(1,2)}{M^+(2,2)}, \frac{\bar{M}^{R1}(1,2)}{\bar{M}^{R1}(2,2)}, b\right)
\end{aligned}$$





$$\begin{aligned}
\bar{M}^{R2}(2,2) &= \underline{A}(M^+(2,2), \bar{M}^{R1}(2,2), b) \\
\bar{M}^{R2}(3,3) &= \underline{A}(M^+(3,3), \bar{M}^{R1}(3,3), b) \quad (\text{membrane}) \\
\bar{B}^{R2}(1,1) &= \bar{A}(B^+(1,1), \bar{B}^{R1}(1,1), b) - \bar{A}\left(\frac{B^+(1,2)^2}{B^+(2,2)}, \frac{\bar{B}^{R1}(1,2)^2}{\bar{B}^{R1}(2,2)}, b\right) + \\
&\quad \bar{A}^2\left(\frac{B^+(1,2)}{B^+(2,2)}, \frac{\bar{B}^{R1}(1,2)}{\bar{B}^{R1}(2,2)}, b\right) \underline{A}(B^+(2,2), \bar{B}^{R1}(2,2), b) \\
\bar{B}^{R2}(1,2) &= \bar{B}^{R2}(2,1) = \underline{A}(B^+(2,2), \bar{B}^{R1}(2,2), b) \bar{A}\left(\frac{B^+(1,2)}{B^+(2,2)}, \frac{\bar{B}^{R1}(1,2)}{\bar{B}^{R1}(2,2)}, b\right) \\
\bar{B}^{R2}(2,2) &= \underline{A}(B^+(2,2), \bar{B}^{R1}(2,2), b) \\
\bar{B}^{R2}(3,3) &= \underline{A}(B^+(3,3), \bar{B}^{R1}(3,3), b) \quad (\text{bending}) \\
\bar{S}^{R2}(1,1) &= \bar{A}(S^+(1,1), \bar{S}^{R1}(1,1), b) \\
\bar{S}^{R2}(2,2) &= \underline{A}(S^+(2,2), \bar{S}^{R1}(2,2), b) \quad (\text{shear}) \quad (2.1.18)
\end{aligned}$$

where “ $b$ ” is the area fraction of the strong plate in the second direction (Figure 2.8). The superscript “R2” indicates that a rank-2 layered material is assumed. Layered materials of second rank were also used by Lurie and Cherkayev (1986) for Kirchhoff (thin) plates, where homogenized transverse shear stiffness ( $\bar{S}^{R2}$ ) cannot be computed. In the case of rotationally symmetric bending of thin plates the rank-2 micro structure was also used by Rozvany, *et al.* (1987).

The effective properties in (2.1.18) summarize the result of this section. They express the average properties of a plate whose cross section varies in the small scale in terms of mixture of strong and weak materials  $E^+$  and  $E^-$ . Formulas (2.1.18) can be applied to ribbed, honeycomb, and perforated plates, simply by assembling the plies in the weak plate in a different order, as outlined in Figure 2.6. The properties of a ribbed plate are obtained setting the stiffness of the weak material to zero. The formulas are used in this manner in optimization formulations for shape and layout of plate structures, as outlined below.



## 2.2 Comparison With Other Models For Ribbed Plates

Several models for the calculation of homogenized properties of plates of rapidly varying thickness have appeared in the recent literature. Some of these models are suitable for optimization of the plate geometry and its shape. In this section we present results that can be used to compare four such models. To facilitate the presentation the study is limited to plates with only one family of ribs, with cross sections as shown in Figure 2.9 and built using a rank-1 material. It should be observed that even though shape optimization problems call for the use of a rank-2 material, when the optimum solution prescribes that ribs be used, it is typical that ribs are aligned along a single direction in ribbed and honeycomb plates.

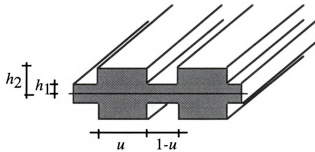


Figure 2.9. Geometry of plate cross section.

The homogenized plate models compared are

### Mindlin Plate Model (M)

This is the model discussed in the previous section and summarized in (2.1.15b).

### Laminated Plate Model (L)

In this model the plate is made assembling three plies. The external plies have homogenized properties computed using the plane elasticity equations. This idea was discussed by Caillerie (1984) and implemented by Suzuki and Kikuchi (1991b).

### Kirchhoff Plate Models (K and K')

This refers to two models derived by Kohn and Vogelius (1984).

The following properties of isotropic materials will be used in the homogenized stiffness

$$D^{iso} = \begin{bmatrix} E_{1111} & E_{1122} & 0 \\ & E_{2222} & 0 \\ \text{sym} & & E_{1212} \end{bmatrix} = \frac{E}{1-\nu^2} \begin{bmatrix} 1 & \nu & 0 \\ \nu & 1 & 0 \\ 0 & 0 & \frac{1-\nu}{2} \end{bmatrix} \quad (\text{in plane stress}) \quad (2.2.1a)$$

$$D_S^{iso} = \begin{bmatrix} E_{1313} & 0 \\ 0 & E_{2323} \end{bmatrix} = \frac{E}{2(1+\nu)} \begin{bmatrix} 1 & 0 \\ 0 & 1 \end{bmatrix} \quad (\text{in transverse shear}) \quad (2.2.1b)$$

where  $E$  is the Young's modulus, and  $\nu$  the Poisson ratio. The ribs are aligned along direction "2" of the local material axes.

To facilitate the comparison we introduce the following arithmetic and harmonic averages of the stiffness of two plates of thickness  $2h_1$  and  $2h_2$ , respectively:

$$UB_{ijkl} = \frac{2}{3} E_{ijkl}^+ \bar{A}(h_2^3, h_1^3, u) \quad (\text{for bending}) \quad (2.2.2a)$$

$$UB_{ijkl} = 2E_{ijkl}^+ \bar{A}(h_2, h_1, u) \quad (\text{for transverse shear}) \quad (2.2.2b)$$

$$LB_{ijkl} = \frac{2}{3} E_{ijkl}^+ \underline{A}(h_2^3, h_1^3, u) \quad (\text{for bending}) \quad (2.2.2c)$$

$$LB_{ijkl} = 2E_{ijkl}^+ \underline{A}(h_2, h_1, u) \quad (\text{for shear}) \quad (2.2.2d)$$

The reader may notice that  $UB$  corresponds to the classical Voigt bound for elastic properties of a mixture of two materials while  $LB$  corresponds to the Reuss classical bound. These should not be confused with optimal bounds found in the literature, such as for example those in Francfort and Murat (1986). Bounds  $UB$  and  $LB$  are used here only to illustrate the relative magnitudes of properties computed using different modeling assumptions.

### 2.2.1 Comparison of Effective Properties in Bending

#### Homogenized Mindlin Plate Model (M)

This is the model developed in Section 2.1 using a rank-2 layered material. The homogenized properties are the same as  $\bar{B}^{R1}$  and  $\bar{S}^{R1}$  in (2.1.15b)

$$\begin{aligned}
\bar{B}^M(1,1) &= \frac{2}{3} \underline{A}(E_{1111}^+ h_2^3, E_{1111}^+ h_1^3 + E_{1111}^-(h_2^3 - h_1^3), u) \\
\bar{B}^M(1,2) &= \bar{B}^M(2,1) = \frac{2}{3} \underline{A}(E_{1122}^+ h_2^3, E_{1122}^+ h_1^3 + E_{1122}^-(h_2^3 - h_1^3), u) \\
\bar{B}^M(2,2) &= \frac{2}{3} ((1 - \nu^2) \bar{A}(E_{2222}^+ h_2^3, E_{2222}^+ h_1^3 + E_{2222}^-(h_2^3 - h_1^3), u) + \\
&\quad \nu^2 \underline{A}(E_{2222}^+ h_2^3, E_{2222}^+ h_1^3 + E_{2222}^-(h_2^3 - h_1^3), u)) \\
\bar{B}^M(3,3) &= \frac{2}{3} \underline{A}(E_{1212}^+ h_2^3, E_{1212}^+ h_1^3 + E_{1212}^-(h_2^3 - h_1^3), u) \tag{2.2.3}
\end{aligned}$$

The superscript “M” (instead of R1) is used here to indicate that this is the result associated with the “Mindlin” model.

All entries in  $\bar{B}^M$ , except entry (2,2), are at the *lower* bound  $LB$  (recall that ribs are aligned along direction “2”). Entry (2,2) is a convex combination of the lower and upper bounds. For typical values of Poisson’s ratio, the bending stiffness along the rib direction is essentially equal to the *upper bound*.

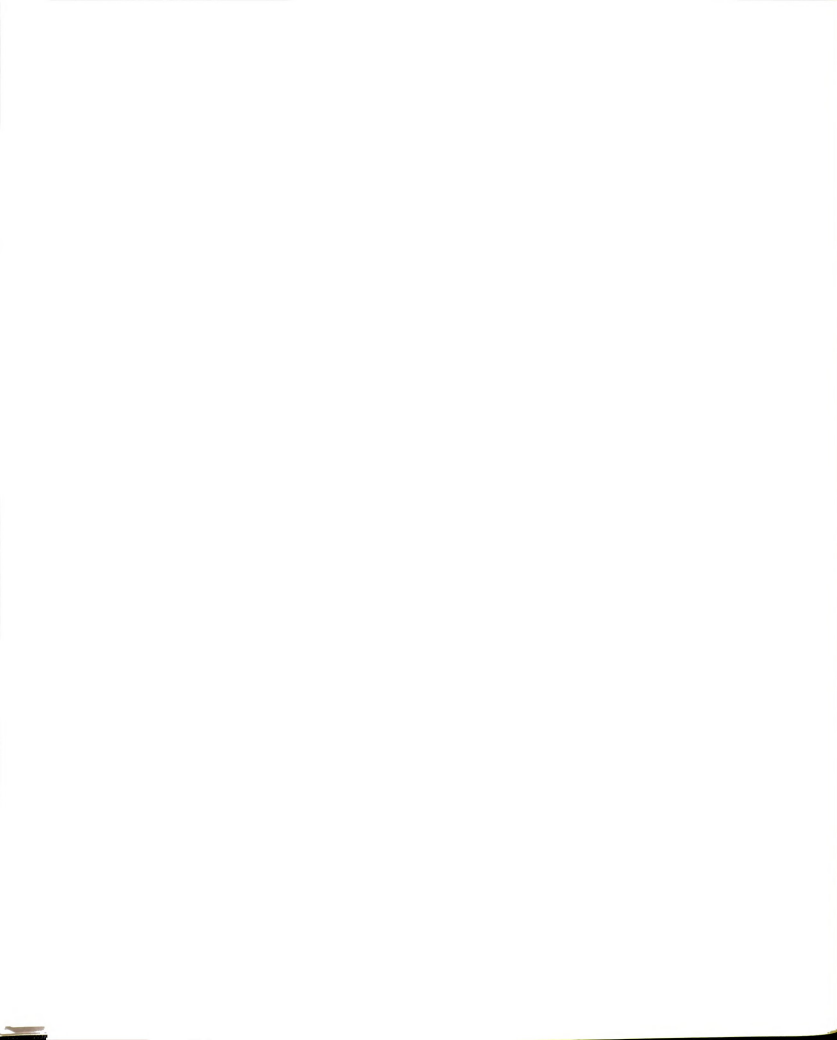
#### Homogenized Laminated Model (L)

In this model the plate is made by three plies as shown in Figure 2.10. In contrast to the Mindlin model the properties of the external plies are the homogenized material properties obtained from plane elasticity equations. The central ply is made of an isotropic material and the external plies of a layered rank-1 material. The homogenized properties are given by (2.1.16) and the assembly process is described by the following equation:

$$\bar{B}^L = D^{cp} \int_{-h_0}^{h_0} z^2 dz + 2D^{ep} \int_{h_0}^{h_1} z^2 dz = \frac{2}{3} [(h_2^3 - h_1^3) D^{R1} + h_1^3 D^{iso}] \tag{2.2.4}$$

The homogenized plate properties of the laminated plate are derived using (2.2.4).

$$\begin{aligned}
\bar{B}^L(1,1) &= \frac{2}{3} ((h_2^3 - h_1^3) \underline{A}(E_{1111}^+, E_{1111}^-, u) + h_1^3 E_{1111}^+) \\
\bar{B}^L(1,2) &= \bar{B}^L(2,1) = \frac{2}{3} ((h_2^3 - h_1^3) \underline{A}(E_{1122}^+, E_{1122}^-, u) + h_1^3 E_{1122}^+) \\
\bar{B}^L(2,2) &= \frac{2}{3} [(h_2^3 - h_1^3) \times \\
&\quad ((1 - \nu^2) \bar{A}(E_{2222}^+, E_{2222}^-, u) + \nu^2 \underline{A}(E_{2222}^+, E_{2222}^-, u)) + h_1^3 E_{2222}^+]
\end{aligned}$$



$$\bar{B}^L(3,3) = \frac{2}{3} \left( (h_2^3 - h_1^3) \underline{A} (E_{1212}^+, E_{1212}^-, u) + h_1^3 E_{1212}^+ \right) \quad (2.2.5)$$

In model L (laminated) the assembly of the plies (Figure 2.10) is carried out *after* the homogenized properties of each ply are obtained. As a result, in model L the thicknesses  $h_1$  and  $h_2$  do not appear inside the averages  $\underline{A}$  and  $\bar{A}$ . In contrast, in model M (2.2.3) the assembly of the plies occurs *before* the homogenization step. Core and rib thicknesses and material properties are homogenized *together*. This is a fundamental difference between models M (Mindlin) and L (laminated). The particular case of a plate with uniform thickness (i.e., when  $u$  is set to 1 in Figure 2.9) is correctly predicted by equations (2.2.5).

#### Homogenized Kirchhoff Plate Models (K and K')

Kohn and Vogelius (1984) developed expressions to compute homogenized stiffness values for a thin ribbed plate using three-dimensional elasticity equations and the following asymptotic expansion

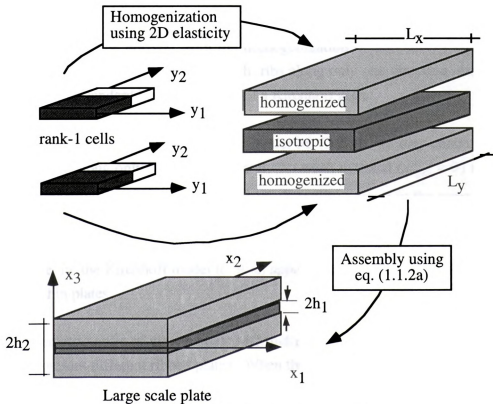


Figure 2.10. Laminated plate model.



$$u^\varepsilon = \sum_{n=0}^k \varepsilon^n u^{(n)}(x, x/\varepsilon^a, z/\varepsilon) \quad a > 0$$

The parameter “ $a$ ” determines the length scale of the thickness variation. They found three types of homogenized properties, depending on the value of the parameter “ $a$ ”. Here we summarize the results for  $a < 1$  and  $a > 1$ . In both cases it is assumed from the start that the “weak” material  $E^-$  is absent.

For  $a < 1$  the length scale of the variation of the plate thickness is larger than the mean thickness. The homogenized plate stiffness properties in this case are (Kohn and Vogelius, (1984))

$$\bar{B}^K = \frac{2}{3} \begin{bmatrix} E_{1111} \underline{A}(h_2^3, h_1^3, u) & E_{1122} \underline{A}(h_2^3, h_1^3, u) & 0 \\ & E_{2222} \left( (1 - \nu^2) \bar{A}(h_2^3, h_1^3, u) + \nu^2 \underline{A}(h_2^3, h_1^3, u) \right) & 0 \\ \text{sym} & & E_{1212} \bar{A}(h_2^3, h_1^3, u) \end{bmatrix} \quad (2.2.6a)$$

This result can also be derived from the homogenization of Kirchhoff's equations by Duvaut (1976). Therefore, in plates with ribs along only one direction the case  $a < 1$  corresponds to the standard homogenization of a Kirchhoff plate.

Comparing (2.2.6a) with the result from model M (2.2.3) we may conclude that in plates with ribs along only one direction and no weak material ( $E_{ijkl}^- = 0$ ) models K (Kohn and Vogelius (1984) with  $a < 1$ ) and M (Mindlin) result in the same averaged properties  $\bar{B}_2(1,1)$ ,  $\bar{B}_2(1,2)$ , and  $\bar{B}_2(2,2)$ . The models, however, predict different values of the twisting stiffness  $\bar{B}_2(3,3)$ . In the Mindlin model  $\bar{B}_2(3,3)$  is a *lower bound* while in the Kirchhoff model it is an *upper bound*. This difference will play a role even in thin plates.

From the geometric point of view models M (Mindlin) and K (Kohn and Vogelius (1984) with  $a < 1$ ) represent different ribbed plates. When the size of the cell  $\varepsilon$  tends to zero in the homogenization process, the periodicity increases and ribs become thinner compared to the plate thickness. Therefore, model M (Mindlin) corresponds to plates with slender ribs. Instead, model K (Kohn and Vogelius (1984) with  $a < 1$ ) corresponds to the case when the

period is much greater than the plate thickness (“stubby” ribs). This fundamental difference is only manifested in the twisting stiffness  $\bar{B}_{2(3,3)}$ . The comparison of these two models is still useful since they are the most used plate models in the engineering practice.

The *second* model derived by Kohn and Vogelius corresponds to values of the parameter  $a > 1$ . In this case, the thickness varies in a scale smaller than the mean plate thickness. The homogenized plate stiffness properties are

$$\bar{B}^{K'} = \frac{2}{3} \begin{bmatrix} E_{1111}h_1^3 & E_{1122}h_1^3 & 0 \\ & E_{2222}\left((1-\nu^2)\bar{A}(h_2^3, h_1^3, u) + \nu^2 h_1^3\right) & 0 \\ sym & & E_{1212}h_1^3 \end{bmatrix} \quad (2.2.6b)$$

Notice that these equations, derived by Kohn and Vogelius from three-dimensional elasticity, are not valid for plates of uniform thickness  $2h_2$  (i.e., when  $u$  is set to 1 in Figure 2.9). Setting  $u=1$  in (2.2.6b) all entries in the stiffness matrix depend on  $h_1$ , *even though the plate is of uniform thickness  $2h_2$* . Also notice that another way to derive equations (2.2.6b) is setting  $E_{ijkl}^- = 0$  in equations (2.2.5). However, this is considered an improper operation since the homogenization procedure carried out in two-dimensional elasticity is only possible under the assumption of positive definiteness of the elasticity tensor at each point of the microscopic cell. Using  $E_{ijkl}^- = 0$  in equations (2.2.5) violates this assumption.

A summary of the results for each model is presented in Table 2.1, where properties of the weak material  $E^-$  have been set to zero throughout. In order to show the fundamental difference between model M and model L we also include the model L for the particular (but improper) case when  $E_{ijkl}^- = 0$ . These results are presented in graphical form in Figures 2.11, 2.12, 2.13, and 2.14, displaying the effect of changes in the rib thicknesses and height on individual entries of the plate *bending* stiffness matrices. The plate cross section is as shown in Figure 2.9. An isotropic “strong” material with  $(E, \nu) = (100, 0.3)$  is used in computations.

**Effect of Rib Width** This experiment measures changes in the stiffness of the plate as the width of the rib ( $u$ ) increases. The core thickness ( $2h_1$ ) and the total plate thickness ( $2h_2$ )

Table 2.1 Summary of homogenized properties of one-family, ribbed plates.

Mindlin Model (M):

$$\bar{B}^M = \frac{2}{3} \begin{bmatrix} E_{1111} \underline{A}(h_2^3, h_1^3, u) & E_{1122} \underline{A}(h_2^3, h_1^3, u) & 0 \\ & E_{2222} \left( (1-v^2) \bar{A}(h_2^3, h_1^3, u) + v^2 \underline{A}(h_2^3, h_1^3, u) \right) & 0 \\ \text{sym} & & E_{1212} \underline{A}(h_2^3, h_1^3, u) \end{bmatrix}$$

Kirchhoff model for  $a < 1$  (K):

$$\bar{B}^K = \frac{2}{3} \begin{bmatrix} E_{1111} \underline{A}(h_2^3, h_1^3, u) & E_{1122} \underline{A}(h_2^3, h_1^3, u) & 0 \\ & E_{2222} \left( (1-v^2) \bar{A}(h_2^3, h_1^3, u) + v^2 \underline{A}(h_2^3, h_1^3, u) \right) & 0 \\ \text{sym} & & E_{1212} \bar{A}(h_2^3, h_1^3, u) \end{bmatrix}$$

Kirchhoff model for  $a > 1$  (K'):

$$\bar{B}^{K'} = \frac{2}{3} \begin{bmatrix} E_{1111} h_1^3 & E_{1122} h_1^3 & 0 \\ & E_{2222} \left( (1-v^2) \bar{A}(h_2^3, h_1^3, u) + v^2 h_1^3 \right) & 0 \\ \text{sym} & & E_{1212} h_1^3 \end{bmatrix}$$

Laminated model with rank-1 material (L):

$$\bar{B}^L = \frac{2}{3} \begin{bmatrix} E_{1111} h_2^3 & E_{1122} h_1^3 & 0 \\ & E_{2222} \left( u(1-v^2) h_2^3 + (1-u(1-v^2)) h_1^3 \right) & 0 \\ \text{sym} & & E_{1212} h_1^3 \end{bmatrix}$$

are fixed. This is the way these formulas are used in layout and shape optimization of plates (Suzuki and Kikuchi (1991b)).

Figure 2.11 shows results for  $\bar{B}_2(2,2)$ , and  $\bar{B}_2(1,2)$ . As expected stiffness in the rib direction (measured by  $\bar{B}_2(2,2)$ , Figure 2.11 (a)) increases with the addition of material for all models. Differences between models are not very significant. Figure 2.11 (b) illustrates the interesting observation that in models K' (Kirchhoff with  $a>1$ ) and L (laminated)  $\bar{B}_2(1,2)$  is *below* the lower bound LB and does not change with the rib width  $u$ . From Table 2.1 we may conclude that the same may be said about other terms involving stiffness in the direction perpendicular to the ribs,  $\bar{B}_2(1,1)$  and  $\bar{B}_2(3,3)$ . This can be explained by the fact that  $a>1$  in the Kohn-Vogelius model implies that ribs are modeled as beam elements with no transverse *bending* stiffness.

All models predict a monotonic increase in bending stiffness along the rib direction as rib width  $u$  increases. This is an important property used in optimization algorithms based on optimality criteria methods.

**Effect of Rib Height** This experiment measures the change in stiffness when ribs are added to a core plate of constant thickness  $2h_1$ . The height of the ribs is increased but the amount of material used to build the ribs is kept constant, i.e., taller ribs are thinner. A low amount of material, equivalent to 20% of the core material, was available to build the ribs.

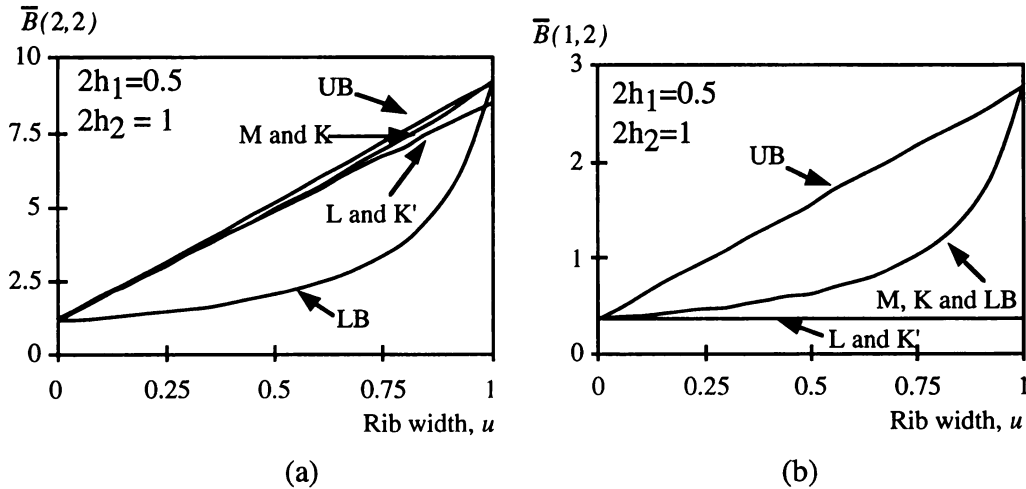


Figure 2.11. Effect of rib width on material properties



Figure 2.12 shows results for  $\bar{B}_2(2,2)$  and  $\bar{B}_2(1,1)$ . As expected, all models predict a stiffening of the plate in the rib direction (as measured by  $\bar{B}_2(2,2)$ , Figure 2.12 (a)) as rib height increases. But increasing rib height may have the opposite effect on the stiffness in the direction perpendicular to the ribs, direction 1. Figure 2.12 (b) shows that in models M (Mindlin) and K (Kirchhoff,  $a < 1$ ) as the rib height increases, the stiffness  $\bar{B}_2(1,1)$  decreases, approaching the value of  $\bar{B}_2^{\text{core}}(1,1)$  for very tall and thin ribs. This is not the case in models L (laminated) and K' (Kirchhoff for  $a > 1$ ), where  $\bar{B}_2(1,1)$  is *equal* to the core stiffness for any rib height, as shown in Table 2.1. In these models the addition of ribs does not have any effect on the stiffness of the plate along directions perpendicular to the rib. This qualitative difference will be of importance later, when results are presented that display the effect of changing the rib width on a plate built with only one family of ribs.

The addition of ribs to a core of uniform thickness always stiffens the plate. Increasing rib height while keeping a constant volume of rib material has a stiffening effect on values in  $\bar{B}$  defined as upper bounds (typically,  $\bar{B}_2(2,2)$  in all models) and a weakening effect on entries defined as lower bounds (typically,  $\bar{B}_2(1,1)$  in all models).

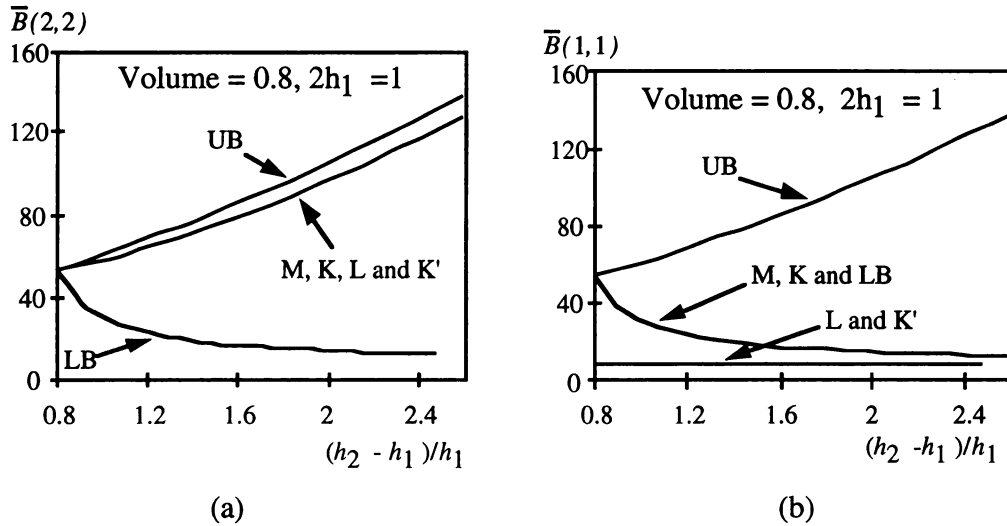


Figure 2.12. Effect of rib height on material properties.

### 2.2.2 Comparison Based on the Mean Compliance of a Simply Supported Plate

Here we use a simple plate structure to highlight the differences between the models discussed in the previous section. The global stiffness of the plate is measured through the computation of the mean compliance defined as

$$C = \int_{\Omega_0} f^t d \, d\Omega \quad (2.2.7)$$

where  $f$  is the vector of applied loads and  $d$  the vector of generalized displacements. This is a measure that is commonly used in layout and shape optimization problems. In what follows  $C$  is normalized using the compliance of the plate without ribs analyzed using Kirchhoff's model  $K$  ( $\alpha < 1$ ).

Consider a square plate simply supported on all sides subjected to a uniformly distributed transverse load. The analysis of this plate is performed using a finite element discretization and 4-noded quadrilateral elements. A single material is used in all elements but the orientation of ribs may vary from element to element. The orientation of ribs within each element,  $\Theta$ , is set to match the angle that minimizes the mean compliance of a transversely orthotropic plate subjected to a uniform transverse load (Pedersen, (1989)). Notice, however, that *all* plate stiffness components play a role in the computation of the mean compliance, even when the orientation of the ribs is chosen to take full advantage of the stiffest material direction.

Homogenized properties derived from plane elasticity equations do not provide for a mechanism to compute the transverse shear terms  $\bar{S}$ . A typical approach followed in practice is to view the transverse shear term ( $S$  in (2.1)) as a penalty contribution in the strain energy that enforces Kirchhoff's assumptions ( $\gamma = 0$ ), that is,

$$\bar{S} = \frac{1}{\varepsilon} \begin{bmatrix} 1 & 0 \\ 0 & 1 \end{bmatrix} \quad 0 < \varepsilon \ll 1 \quad (2.2.8)$$

This view is adopted here in the analysis of the plate using the L (laminated) model. For comparison, results are also shown of the analysis associated with model M (Mindlin), modified to enforce the same condition. These results are identified as model M' in Figures 2.13 and 2.14. All computations of Kirchhoff plates were done using the finite element model for the Mindlin equations along with condition (2.2.8). This procedure

produces good results for the simple case studied in here. Comparisons with analytical solutions for uniform thickness Kirchhoff plates validate this procedure.

### Effect of Rib Width

Here we study variations in the mean compliance of a ribbed plate when the width of the ribs is varied without changing the core or rib thicknesses.

For thin plates, Figures 2.13 (a) and 2.13 (b) show that plates whose effective properties are computed using model M are consistently stiffer than plates analyzed using the laminated model L. If the total amount of available material is fixed, model M may predict that it is possible to achieve a prescribed stiffness using a plate with thinner ribs ( $u$  near 0). However, to achieve a similar stiffness using model L it may be necessary to rely on plates of nearly uniform but higher width ( $u$  near 1). This suggests that in an optimization problem where compliance is the cost function model M is more likely to produce results that call for the use of ribs. Figures 2.13 (a) and 2.13 (b) indicate that the difference will be more pronounced in plates with shorter ribs ( $(h_2-h_1)/h_1 = 0.25$ ). Examples in Chapter 4 will show this phenomenon.

Differences between thick and thin plates depend on the contribution of the transverse shear stiffness  $\bar{S}$ , present only in model M. As expected, Figures 2.13 (c) and 2.13 (d) show qualitative changes only in model M and then only when shorter ribs are used (Figure 2.13 (c)). In that case the effect of the choice of model on the stiffest solution is unclear. Then it is more likely that differences between optima associated with models M and L arise because of other factors, such as the effect of the transverse shear contribution to the objective function on the optimum orientation angle  $\Theta$ .

### Effect of Rib Height

Here we study variations in mean compliance when a fixed amount of material is used to add ribs of varying heights ( $h_2$ ) to a plate of uniform thickness  $2h_1$ .

Figure 2.14 shows the results for a thin and a thick plates and different amounts of rib material. It is observed that although the ribs increase the stiffness of a plate of uniform thickness, taller ribs are not always associated with lower mean compliance. This occurs here because in some models (e.g. M and K), increasing rib height may actually *decrease* stiffness in the direction transverse to the ribs. The non monotonic behavior of the compliance as a function of rib height is more pronounced in the Mindlin model



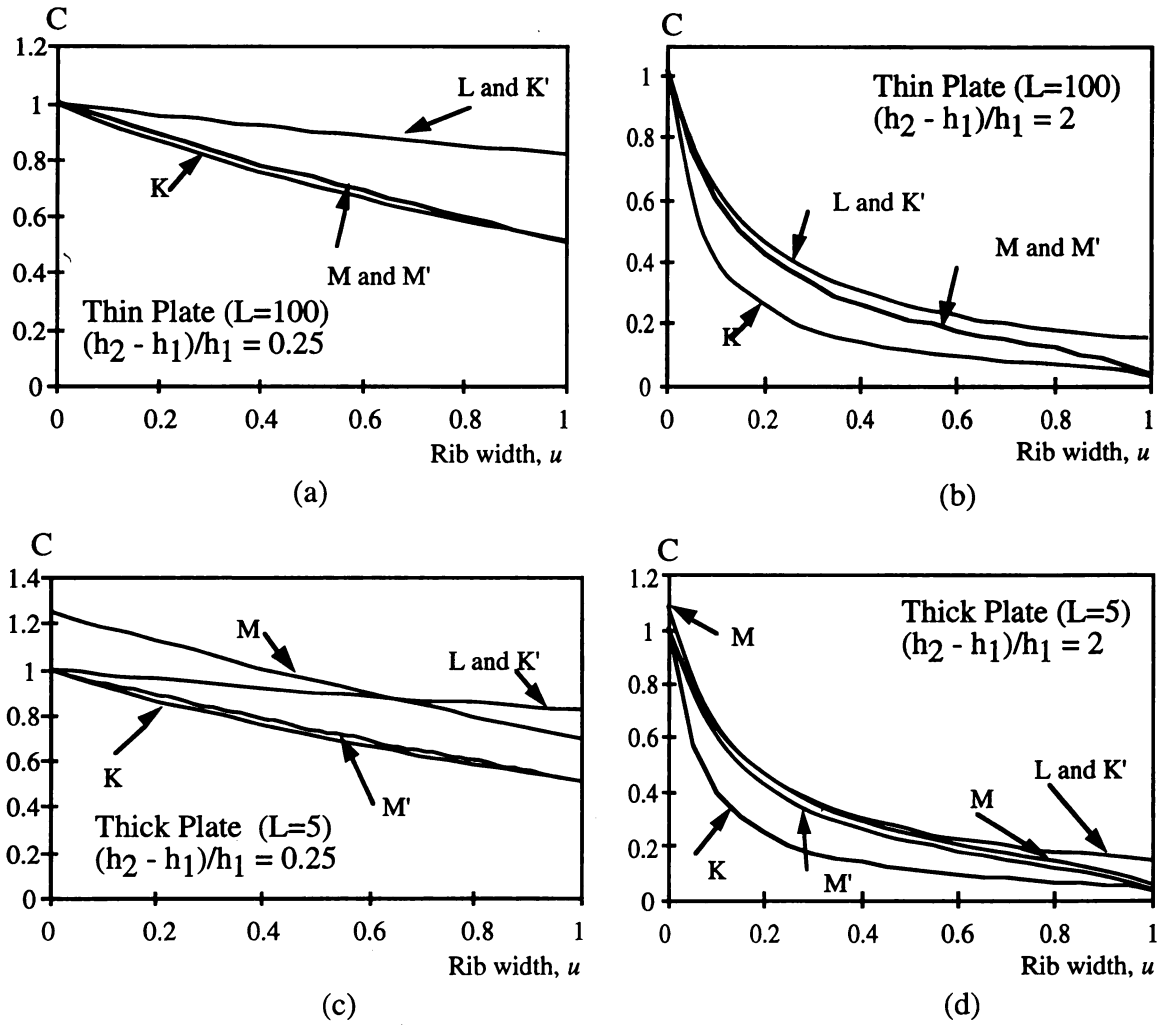


Figure 2.13. Effect of rib width on mean compliance.

because *all* transverse stiffness terms in that model *decrease* with rib height. Model K (Kirchhoff with  $a < 1$ ) presents a similar behavior, less pronounced because the twisting stiffness  $\bar{B}(3,3)$  in model K *increases* with rib height. In contrast, the compliances of plates modeled using models K' (Kirchhoff with  $a > 1$ ) and L (laminated) varies monotonically with rib height, since twisting stiffness terms in these models are independent  $h_1$ .

The presence of “weak” (lower bound) entries in the twisting stiffness entries in  $\bar{B}$  makes it possible that increasing the height of short ribs within a constant amount of material result in more compliant plates. However, there appears to exist a rib height beyond which this behavior is reversed and the addition higher and thinner ribs does result in stiffer plates.

Regarding the differences between Mindlin and Kirchhoff model K ( $a > 1$ ), it is interesting to note that these differences are not limited to the effect of transverse shear deformations. When transverse shear contributions are neglected (as in model M'), differences in the mean compliance associated with these models can only be explained by differences in the *twisting* stiffness term  $\bar{B}(3,3)$ , as it is easily appreciated comparing  $\bar{B}^M$  and  $\bar{B}^K$  in Table 2.1. Figures 2.13 and 2.14 suggest that the effect of this term, far from being negligible, may be comparable to the effect of differences in the treatment of transverse shear deformations.

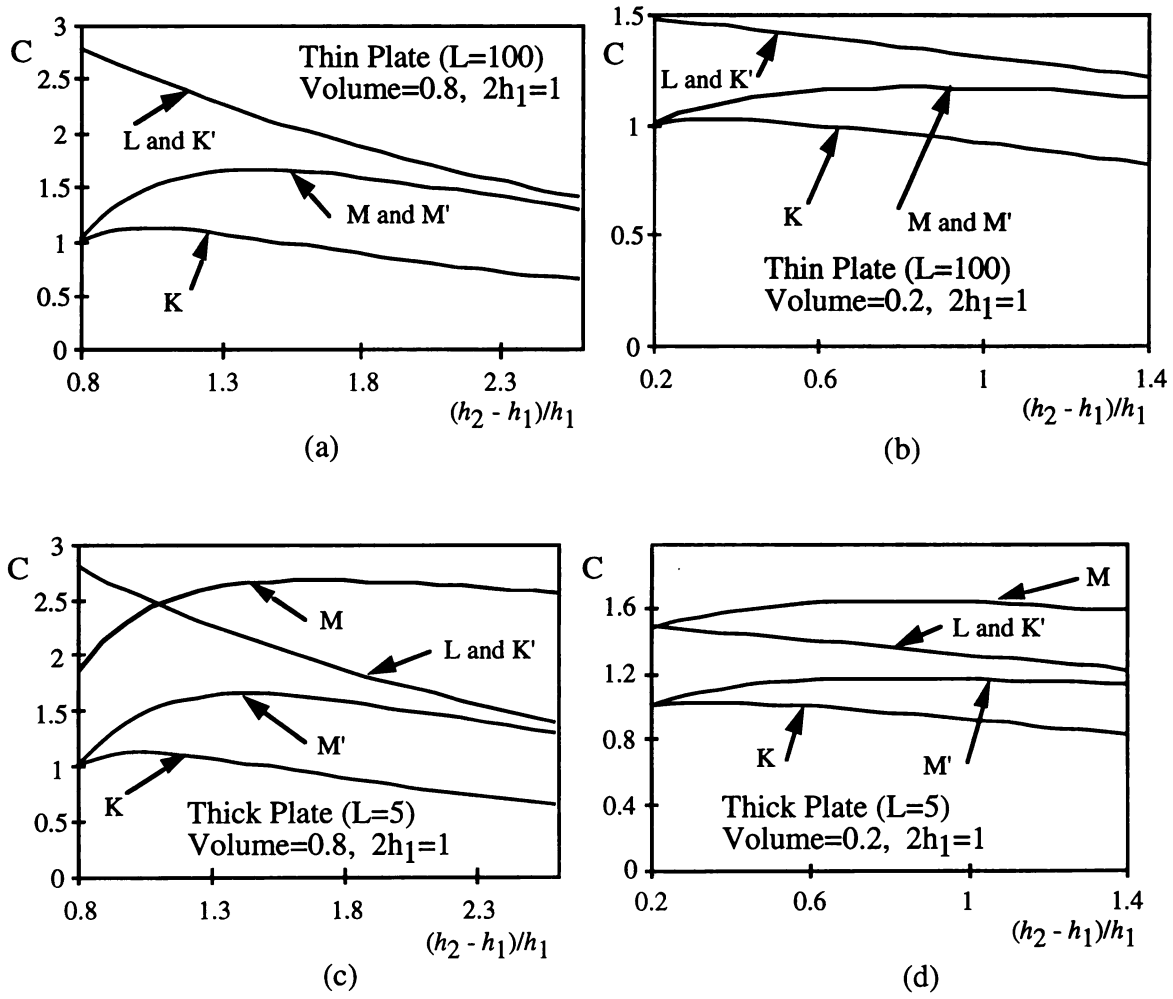


Figure 2.14. Effect of rib height on mean compliance.

### CHAPTER 3

## HOMOGENIZED PROPERTIES OF RANK- $L$ MINDLIN PLATES - MOMENT REPRESENTATION

In this chapter formulas for stiffness properties of Mindlin plates made of layering materials of rank  $L$  ( $L \in \mathbb{N}^+$ ) are developed (see Figure 3.1). The approach is different from the one used in Chapter 2, and it is justified by the following observations:

- These new formulas describe plates with  $L$  different layers of ribs oriented in any direction and having arbitrary widths. This is a more general model than the one presented in Chapter 2.
- This formulation uses only four variables to describe the full anisotropy of the plates. Even though there are  $L$  layers -- each one with a different width and orientation -- it is possible to condense all the information in just four variables once the amount of material is prescribed.
- It will be seen later in this chapter that the stiffest micro structure for plate problems is made of at most three layers, which is a special case of the rank- $L$  material plates.

The derivation will be presented for the bending and transverse shear deformation only. Membrane effective properties were derived by Avellaneda and Milton (1989) and will be presented here in their final form.

#### Notation Convention

The following notation convention is adopted in this chapter: indices repeated twice imply summation; Latin indices take values 1 and 2, while Greek indices take values 1, 2 and 3. When index notation is used the convention is as follows: let  $a$  and  $b$  be vectors,  $C$  and  $D$  be second order tensors (matrices), and  $E$  and  $F$  be fourth order tensors. Then,

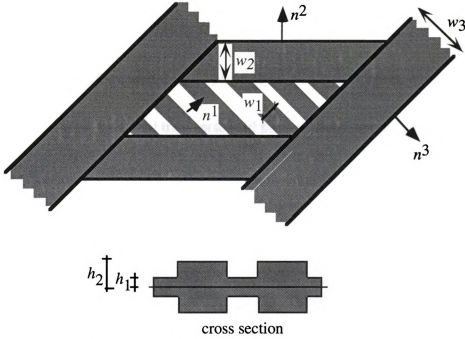


Figure 3.1. Rank-L layer plate ( $L=3$  in this picture).

$$a \cdot b = a_i b_i \quad (a \text{ scalar})$$

$$C : D = C_{ij} D_{ij} \quad (a \text{ scalar})$$

$$E :: F = E_{ijkl} F_{ijkl} \quad (a \text{ scalar})$$

$$Da = D_{ij} a_j \quad (a \text{ vector})$$

$$a \otimes b = a_i b_j \quad (a \text{ matrix})$$

$$BD = B_{ijkl} D_{kl} \quad (a \text{ matrix})$$

$$a \otimes a \otimes a \otimes a = a_i a_j a_k a_l \quad (a \text{ fourth order tensor})$$

### 3.1 Effective Properties for Rank-L Material Plates

Two plates of thickness  $2h_1$  and  $2h_2$  ( $h_2 > h_1$ ) (see Figure 3.1) are mixed in a small scale to build a plate of rapidly varying thickness. There are ribs in  $L$  different directions and of arbitrary widths arranged in  $L$  different scales in a layering arrangement as shown in Figure 2.5. The goal is to obtain an expression for the effective properties of this plate.

#### 3.1.1 Set up of the Mindlin Plate Equations

As before, the plate occupies a domain

$$\Omega = \{x \in \mathbb{R}^3 : (x_1, x_2) \in \Omega_0 \subset \mathbb{R}^2, -h_2 \leq x_3 \leq h_2\} \quad (3.1.1)$$

where  $\Omega_0$  is identified with the mid plane about which the plate is symmetric.

The plate is loaded by a total transverse load per unit area  $f$  applied over  $\Omega_0$ , a transverse shear force  $q$  applied over the boundary  $\Gamma^q \subseteq \partial\Omega_0$ , and moments  $M = \{M_1, M_2\}$  applied over the boundary  $\Gamma^M \subseteq \partial\Omega_0$ . The notation is simplified replacing rotations  $(\theta_x, \theta_y)$  by  $(\theta_2, -\theta_1)$ , and the transversal displacement  $v_z$  by  $w$ . As before, the transverse shear strain vector,  $\gamma = \{\gamma_1, \gamma_2\}$ , is defined as

$$\gamma_i = \frac{\partial w}{\partial x_i} - \theta_i, \quad i=1,2 \quad (3.1.2)$$

Equilibrium of the Mindlin plate is satisfied by a solution  $u = (\theta_1, \theta_2, w) \in V^\ell$  such that

$$\int_{\Omega_0} (\mathbf{B} \tilde{\nabla} \theta : \tilde{\nabla} \hat{\theta} + S \gamma \cdot \hat{\gamma}) d\Omega = \int_{\Omega_0} \hat{w} f d\Omega + \int_{\Gamma^q} \hat{w} q d\Gamma - \int_{\Gamma^M} \hat{\theta} \cdot M d\Gamma, \quad (3.1.3)$$

for arbitrary functions  $\hat{u} = (\hat{\theta}_1, \hat{\theta}_2, \hat{w})$  in the space of kinematically admissible solutions,

$$V^\ell = \{u = (\theta_1, \theta_2, w) \in H^1(\Omega_0)^3 : (\theta_1, \theta_2) = 0 \text{ on } \Gamma^M, w = 0 \text{ on } \Gamma^q\} \quad (3.1.4)$$

The operator  $\tilde{\nabla}$  is defined as  $\tilde{\nabla}_i \theta_j \equiv \frac{1}{2}(\nabla_i \theta_j + \nabla_j \theta_i)$ . The tensors  $\mathbf{B}(x_1, x_2)$  and  $\mathbf{S}(x_1, x_2)$  are, respectively, the bending and shear rigidity tensors obtained after integration through the thickness of the material properties at location  $(x_1, x_2) \in \Omega_0$ . Let  $\mathbf{B}^k$  and  $\mathbf{S}^k$  be the rigidity tensors corresponding to the cross section  $k$ ,  $k=1,2$ . These tensors have the symmetries

$$\mathbf{B}^k_{mnpq} = \mathbf{B}^k_{pqmn} \quad \text{and} \quad \mathbf{B}^k_{mnpq} = \mathbf{B}^k_{qpmn} = \mathbf{B}^k_{mnqp} \quad (3.1.5a)$$

and

$$\mathbf{S}^k_{mn} = \mathbf{S}^k_{nm} \quad (3.1.5b)$$



It is assumed that properties  $B^2$ , and  $S^2$  correspond to a cross section of thickness  $2h_2$  built using an isotropic material, i.e., for a material with Young's modulus  $E$  and Poisson's ration  $\nu$ ,  $B^2$  and  $S^2$  are of the form

$$B_{1111}^2 = B_{2222}^2 = B_0 \quad B_{1122}^2 = \nu B_0 \quad B_{1212}^2 = \frac{(1-\nu)}{2} B_0, \quad (3.1.6a)$$

$$S_{11}^2 = S_{22}^2 = S_0 \quad S_{12}^2 = 0, \quad (3.1.6b)$$

where

$$B_0 \equiv \frac{2}{3} \frac{E h_2^3}{(1-\nu^2)} \quad S_0 \equiv \frac{E h_2}{1+\nu}. \quad (3.1.7)$$

$B^2$  is the “strong” cross section. In layout optimization  $B^2$  corresponds to the section of the plate reinforced with stiffeners.  $B^1$  is the “weak” or unreinforced cross section, and it is assumed that  $B^1 < B^2$ . No special orthotropy on  $B^1$  is assumed.

### 3.1.2 Computation of Homogenized Stiffness Properties

As in the previous chapter, stiffness properties  $B$  and  $S$  depend on  $x$  and  $y=x/\epsilon$ , and are  $Y$ -periodic, i.e.,  $B = B^\epsilon(x, y=x/\epsilon)$ ,  $S = S^\epsilon(x, y=x/\epsilon)$ ,  $B^\epsilon(x, y) = B^\epsilon(x, y+Y)$ ,  $S^\epsilon(x, y) = S^\epsilon(x, y+Y)$ .

Accordingly, the rotations  $\theta_i$  and displacement  $w$  also depend on the small scale parameter  $y$ , therefore,  $\theta = \theta^\epsilon(x, y=x/\epsilon)$  and  $w = w^\epsilon(x, y=x/\epsilon)$  and the weak equilibrium equations (3.1.3) is

$$\int_{\Omega_0} \int_Y \{ B^\epsilon(x, y) \tilde{\nabla} \theta^\epsilon(x, y) : \tilde{\nabla} \hat{\theta} + S^\epsilon(x, y) \gamma^\epsilon(x, y) \cdot \hat{\gamma} \} dY d\Omega = \int_{\Omega_0} \hat{w} f d\Omega + \int_{\Gamma^q} \hat{w} q d\Gamma - \int_{\Gamma^M} \hat{\theta} \cdot M d\Gamma \quad (3.1.8)$$

In (3.1.8) it was assumed that the external loads are independent of  $y$  and have made use of the simplified notation



$$\frac{1}{\|Y\|} \int_Y [\bullet] dY \equiv \int_Y [\bullet] d\bar{Y}. \quad (3.1.9)$$

We seek average tensors  $\bar{\mathbf{B}}$  and  $\bar{\mathbf{S}}$  that represent the limiting behavior of tensors  $\mathbf{B}^\varepsilon$  and  $\mathbf{S}^\varepsilon$ , respectively, as  $\varepsilon \rightarrow 0$ . That is, let  $u^\varepsilon$  be the solution of (3.1.8) with  $\mathbf{B}^\varepsilon$  and  $\mathbf{S}^\varepsilon$ . We seek effective properties  $\bar{\mathbf{B}}$  and  $\bar{\mathbf{S}}$  such that, if  $u^\varepsilon \rightarrow \bar{u}$  as  $\varepsilon \rightarrow 0$ , then  $\bar{u}$  is the solution of (3.1.8) with  $(\mathbf{B}^\varepsilon, \mathbf{S}^\varepsilon)$  replaced by  $(\bar{\mathbf{B}}, \bar{\mathbf{S}})$ . The computation of  $\bar{\mathbf{B}}$  and  $\bar{\mathbf{S}}$  is again carried out using the asymptotic expansion in (2.1.5a). Only the first two terms of the expansion will be considered; this yields, in terms of the displacement vector,

$$u^\varepsilon(x, y) = \{\theta_1^\varepsilon, \theta_2^\varepsilon, w^\varepsilon\} = \{\theta_1^0(x), \theta_2^0(x), w^0(x)\} + \varepsilon \{\theta_1^1(x, y), \theta_2^1(x, y), w^1(x, y)\} \quad (3.1.10)$$

The equilibrium statement for the small scale domain is:

For a fixed point  $x \in \Omega_0$ ,

$$\int_Y \mathbf{B}(\bar{\kappa} + \kappa^*) : \tilde{\nabla}_y \hat{\theta} dY = 0, \quad \text{for all } Y\text{-periodic } \hat{\theta}(y) \in H^1(Y)^2 \quad (3.1.11a)$$

and

$$\int_Y \mathbf{S}(\bar{\gamma} + \gamma^*) \cdot \nabla_y \hat{w} dY = 0, \quad \text{for all } Y\text{-periodic } \hat{w}(y) \in H^1(Y), \quad (3.1.11b)$$

where the following notation was introduced,

$$\begin{aligned} \bar{\kappa}(x) &\equiv \tilde{\nabla}_x \theta^0(x) && \text{the mean value of the bending strain;} \\ \bar{\gamma}(x) &\equiv \nabla_x w^0(x) - \theta^0(x) && \text{the mean value of the shear strain;} \\ \kappa^*(x, y) &\equiv \tilde{\nabla}_y \theta^1(x, y) && \text{the fluctuating part of the bending strain, and} \\ \gamma^*(x, y) &\equiv \nabla_y w^1(x, y) - \theta^1(x, y) && \text{the fluctuating part of the shear strain.} \end{aligned} \quad (3.1.12)$$

Subscripts  $x$  and  $y$  in (3.1.12) indicate that the partial derivatives are with respect to the  $x$  and  $y$  coordinates, respectively.

The equilibrium equation for the large scale domain is

$$\begin{aligned} \int_{\Omega^o} \left\{ \frac{1}{\|Y\|} \int_Y \mathbf{B}(\bar{\kappa} + \kappa^*) dY \right\} : \hat{\kappa} d\Omega + \int_{\Omega^o} \left\{ \frac{1}{\|Y\|} \int_Y \mathbf{S}(\bar{\gamma} + \gamma^*) dY \right\} \cdot \hat{\gamma} d\Omega = \\ \int_{\Omega_0} w f d\Omega + \int_{\Gamma^q} w q d\Gamma - \int_{\Gamma^M} \theta \cdot M d\Gamma \quad \forall \hat{u} \in V^\ell \end{aligned} \quad (3.1.13a)$$

where  $\hat{\kappa}$  and  $\hat{\gamma}$  are defined as follows,

$$\hat{\kappa}(x) = \tilde{\nabla}_x \hat{\theta}, \quad \hat{\gamma}(x) = \nabla_x \hat{w} - \hat{\theta}. \quad (3.1.13b)$$

Equation (3.1.13) is the equilibrium equation of a plate with effective stiffness properties  $\bar{\mathbf{B}}(x)$  and  $\bar{\mathbf{S}}(x)$  defined as

$$\bar{\mathbf{B}} \bar{\kappa} = \frac{1}{\|Y\|} \int_Y \mathbf{B}(\bar{\kappa} + \kappa^*) dY \quad (3.1.14a)$$

$$\bar{\mathbf{S}} \bar{\gamma} = \frac{1}{\|Y\|} \int_Y \mathbf{S}(\bar{\gamma} + \gamma^*) dY. \quad (3.1.14b)$$

The geometric configuration of the basic cell  $Y$  is now prescribed in order to solve (3.1.11).

#### Rank-1 material plate

In this section homogenized stiffness properties of a plate with ribs orthogonal to a generic unit vector  $n$  are derived. The plate is built by repetition of the basic cell shown in Figure 3.2 and defined as

$$\begin{aligned} Y &= Y_1 \cup Y_2, \\ Y_1 &= \{(y_1, y_2, y_3) : (y_1, y_2) \in [\rho, 1] \times \mathfrak{R}, y_3 \in [-h_1, h_1], \rho \in [0, 1]\} \\ Y_2 &= \{(y_1, y_2, y_3) : (y_1, y_2) \in [0, \rho] \times \mathfrak{R}, y_3 \in [-h_2, h_2], \rho \in [0, 1]\}. \end{aligned} \quad (3.1.15)$$

It is assumed that stiffness properties, bending strains and transverse shear deformations are constant in the sub domains  $Y_1$  and  $Y_2$ , i.e.,

$$\mathbf{B} = \chi_1 \mathbf{B}^1 + \chi_2 \mathbf{B}^2$$

$$\begin{aligned}
S &= \chi_1 S^1 + \chi_2 S^2 \\
\bar{\kappa} + \kappa^* &= \chi_1 \kappa^1 + \chi_2 \kappa^2 \\
\bar{\gamma} + \gamma^* &= \chi_1 \gamma^1 + \chi_2 \gamma^2
\end{aligned} \tag{3.1.16}$$

where  $\chi_i$  are defined as  $\chi_i(Y_j) = \delta_{ij}$ , i.e.,

$$\chi_i = \begin{cases} 1 & \text{on the set occupied by plate with thickness } 2h_i \\ 0 & \text{elsewhere} \end{cases} \tag{3.1.17}$$

Under these assumptions and using (3.1.14) it is possible to write

$$\bar{B} \bar{\kappa} = (1 - \rho) B^1 \kappa^1 + \rho B^2 \kappa^2 \tag{3.1.18a}$$

$$\bar{S} \bar{\gamma} = (1 - \rho) S^1 \gamma^1 + \rho S^2 \gamma^2 \tag{3.1.18b}$$

and

$$\bar{\kappa} = (1 - \rho) \kappa^1 + \rho \kappa^2 \tag{3.1.19a}$$

$$\bar{\gamma} = (1 - \rho) \gamma^1 + \rho \gamma^2 \tag{3.1.19b}$$

where the superscripts '1' and '2' refer to the plate of thickness  $2h_1$  and  $2h_2$ , respectively, and  $\rho$  is the area fraction of the thicker plate. The goal here is to solve for  $\bar{B}$  and  $\bar{S}$  in terms of the constituents  $B^1, B^2, S^1, S^2$  and the cell geometry.

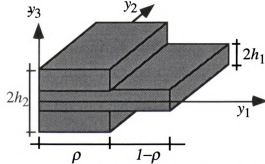


Figure 3.2. Basic cell for a rank-1 material plate.

Additional equations are required to solve for  $\bar{B}$  and  $\bar{S}$ . They are derived from the continuity conditions at the interface of the two sub-domains. From static equilibrium on the interface  $\Gamma^{1,2}$  between  $Y_1$  and  $Y_2$ , continuity of stresses is required. This can be written in term of bending moments and shear forces as follows

$$\left. \begin{aligned} (\mathbf{B}^2 \boldsymbol{\kappa}^2 - \mathbf{B}^1 \boldsymbol{\kappa}^1) \mathbf{n} &= 0 \\ (\mathbf{S}^2 \boldsymbol{\gamma}^2 - \mathbf{S}^1 \boldsymbol{\gamma}^1) \cdot \mathbf{n} &= 0 \end{aligned} \right\} \text{ on } \Gamma^{1,2} \quad (3.1.20a)$$

For convenience, condition (3.1.20a)<sub>1</sub> is expressed in the normal and tangential directions along the interface  $\Gamma^{1,2}$ , i.e.,

$$(\mathbf{B}^1 \boldsymbol{\kappa}^1 - \mathbf{B}^2 \boldsymbol{\kappa}^2) \mathbf{n} \cdot \mathbf{n} = 0 \quad (3.1.20b)$$

$$(\mathbf{B}^1 \boldsymbol{\kappa}^1 - \mathbf{B}^2 \boldsymbol{\kappa}^2) \mathbf{n} \cdot \mathbf{t} = 0 \quad (3.1.20c)$$

where  $\mathbf{t}$  is a unit vector tangent to the boundary  $\Gamma^{1,2}$ . Additionally, there are continuity conditions on the displacements. The solution  $\mathbf{u}$  of the equilibrium equations in the small scale domain  $Y$  is required to be  $Y$ -periodic and

$$\mathbf{u} = \{\theta_1, \theta_2, w\} \in \left(H^1(Y)\right)^3. \quad (3.1.21)$$

This continuity is achieved if we assume  $\theta_1$ ,  $\theta_2$  and  $w$  are continuous across the interface  $\Gamma^{1,2}$ , i.e.,

$$\mathbf{u} = \{\theta_1, \theta_2, w\} \in \left(C^0(Y)\right)^3. \quad (3.1.22)$$

This means that the displacements in  $Y_I$  and  $Y_2$  have to be the same on the interface  $\Gamma^{1,2}$ . A sufficient condition for a function  $f : Y \rightarrow \mathfrak{R}$  to be continuous on  $\Gamma^{1,2}$  is that the gradients in  $Y_I$  and  $Y_2$  have the same component along  $\Gamma^{1,2}$ , that is,

$$\nabla f|_2 \cdot \mathbf{t} = \nabla f|_1 \cdot \mathbf{t}. \quad (3.1.23)$$

Which in terms of this problem is written as

$$\begin{aligned} \nabla_i \theta_j^1 - \nabla_i \theta_j^2 &= \alpha_1 n_i n_j + \alpha_2 n_i t_j \\ w_{,i}^1 - w_{,i}^2 &= \alpha_3 n \end{aligned} \quad \alpha_1, \alpha_2, \alpha_3 \in \mathfrak{R} \quad (3.1.24)$$

Using the definition of bending strains and transverse shear strains the following kinematic admissibility conditions are obtained from (3.1.24):

$$\kappa^1 - \kappa^2 = \beta_1 n \otimes n + \beta_2 (t \otimes n + n \otimes t) \quad (3.1.25a)$$

$$\gamma^1 - \gamma^2 = \beta_3 n \quad (3.1.25b)$$

for some  $\beta_1, \beta_2, \beta_3 \in \mathfrak{R}$ . Equations (3.1.18), (3.1.19), (3.1.20) and (3.1.25) form a set of equations from which the effective properties  $\bar{\mathbf{B}}$  and  $\bar{\mathbf{S}}$  can be obtained. What follows is the solution of these equations.

### Effective Properties in Bending

Using (3.1.19a) in (3.1.18a),

$$(\mathbf{B}^2 - \bar{\mathbf{B}})\bar{\kappa} = (1 - \rho)(\mathbf{B}^2 - \mathbf{B}^1)\kappa^1 = (1 - \rho)\eta_b, \quad (3.1.26)$$

where  $\eta_b$  is an arbitrary symmetric 2<sup>nd</sup> tensor often called the *polarization* tensor in the literature (Lipton, (1993a)). Solving for  $\kappa^2$  in (3.1.25a),

$$\kappa^2 = \kappa^1 - \beta_1 n \otimes n - \beta_2 (t \otimes n + n \otimes t). \quad (3.1.27)$$

Using this expression in (3.1.20b) leads to,

$$\left[ \mathbf{B}^1 \kappa^1 - \mathbf{B}^2 (\kappa^1 - \beta_1 n \otimes n - \beta_2 (t \otimes n + n \otimes t)) \right] : n \otimes n = 0 \quad (3.1.28)$$

Since  $\mathbf{B}^2$  is isotropic,  $\mathbf{B}^2 :: (t \otimes n \otimes n \otimes n) = \mathbf{B}^2 :: (n \otimes t \otimes n \otimes n) = 0$ . Therefore,

$$\beta_1 = \frac{(\mathbf{B}^2 - \mathbf{B}^1)\kappa^1 : n \otimes n}{B_0} = \frac{\eta_b n \cdot n}{B_0} \quad (3.1.29)$$

with  $B_0 = \mathbf{B}^2 :: (n \otimes n \otimes n \otimes n) = \mathbf{B}^2_{1111} = \frac{2}{3} \frac{E}{1 - \nu^2} h_2^3$ .

Using (3.1.20c) and (3.1.27),  $\beta_2$  is obtained as,

$$\beta_2 = \frac{(\mathbf{B}^2 - \mathbf{B}^1)\kappa^1 : n \otimes t}{\mathbf{B}^2 :: (t \otimes n \otimes n \otimes t + n \otimes t \otimes n \otimes t)} = \frac{\eta_b n \cdot t}{(1 - \nu)B_0}. \quad (3.1.30)$$



Substituting the expressions of  $\beta_1$  and  $\beta_2$  back in (3.1.27) gives,

$$\kappa^2 = \kappa^1 - \frac{1}{B_0} \left[ n \otimes n \otimes n \otimes n + \frac{1}{(1-\nu)} (t \otimes n \otimes n \otimes t + n \otimes t \otimes n \otimes t) \right] \eta_b. \quad (3.1.31)$$

which we re-write as

$$\kappa^2 = \kappa^1 - \frac{1}{B_0} \left[ n \otimes n \otimes n \otimes n + \frac{1}{2(1-\nu)} (n \otimes t \otimes n \otimes t + t \otimes n \otimes n \otimes t + n \otimes t \otimes t \otimes n + t \otimes n \otimes t \otimes n) \right] \eta_b. \quad (3.1.32)$$

where the following identity was used

$$\eta_b(n \otimes t \otimes n \otimes t + t \otimes n \otimes n \otimes t) = \eta_b(n \otimes t \otimes t \otimes n + t \otimes n \otimes t \otimes n), \quad (3.1.33)$$

With equation (3.1.32), and using (3.1.26) to express  $\bar{\kappa}$  and  $\kappa^1$  in terms of  $\eta_b$ , the following version of (3.1.19a) can be written,

$$(1-\rho)(B^2 - \bar{B})^{-1} \eta_b = (B^2 - B^1)^{-1} \eta_b - \frac{\rho}{B_0} \mathbf{A}_b \eta_b, \quad (3.1.34)$$

where

$$\mathbf{A}_b = n \otimes n \otimes n \otimes n + \frac{1}{2(1-\nu)} (t \otimes n \otimes t \otimes n + n \otimes t \otimes n \otimes t + n \otimes t \otimes t \otimes n + t \otimes n \otimes n \otimes t). \quad (3.1.35)$$

and  $\mathbf{A}_b$  has all the major symmetries. Since  $\eta_b$  is arbitrary (3.1.34) leads to the final result when it is dropped

$$\bar{B} = B^2 - (1-\rho) \left[ (B^2 - B^1)^{-1} - \frac{\rho}{B_0} \mathbf{A}_b \right]^{-1}. \quad (3.1.36a)$$

This is the final expression for the effective properties in bending. The fourth order tensor

$\mathbf{A}_b$  can be written in a convenient way in terms of the normal vector  $n$ , and the Kronecker delta  $\delta_{ij}$  as

$$\mathbf{A}_{bijkl} = \frac{1}{2(1-\nu)}(n_i n_k \delta_{jl} + n_i n_l \delta_{jk} + n_j n_k \delta_{il} + n_l n_j \delta_{ik} - 2(1+\nu) n_i n_j n_k n_l) \quad (3.1.36b)$$

### Effective Properties in Transverse Shear

The effective shear stiffness is computed following a similar procedure. Using (3.1.19b) in (3.1.18b), gives

$$(\mathbf{S}^2 - \bar{\mathbf{S}})\bar{\gamma} = (1-\rho)(\mathbf{S}^2 - \mathbf{S}^1)\gamma^1 = (1-\rho)\eta_s \quad (3.1.37)$$

where  $\eta_s$  is an arbitrary polarization vector. Solving for  $\gamma^2$  in (3.1.25b),

$$\gamma^2 = \gamma^1 - \beta_3 n, \quad (3.1.38)$$

which can be used in (3.1.20a)<sub>2</sub> to get

$$[\mathbf{S}^1 \gamma^1 - \mathbf{S}^2 (\gamma^1 - \beta_3 n)] \cdot n = 0. \quad (3.1.39)$$

From this equation  $\beta_3$  is solved to obtain

$$\beta_3 = \frac{(\mathbf{S}^2 - \mathbf{S}^1)\gamma^1 \cdot n}{S_0} = \frac{\eta_s \cdot n}{S_0} \quad (3.1.40)$$

where

$$S_0 = \mathbf{S}^2 n \cdot n = \mathbf{S}_{11}^2 = h_2 \frac{E}{1+\nu}. \quad (3.1.41)$$

Using this expression of  $\beta_3$  back in (3.1.38), gives

$$\gamma^2 = \gamma^1 - \frac{1}{S_0} n \otimes n \eta_s \quad (3.1.42)$$



With (3.1.42), and using (3.1.37) to express  $\bar{\gamma}$  and  $\gamma^1$  in terms of  $\eta_s$ , (3.1.19b) can be written as

$$(1 - \rho)(S^2 - \bar{S})^{-1}\eta_s = (S^2 - S^1)^{-1}\eta_s - \rho \frac{n \otimes n}{S_0} \eta_s. \quad (3.1.43)$$

Since the vector  $\eta_s$  is arbitrary, it is possible to obtain the effective transverse shear stiffness from (3.1.43):

$$\bar{S} = S^2 - (1 - \rho) \left[ (S^2 - S^1)^{-1} - \frac{\rho}{S_0} \mathbf{A}_s \right]^{-1}, \quad (3.1.44a)$$

where

$$\mathbf{A}_s = n \otimes n. \quad (3.1.44b)$$

Next, effective stiffness properties for plates with ribs in more than one direction are derived.

#### Homogenized properties of a rank-L material plate

Plates with more than one layer of ribs are constructed recursively, that is, a rank-(i+1) ribbed plate is built by mixing a plate of rank-(i) and a layer of strong plate in an given direction. This process start with a rank-1 plate and is performed  $L$  times in order to create rank-L plates with  $L$  different scales of ribs as shown in Figure 3.1. The properties of a rank-L laminate can be derived by the recursive use of the formulas for the rank-1 laminate (3.1.36). They are

$$\bar{\mathbf{B}} = \mathbf{B}^2 - (1 - \rho) \left[ (\mathbf{B}^2 - \mathbf{B}^1)^{-1} - \frac{\rho}{B_0} \sum_{\ell=1}^L p_{\ell} \mathbf{A}_b(n^{\ell}) \right]^{-1} \quad (3.1.45a)$$

$$\sum_{\ell=1}^L p_{\ell} = 1, \quad p_{\ell} \geq 0 \quad (3.1.45b)$$

where  $\rho$  now represents the total area fraction of the plate with thickness  $2h_2$ , and  $p_i$  is called 'relative widths' of layer  $i$ . Actual widths of each layer ( $w_i$  in Figure 3.1) can be recovered from  $\rho$  and  $p_i$ 's.

Next, formula (3.1.45) is proved by induction. For  $L=1$ , formula (3.1.45) reduces to (3.1.36). Now assume that formula (3.1.45) is valid for  $L=K-1$ , i.e.,

$$\rho_1^{K-1}(\mathbf{B}^2 - \bar{\mathbf{B}}^{K-1})^{-1} = (\mathbf{B}^2 - \mathbf{B}^1)^{-1} - \frac{\rho_2^{K-1}}{B_0} \sum_{\ell=1}^{K-1} p_\ell^{K-1} \mathbf{A}_b(n^\ell) \quad (3.1.46)$$

where 'K-1' is used as superscript and  $\rho_2^{K-1} \equiv \rho$ ,  $\rho_1^{K-1} \equiv 1 - \rho$ . Consider now the following mixture of two plates: one of properties  $\mathbf{B}^2$  and another of properties  $\bar{\mathbf{B}}^{K-1}$ , corresponding to the effective properties of a rank-(K-1) laminate (3.1.46). Since  $\bar{\mathbf{B}}^{K-1} < \mathbf{B}^2$ , and no other particular assumption on the orthotropy of  $\mathbf{B}^1$  was made to derive (3.1.36), the same procedure and results apply. Taking care to use a different lamination direction, identified by the normal vector  $n^K$ , it holds now

$$\rho_1^K(\mathbf{B}^2 - \bar{\mathbf{B}}^K)^{-1} = (\mathbf{B}^2 - \bar{\mathbf{B}}^{K-1})^{-1} - \frac{\rho_2^K}{B_0} \mathbf{A}_b(n^K). \quad (3.1.47)$$

Using (3.1.46) in (3.1.47),

$$\begin{aligned} \rho_1^{K-1} \rho_1^K (\mathbf{B}^2 - \bar{\mathbf{B}}^K)^{-1} &= (\mathbf{B}^2 - \mathbf{B}^1)^{-1} - \\ &\quad \frac{1}{B_0} [\rho_2^{K-1} \sum_{\ell=1}^{K-1} p_\ell^{K-1} \mathbf{A}_b(n^\ell) + \rho_1^{K-1} \rho_2^K \mathbf{A}_b(n^K)]. \end{aligned} \quad (3.1.48)$$

New area fractions for material 1 and 2 in the rank-K mixture are defined as

$$\rho_1 \equiv \rho_1^{K-1} \rho_1^K \quad \text{and} \quad \rho_2 \equiv \rho_2^{K-1} p_\ell^{K-1} + \rho_1^{K-1} \rho_2^K \quad (3.1.49)$$

yielding

$$\rho_1(\mathbf{B}^2 - \bar{\mathbf{B}}^K)^{-1} = (\mathbf{B}^2 - \mathbf{B}^1)^{-1} - \frac{\rho_2}{B_0} \left[ \sum_{\ell=1}^{K-1} p_\ell \mathbf{A}_b(n^\ell) + p_K \mathbf{A}_b(n^K) \right], \quad (3.1.50a)$$



where

$$p_\ell \equiv \frac{\rho_2^{K-1}}{\rho_2} p_\ell^{K-1}, \quad \ell = 1, \dots, K-1 \quad \text{and} \quad p_K \equiv \frac{\rho_1^{K-1} \rho_2^K}{\rho_2}. \quad (3.1.50b)$$

It is easy to show that (3.1.45b) is satisfied. Using  $\rho \equiv \rho_2$ ,  $\rho_1 = 1 - \rho$ , and changing  $K$  by  $L$ , formula (3.1.45) is obtained. This finishes the proof.

The result for the shear stiffness of a rank- $L$  laminate can be obtained following similar steps,

$$\bar{S} = S^2 - (1 - \rho) \left[ (S^2 - S^1)^{-1} - \frac{\rho}{S_0} \sum_{\ell=1}^L p_\ell \mathbf{A}_s(n^\ell) \right]^{-1}. \quad (3.1.51)$$

As expected, when  $L=2$ ,  $n^1 = \{1, 0\}^t$  and  $n^2 = \{0, 1\}^t$ , formulas (3.1.45) and (3.1.51) gives the same effective properties derived in Chapter 2 setting  $E^- = 0$ .

### Membrane Effective Stiffness

The same procedure outlined here can be followed to obtain the in-plane effective stiffness of plates with  $L$  layers of ribs. This was done in (Avellaneda and Milton, (1989)) and the result is shown here for completeness.

$$\bar{M} = M^2 - (1 - \rho) \left[ (M^2 - M^1)^{-1} - \frac{\rho}{M_0} \sum_{\ell=1}^L p_\ell \mathbf{A}_m(n^\ell) \right]^{-1} \quad (3.1.52a)$$

where

$$\mathbf{A}_{mijkl} = \frac{1}{2(1 - \nu)} (n_i n_k \delta_{jl} + n_i n_l \delta_{jk} + n_j n_k \delta_{il} + n_l n_j \delta_{ik} - 2(1 + \nu) n_i n_j n_k n_l), \quad (3.1.52b)$$

$$M_0 \equiv \frac{2Eh_2}{(1 - \nu^2)}, \quad (3.1.52c)$$

and  $M^k$  are fourth order tensors of stiffness properties of a plate of thickness  $2h_k$  ( $k=1,2$ ), and have the same structure of (3.1.6a) replacing  $B_0$  by  $M_0$ . Table 3.1 summaries the formulas presented in this section.

### Other Effective Stiffness

To finish this Section some comments about other effective properties similar to (3.1.36) are presented. For Kirchhoff plates, the bending stiffness is given by the same expression in (3.1.36) except that the tensor  $A_b$  is defined as (Lipton, (1993a)):

$$A_b = (n \otimes n \otimes n \otimes n) \text{ for Kirchhoff's plates.} \quad (3.1.53)$$

All results presented in this section can be also applied to plates with honeycomb cross sections (see Figure 1.6). The only change is in the properties of the “weak plate”. For example, the bending stiffness tensor for honeycomb plates would be

$$B_{1111}^1 = B_{1111}^1 = B_0^1 \quad B_{1122}^1 = \nu B_0^1 \quad B_{1212}^1 = \frac{(1-\nu)}{2} B_0^1 \quad (3.1.54a)$$

$$B_0^1 \equiv \frac{2}{3} \frac{E(h_2^3 - h_1^3)}{(1-\nu^2)}. \quad (3.1.54b)$$

A similar argument can be used for perforated plates (Figure 2.6). In this case a weak material with  $0 < E^- \ll 1$  is used. As commented before, it is not possible to use  $h_1=0$  since the positive definiteness property of  $B$  is lost, the G-convergence theory would not be applicable, and the homogenization process would fail. Therefore, the problem is “regularized” using a weak material to simulate transverse perforations.

## **3.2 Moment Representation of the Homogenized Properties**

The effective properties derived in the previous section depend on the relative width ( $p_i$ ) and orientation ( $n_i$ ) of each layer  $i$  (i.e., two variables per layer). In this section we introduce a transformation that allows us to express these average properties as a function of at most four independent variables for *any* number of layers. Specifically, new expressions are derived for (3.1.53) and (3.1.54) in terms of  $\Theta$ ,  $m_1$ ,  $m_2$  and  $m_3$ , which are, respectively, the global angle of orientation of the whole micro structure, and three “moments”, describing the internal geometry of the basic cell, i.e., relative widths and

Table 3.1. Effective stiffness for rank-L material plates.

Membrane

$$\bar{\mathbf{M}} = \mathbf{M}^2 - (1 - \rho) \left[ (\mathbf{M}^2 - \mathbf{M}^1)^{-1} - \frac{\rho}{M_0} \sum_{\ell=1}^L p_{\ell} \mathbf{A}_m(n^{\ell}) \right]^{-1}$$

$$\mathbf{A}_{mijkl} = \frac{1}{2(1-\nu)} (n_i n_k \delta_{jl} + n_i n_l \delta_{jk} + n_j n_k \delta_{il} + n_l n_j \delta_{ik} - 2(1+\nu) n_i n_j n_k n_l)$$

Bending

$$\bar{\mathbf{B}} = \mathbf{B}^2 - (1 - \rho) \left[ (\mathbf{B}^2 - \mathbf{B}^1)^{-1} - \frac{\rho}{B_0} \sum_{\ell=1}^L p_{\ell} \mathbf{A}_b(n^{\ell}) \right]^{-1}$$

$$\mathbf{A}_{bijkl} = \frac{1}{2(1-\nu)} (n_i n_k \delta_{jl} + n_i n_l \delta_{jk} + n_j n_k \delta_{il} + n_l n_j \delta_{ik} - 2(1+\nu) n_i n_j n_k n_l)$$

Transverse Shear

$$\bar{\mathbf{S}} = \mathbf{S}^2 - (1 - \rho) \left[ (\mathbf{S}^2 - \mathbf{S}^1)^{-1} - \frac{\rho}{S_0} \sum_{\ell=1}^L p_{\ell} \mathbf{A}_s(n^{\ell}) \right]^{-1}$$

$$\mathbf{A}_s = \mathbf{n} \otimes \mathbf{n}$$

$$\sum_{\ell=1}^L p_{\ell} = 1, \quad p_{\ell} \geq 0$$

orientations of layers. This transformation has been used in two-dimensional elasticity by Avellaneda and Milton (1989) whose final results will be presented here. Only formulas for bending and transverse shear deformation are derived here.

### Change of Basis

Instead of working with fourth order tensors, it is more convenient to work with their matrix representation in a suitable basis. The corresponding (3x3) matrix representation of fourth order tensors will be denoted using capital letters, e.g.,  $B_{\alpha\beta}$  ( $\alpha, \beta=1,2,3$ ) is the matrix representation of  $B_{ijkl}$ . Membrane and bending strain tensors are expressed in the following convenient basis

$$\xi^1 = \frac{1}{\sqrt{2}} \begin{pmatrix} 1 & 0 \\ 0 & -1 \end{pmatrix}, \quad \xi^2 = \frac{1}{\sqrt{2}} \begin{pmatrix} 0 & 1 \\ 1 & 0 \end{pmatrix}, \quad \xi^3 = \frac{1}{\sqrt{2}} \begin{pmatrix} 1 & 0 \\ 0 & 1 \end{pmatrix} \quad (3.2.1)$$

For in-plane deformations, tensor  $\xi^3$  correspond to radial expansion, and tensors  $\xi^1$  and  $\xi^2$  to in-plane shear deformations in two orthogonal axes. For bending deformations, tensor  $\xi^3$  is an axisymmetric bending strain (i.e., the one produced by a transverse displacement  $w(x,y) = (x^2+y^2)/2$ ), and tensors  $\xi^1$  and  $\xi^2$  are twisting bending strains in two orthogonal directions (i.e., those in  $w(x,y) = (x^2 - y^2 + 2xy)/2$ ). The use of the basis (3.2.1) allows one to state the following properties that can be easily proved and will be used in this section. Properties will be stated for bending deformations. The version for membrane deformations can be easily derived.

1) A generic bending strain tensor  $\kappa_{ij}$  is expressed as:

$$\begin{aligned} \kappa_{ij} &= c^{\alpha} \xi_{ij}^{\alpha} = \kappa_{lm} \xi_{lm}^{\alpha} \xi_{ij}^{\alpha} \\ &= \frac{\kappa_{11} - \kappa_{22}}{\sqrt{2}} \xi_{ij}^1 + \frac{\sqrt{2} \kappa_{12}}{\sqrt{2}} \xi_{ij}^2 + \frac{\kappa_{11} + \kappa_{22}}{\sqrt{2}} \xi_{ij}^3. \end{aligned} \quad (3.2.2)$$

2) The bending strain energy density is:

$$\mu_b = \frac{1}{2} B_{ijkl} \kappa_{ij} \kappa_{kl} = \frac{1}{2} B_{ijkl} \kappa_{pq} \xi_{pq}^{\alpha} \xi_{ij}^{\alpha} \kappa_{rs} \xi_{rs}^{\beta} \xi_{kl}^{\beta}. \quad (3.2.3)$$

From (3.2.3), we define the following (3x3) matrices,

$$B_{\alpha\beta} \equiv B_{ijkl} \xi_{kl}^{\beta} \xi_{ij}^{\alpha}, \quad (3.2.4)$$

$$K_{\alpha\beta} \equiv \kappa_{pq} \kappa_{rs} \xi_{pq}^{\alpha} \xi_{rs}^{\beta}. \quad (3.2.5)$$

3) A planar rotation  $\Theta$  of the unit vectors  $n^{\ell}$  in equation (3.1.35) produces the following change in  $\Lambda_b$  :

$$\Lambda_{bijkl}(R^t n^{\ell}) = R_{pi} R_{qj} R_{rk} R_{sl} \Lambda_{bpqrs}(n^{\ell}), \quad R = \begin{bmatrix} \cos(\Theta) & \sin(\Theta) \\ -\sin(\Theta) & \cos(\Theta) \end{bmatrix}, \quad (3.2.6)$$

and its matrix representation, using the same transformation in (3.2.4), is

$$M_b \equiv \Lambda_b(R^t n^{\ell}) = Q^t \Lambda_b(n^{\ell}) Q, \quad (3.2.7)$$

where

$$Q = \begin{bmatrix} \cos(2\Theta) & \sin(2\Theta) & 0 \\ -\sin(2\Theta) & \cos(2\Theta) & 0 \\ 0 & 0 & 1 \end{bmatrix}. \quad (3.2.8)$$

4) If  $B_{ijkl}$  is a fourth order tensor with all minor and major symmetries, it can be proved that

$$\left( \xi_{ij}^{\alpha} B_{ijkl} \xi_{kl}^{\beta} \right)^{-1} = \xi_{ij}^{\alpha} \left( B_{ijkl} \right)^{-1} \xi_{kl}^{\beta}. \quad (3.2.9)$$

5) Using the transformation (3.2.4), an isotropic fourth order tensor such as that in (3.1.6), is of the form

$$B = \frac{2}{3} h^3 \frac{E}{1-\nu^2} \begin{bmatrix} 1-\nu & 0 & 0 \\ 0 & 1-\nu & 0 \\ 0 & 0 & 1+\nu \end{bmatrix}. \quad (3.2.10)$$

Entries (1,1) and (2,2) in (3.2.10) are associated with the twisting bending in two orthogonal directions, and entry (3,3) with the axisymmetric bending.





### 3.2.1 Moment Representation of Bending Stiffness

Using transformation (3.2.4) and property (3.2.9) it is possible to write formula (3.1.45) in a (3x3) matrix form as

$$\bar{B} = B^2 - (1 - \rho) \left[ (B^2 - B^1)^{-1} - \frac{\rho}{B_0} \sum_{\ell=1}^L p_{\ell} \Lambda_b(n^{\ell}) \right]^{-1}. \quad (3.2.11)$$

Using unit vectors of the form  $n^{\ell} = \{ \cos(\varphi_{\ell}), \sin(\varphi_{\ell}) \}^t$ , the formula for  $\Lambda_b(n^{\ell})$  gives, after trigonometric simplifications,

$$\Lambda_b = \begin{bmatrix} \frac{3 - \nu - (1 + \nu)\cos(4\varphi_{\ell})}{4(1 - \nu)} & -\frac{1 + \nu}{4(1 - \nu)}\sin(4\varphi_{\ell}) & \frac{\cos(2\varphi_{\ell})}{2} \\ \frac{3 - \nu + (1 + \nu)\cos(4\varphi_{\ell})}{4(1 - \nu)} & \frac{\sin(2\varphi_{\ell})}{2} & \frac{1}{2} \\ \text{symmetric} & & \end{bmatrix} \quad (3.2.12)$$

or, defining

$$\begin{aligned} m_1(p, \varphi) &= \sum_{\ell=1}^L p_{\ell} \cos(2\varphi_{\ell}), & m_2(p, \varphi) &= \sum_{\ell=1}^L p_{\ell} \sin(2\varphi_{\ell}), \\ m_3(p, \varphi) &= \sum_{\ell=1}^L p_{\ell} \cos(4\varphi_{\ell}), & m_4(p, \varphi) &= \sum_{\ell=1}^L p_{\ell} \sin(4\varphi_{\ell}), \end{aligned} \quad (3.2.13)$$

then,

$$M_b = \sum_{\ell=1}^L p_{\ell} \Lambda_b = \begin{bmatrix} \frac{3 - \nu - (1 + \nu)m_3}{4(1 - \nu)} & -\frac{(1 + \nu)m_4}{4(1 - \nu)} & \frac{m_1}{2} \\ \frac{3 - \nu + (1 + \nu)m_3}{4(1 - \nu)} & \frac{m_2}{2} & \frac{1}{2} \\ \text{symmetric} & & \end{bmatrix}, \quad (3.2.14)$$

and the final form of the bending properties in matrix form is

$$\bar{B} = B^2 - (1 - \rho) \left[ (B^2 - B^1)^{-1} - \frac{\rho}{B_0} M_b \right]^{-1} \quad (3.2.15a)$$



where

$$B^k = \frac{2}{3} h_k^2 \frac{E}{1-\nu^2} \begin{bmatrix} 1-\nu & 0 & 0 \\ 0 & 1-\nu & 0 \\ 0 & 0 & 1+\nu \end{bmatrix}, \quad k=1,2 \quad (3.2.15b)$$

$$B_0 = \frac{2}{3} h_2^2 \frac{E}{1-\nu^2} \quad (3.2.15c)$$

### 3.2.2 Moment Representation of Shear Stiffness

A similar procedure is performed to express the shear stiffness in terms of the moments. Using  $n^\ell = \{ \cos(\varphi_\ell), \sin(\varphi_\ell) \}^t$  in  $A_s(n^\ell)$  (eqn. (3.1.51)), and using the definition of moments in (3.2.13), one obtains

$$M_s = \begin{bmatrix} \frac{1+m_1}{2} & \frac{m_2}{2} \\ \frac{m_2}{2} & \frac{1-m_1}{2} \end{bmatrix}. \quad (3.2.16)$$

and the final formula for the shear properties in matrix form is

$$\bar{S} = S^2 - (1-\rho) \left[ (S^2 - S^1)^{-1} - \frac{\rho}{S_0} M_s \right]^{-1} \quad (3.2.17a)$$

$$S^k = \frac{E}{1+\nu} h_k \begin{bmatrix} 1 & 0 \\ 0 & 1 \end{bmatrix}, \quad k=1,2, \quad S_0 = \frac{E}{1+\nu} h_2 \quad (3.2.17b)$$

### 3.2.3 Moment Representation of Membrane Stiffness

Here the results obtained by Avellaneda and Milton (1989) for plane stress elasticity are slightly modified to take into account the presence of ribs. The result is the moment representation of the effective stiffness for membrane deformations.



$$\bar{M} = M^2 - (1 - \rho) \left[ (M^2 - M^1)^{-1} - \frac{\rho}{M_0} M_m \right]^{-1},$$

$$M_m = \begin{bmatrix} \frac{3 - \nu - (1 + \nu)m_3}{4(1 - \nu)} & -\frac{(1 + \nu)m_4}{4(1 - \nu)} & \frac{m_1}{2} \\ & \frac{3 - \nu + (1 + \nu)m_3}{4(1 - \nu)} & \frac{m_2}{2} \\ \text{symmetric} & & \frac{1}{2} \end{bmatrix},$$

$$M^k = 2h_k \frac{E}{1 - \nu^2} \begin{bmatrix} 1 - \nu & 0 & 0 \\ 0 & 1 - \nu & 0 \\ 0 & 0 & 1 + \nu \end{bmatrix}, \quad k = 1, 2$$

$$M_0 = 2h_2 \frac{E}{1 - \nu^2}. \quad (3.2.18)$$

Notice that  $M_m = M_b$  since  $\Lambda_m = \Lambda_b$ .

In summary, a representation of the homogenized stiffness of Mindlin plates with ribs in L different directions with only four independent variables,  $m_1$ ,  $m_2$ ,  $m_3$ , and  $m_4$ , that describe the local orthotropy, i.e., the relative rib widths,  $p_i$ , and the local orientation of the layers,  $\varphi_i$ .

### 3.2.4 Feasible Set in the Moment Space

In order to perform the optimization in the moment space it is necessary to identify the set of feasible solutions. In this context ‘feasible’ means that a point in the set must represent a realizable material with average stiffness within the known bounds. The identification of this set is done using the approach presented by Avellaneda and Milton, (1989), in plane elasticity. This requires the solution of the trigonometric moment problem (see theorem 2.6 in the text of Krein and Nudel’man, (1977)). Using the identity between tensors  $\Lambda_b$  and  $\Lambda_m$  it is possible to obtain the constraints on the moments for plate problems directly from the work of Avellaneda and Milton. In the four-dimensional moment space, the feasible set is given by

$$H = \{(m_1, m_2, m_3, m_4) : \frac{2m_1^2}{1+m_3} + \frac{2m_2^2}{1-m_3} + \frac{m_4^2}{1-m_3^2} - \frac{4m_1m_2m_4}{1-m_3^2} \leq 1, \quad (3.2.19)$$

$$m_1^2 + m_2^2 \leq 1, \quad -1 \leq m_3 \leq 1\}$$

From the layout optimization point of view, it is important to emphasize the difference between the moment formulation and the formulation presented in Chapter 2. A shape optimization problem based on the formulas given in Chapter 2 requires three design variables, namely,  $a$ ,  $b$  (the width of the layers) and  $\Theta$  (the orientation of the cell), to characterize a rank-2 material plate with orthogonal layers. In the formulation of this chapter we have five design variables, namely,  $\rho$  (the amount of material assigned to a location), and the four moments  $m_1, m_2, m_3, m_4$  (the description of the layering), to characterize a rank-L material plate with arbitrary layer orientation. It was proved in elasticity problems that for multiple load cases (i.e., multiple energy cases) the stiffest micro structure can always be attained using at most rank-3 materials (Lipton, (1994)) which is an special case of rank-L materials. As it will be seen in section 3.2.5, this is also the case of Mindlin plates.

It is important to mention that in Mindlin plates, even under a single load case, there are always at least two sources of strain energies, one coming from the bending deformations and another one coming from the transverse shear deformations. These two energies always come together because of the nature of the Mindlin plate equations. If additionally there are membrane deformations, there will be a third source of strain energy.

### 3.2.5 Determination of the Micro Structure Geometry

Once the optimum moments are determined from the solution of the optimization problem (as will be explained in Chapter 4), it is possible to obtain the geometry of the micro structure, namely, the number of layers, layer widths and directions. Potentially, there are  $2*L$  unknowns to be determined in order to describe the micro structure of the material, i.e.,  $L$  layer widths and  $L$  directions. Recent work, however, has shown that optimum (stiffest) micro structures for multiple load cases are made of at most three layers (Lipton, (1994)), therefore, we can reduce the number of unknowns to six, namely,  $p_i, \phi_i, i=1,2,3$ , which can be solved following the procedure described below.

First, a 3-dimensional set  $\tilde{H}$  is obtained from the 4-dimensional set  $H$  making  $m_4=0$ . This can be done performing a rigid-body rotation,  $\Theta$ , of all layers in the micro structure. Then the micro structure geometry of the three layers can be computed using the convexity of  $\tilde{H}$  and the solution of the micro structure geometry of rank-2 materials on the boundary of  $\tilde{H}$  that appears in (Lipton, (1993c)). The detailed procedure follows.

Noting that the layer angles are measured from an arbitrary reference, one can select a local frame that is rotated an angle  $\Theta$  from the fixed frame. As this is just a planar rotation of the layer direction vectors, it is possible to write, from (3.2.7),

$$\tilde{M}_b = Q^t(\Theta) M_b Q(\Theta). \quad (3.2.20)$$

and select  $\Theta$  so that  $\tilde{M}_b(1, 2) = 0$ . This angle is

$$\Theta = \frac{1}{2} \text{ArcTan}\left(\frac{\sqrt{m_3^2 + m_4^2} + m_3}{m_4}\right). \quad (3.2.21)$$

With this choice,

$$\tilde{M}_b = \begin{bmatrix} \frac{3 - \nu - (1 + \nu)\tilde{m}_3}{4(1 - \nu)} & 0 & \frac{\tilde{m}_1}{2} \\ & \frac{3 - \nu + (1 + \nu)\tilde{m}_3}{4(1 - \nu)} & \frac{\tilde{m}_2}{2} \\ \text{symmetric} & & \frac{1}{2} \end{bmatrix}. \quad (3.2.22)$$

where the new moments are

$$\begin{aligned} \tilde{m}_1(p, \tilde{\varphi}) &= \sum_{\ell=1}^L p_\ell \cos(2\tilde{\varphi}_\ell), & \tilde{m}_2(p, \tilde{\varphi}) &= \sum_{\ell=1}^L p_\ell \sin(2\tilde{\varphi}_\ell), \\ \tilde{m}_3(p, \tilde{\varphi}) &= \sum_{\ell=1}^L p_\ell \cos(4\tilde{\varphi}_\ell) \end{aligned} \quad (3.2.23)$$

and the new angles are  $\tilde{\varphi}_\ell = \varphi_\ell + \Theta$ . The relation between the moments in the 4-dimensional set and those in the 3-dimensional set is given by



$$\begin{aligned}
\tilde{m}_1 &= m_1 \cos(2\theta) - m_2 \sin(2\theta) \\
\tilde{m}_1 &= m_2 \cos(2\theta) + m_1 \sin(2\theta) \\
\tilde{m}_3 &= m_3 \cos(4\theta) - m_4 \sin(4\theta)
\end{aligned}
\tag{3.2.24}$$

The new set of feasible moments,  $\tilde{H}$ , is easily obtained from (3.2.19) setting  $m_4=0$  (see Figure 3.3), i.e.,

$$\tilde{H} = \{(\tilde{m}_1, \tilde{m}_2, \tilde{m}_3) : \frac{2\tilde{m}_1^2}{1+\tilde{m}_3} + \frac{2\tilde{m}_2^2}{1-\tilde{m}_3} \leq 1, \tilde{m}_1^2 + \tilde{m}_2^2 \leq 1, -1 \leq \tilde{m}_3 \leq 1\}
\tag{3.2.25}$$

It can be easily checked that the four points satisfying  $\tilde{m}_1^2 + \tilde{m}_2^2 = 1$ , namely,  $(1,0,1)$ ,  $(0,1,-1)$ ,  $(0,-1,-1)$  and  $(-1,0,1)$ , correspond to rank-1 materials with layer direction equal to  $0^\circ$ ,  $+45^\circ$ ,  $-45^\circ$  and  $90^\circ$ , respectively. Additionally, it is known that all other points on

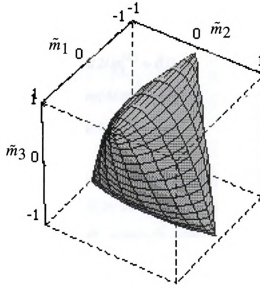


Figure 3.3. Convex set  $\tilde{H}$ .

the boundary  $\partial\tilde{H}$  correspond to rank-2 materials (Lipton, (1993c)). Making use of these characteristics, it is possible to express any interior point in  $\tilde{H}$  as a convex combination of a rank-1 material point  $\tilde{a}$  --one of the 4 points mentioned above-- and another point on the boundary,  $\tilde{b}$ , that is,

$$\tilde{m} = \alpha \tilde{a} + (1 - \alpha) \tilde{b}, \quad 0 \leq \alpha \leq 1 \quad (3.2.26)$$

The point  $\tilde{b}$  is a rank-2 material point on  $\partial \tilde{H}$ , to be determined intersecting the line that connects  $\tilde{a}$  and  $\tilde{m}$  with the boundary  $\partial \tilde{H}$ . This is accomplished solving the non-linear system of equations

$$\begin{aligned} \frac{2\tilde{b}_1^2}{1+\tilde{b}_3} + \frac{2\tilde{b}_2^2}{1-\tilde{b}_3} &= 1 \\ \frac{\tilde{b}_1 - \tilde{a}_1}{\tilde{m}_1 - \tilde{a}_1} &= \frac{\tilde{b}_2 - \tilde{a}_2}{\tilde{m}_2 - \tilde{a}_2} = \frac{\tilde{b}_3 - \tilde{a}_3}{\tilde{m}_3 - \tilde{a}_3} \end{aligned} \quad (3.2.27)$$

with  $-1 \leq \tilde{m}_3 \leq 1$ . Once the point  $\tilde{b}$  is obtained from (3.2.27) it is possible to compute its layer directions  $(\varphi_1^{(\tilde{b})}, \varphi_2^{(\tilde{b})} = \varphi_1^{(\tilde{b})} + \delta)$  and relative widths  $(p_1^{(\tilde{b})}, p_2^{(\tilde{b})} = 1 - p_1^{(\tilde{b})})$  solving the nonlinear system

$$\begin{aligned} \tilde{b}_1 &= p_1^{(\tilde{b})} \cos(2\varphi_1^{(\tilde{b})}) + (1 - p_1^{(\tilde{b})}) \cos(2(\varphi_1^{(\tilde{b})} + \delta)) \\ \tilde{b}_2 &= p_1^{(\tilde{b})} \sin(2\varphi_1^{(\tilde{b})}) + (1 - p_1^{(\tilde{b})}) \sin(2(\varphi_1^{(\tilde{b})} + \delta)) \\ \tilde{b}_3 &= p_1^{(\tilde{b})} \cos(4\varphi_1^{(\tilde{b})}) + (1 - p_1^{(\tilde{b})}) \cos(4(\varphi_1^{(\tilde{b})} + \delta)) \\ 0 &= p_1^{(\tilde{b})} \sin(4\varphi_1^{(\tilde{b})}) + (1 - p_1^{(\tilde{b})}) \sin(4(\varphi_1^{(\tilde{b})} + \delta)) \end{aligned} \quad (3.2.28)$$

A solution of the nonlinear system in (3.2.28) to compute the geometry of  $\tilde{b}$  can be found in (Lipton, (1993c)). The final step is to identify the layer directions,  $\varphi_\ell^{(\tilde{m})}$ , and relative widths,  $p_\ell^{(\tilde{m})}$ , of the interior point  $\tilde{m}$  using (3.2.26). In order to do this, we need to pick one of the four points satisfying  $\tilde{m}_1^2 + \tilde{m}_2^2 = 1$ . We choose  $\tilde{a}=(1,0,1)$ , then (3.2.26) becomes

$$\begin{aligned} \sum_{\ell=1}^3 p_\ell^{(\tilde{m})} \cos(2\varphi_\ell^{(\tilde{m})}) &= \alpha + (1 - \alpha) \{ p_1^{(\tilde{b})} \cos(2\varphi_1^{(\tilde{b})}) + p_2^{(\tilde{b})} \cos(2(\varphi_1^{(\tilde{b})} + \delta)) \} \\ \sum_{\ell=1}^3 p_\ell^{(\tilde{m})} \sin(2\varphi_\ell^{(\tilde{m})}) &= 0 + (1 - \alpha) \{ p_1^{(\tilde{b})} \sin(2\varphi_1^{(\tilde{b})}) + p_2^{(\tilde{b})} \sin(2(\varphi_1^{(\tilde{b})} + \delta)) \} \\ \sum_{\ell=1}^3 p_\ell^{(\tilde{m})} \cos(4\varphi_\ell^{(\tilde{m})}) &= \alpha + (1 - \alpha) \{ p_1^{(\tilde{b})} \cos(4\varphi_1^{(\tilde{b})}) + p_2^{(\tilde{b})} \cos(4(\varphi_1^{(\tilde{b})} + \delta)) \} \end{aligned} \quad (3.2.29)$$



Using equation (3.2.29), the identification of terms results in

$$\begin{aligned} p_1^{(\tilde{m})} &= \alpha; & p_2^{(\tilde{m})} &= (1-\alpha)p_1^{(\tilde{b})}; & p_3^{(\tilde{m})} &= (1-\alpha)p_2^{(\tilde{b})} \\ \varphi_1^{(\tilde{m})} &= 0; & \varphi_2^{(\tilde{m})} &= \varphi_1^{(\tilde{b})}; & \varphi_3^{(\tilde{m})} &= \varphi_1^{(\tilde{b})} + \delta \end{aligned}, \quad (3.2.30)$$

and the final orientation of layers is computed using  $\varphi_\ell = \tilde{\varphi}_\ell - \Theta$ . Notice that different geometries are obtained depending on which point  $\tilde{a}$  is used. This means that we are able to identify at least four different rank-3 layering geometries that have the same moments, i.e., the same stiffness properties. For example, the following two micro structures have the same stiffness properties:

$$\begin{aligned} &(\Theta, p_1^{(\tilde{m})}, p_2^{(\tilde{m})}, p_3^{(\tilde{m})}, \varphi_1^{(\tilde{m})}, \varphi_2^{(\tilde{m})}, \varphi_3^{(\tilde{m})}) \\ \text{micro structure 1:} & \quad (33.7, 0.27, 0.42, 0.31, -33.7, 22.2, 84.3) \\ \text{micro structure 2:} & \quad (33.7, 0.30, 0.34, 0.36, -78.7, -12.7, 38.8) \end{aligned}$$

and correspond to  $m=(0.1, 0.1, 0.1, 0.1)$ .

This non-uniqueness of the layering arrangement is expected since the micro structure geometry is determined solving a non-linear system of five equations and six unknowns, namely, equations in (3.2.13) and (3.1.45b), and unknowns  $p_i, \varphi_i, i=1,2,3$ . The idea of using a convex combination in (3.2.25) to obtain the micro structure geometry is due to (Lipton, (1993d)).



## **CHAPTER 4**

### **FORMULATION AND IMPLEMENTATION OF THE LAYOUT OPTIMIZATION PROBLEM FOR MINIMIZATION OF COMPLIANCE**

A simple way to measure the flexibility of a structure is to compute its mean compliance (external work) for the given loading conditions. Since compliance is an inverse measure of the stiffness, it is meaningful to use the mean compliance as a cost function in order to maximize the global stiffness of the structure. From the mathematical viewpoint, the most important advantage of this choice is that in the formulation of the optimization problem the state variable (the displacement field) and the adjoint variable turn out to be the same, which makes the problem much easier to solve.

As it was said in the introduction, the idea behind the homogenization approach to shape optimization is to fill the domain with a microscopically porous material and to pose the problem as one of optimum distribution of material. Using the functional relation between the stiffness of the material and its volume (a relation computed via the homogenization procedure), it is possible to compute the sensitivity of the stiffness with respect to changes in the amount of material, which is indispensable for any topology optimization approach. This is the basic idea that will be explored throughout this chapter.

The layout and shape optimization problem presented here is based on the moment formulation of the stiffness properties shown in Chapter 3 which allows us to build a two-scale hierarchical statement of the optimization problem as in (Jog, *et al.*, 1992).

In the first part of this chapter the problem of minimization of the mean compliance (maximization of global stiffness) is considered. The second part is devoted to the implementation aspects of the layout optimization problem.

#### 4.1 Hierarchical Moment Formulation of the Stiffness Maximization Problem

The optimization problem in (Bendsøe and Kikuchi, (1988)) was stated in terms of three design variables, namely, the rib widths  $(a(x), b(x))$ , and the global rotation of the micro structure,  $\Theta(x)$ . The strategy used in that case was to implement an iterative procedure based on an optimality criterion approach to solve for all three variables simultaneously. Here we split the optimization problem in two, one at the small scale level where the micro structure of the plate is computed, and another at the large scale where the distribution of material is computed. This is possible using standard variational principles of mechanics that allow one to express the equilibrium state of the structural system from a minimization problem. This idea was first applied in static problems, in two-dimensional elasticity, for a single load case, and using the rank-2 materials, by Jog, Haber and Bendsøe (1992). Mindlin plates under multiple independent load cases are now considered.

As will be seen in the following presentation, the formulation of Jog, Haber and Bendsøe is more convenient than the Bendsøe-Kikuchi's formulation when the effective properties of rank-L material plates are represented through the moment formulation described in Chapter 3. For the moment, it is sufficient to know that the design variables are now the internal geometry of the micro structure, given by the moments  $m(x)=(m_1(x), m_2(x), m_3(x), m_4(x))$  and the distribution of the material resource throughout the plate,  $\rho(x)$ . The notation in this section follows very close the tensorial notation used in section 3.2.

##### 4.1.1 Optimization Problem Statement

Suppose there are  $P$  independent load cases for which a single optimum structural shape is desired. This problem can be stated using a weighted average of the compliances  $c(u^p)$  of each load case  $p$ , i.e.,

Find  $\rho(x)$  and  $m(x)=(m_1(x), m_2(x), m_3(x), m_4(x))$ ,  $x \in \Omega_0$  that

$$\min_{(\rho, m) \in X} C(\{u\}^*) = \sum_{p=1}^P w_p c(u_*^p) \quad (4.1.6a)$$

where  $\rho$ , and  $m=\{m_1, m_2, m_3, m_4\}$  are the design variables in the set

$$X = X_G \times H, \quad (4.1.6b)$$

$$X_G = \{ \rho(x) : x \in \Omega_0, \int_{\Omega^0} \rho d\Omega \leq V_{max}, 0 < \rho_{min} \leq \rho \leq 1 \}, \quad (4.1.6c)$$

where  $H$  is the four-dimensional moment space defined in (3.2.19) and  $u_*^P = \{v_1, v_2, v_3, \theta_1, \theta_2\}^P \equiv \{v_x, v_y, v_z, -\theta_y, \theta_x\}^P$  represents the plate displacement fields at equilibrium.  $V_{max} < |\Omega_0|$  and  $\rho_{min}$  are given data. The subscript '\*' in the displacement vector emphasizes that it is the equilibrium solution and hence minimizes the potential energy of the structure.

To identify the local and global problems the following series of equalities are used

$$\min_{(\rho, m) \in X} \sum_{p=1}^P w_p c(u_*^P) = \min_{(\rho, m) \in X} -2 \sum_{p=1}^P w_p \Pi(u_*^P) \quad (4.1.7)$$

where  $\Pi$  is the potential energy. Equality (4.1.7) uses the Clapeyron's work theorem (Fung, (1965)). Applying the principle of minimum potential energy:

$$\min_{(\rho, m) \in X} -2 \sum_{p=1}^P w_p \Pi(u_*^P) = \min_{\rho \in X_G} \{ -2 \max_{m \in H} \sum_{p=1}^P w_p \min_{u^P \in V} [U(u^P) - c(u^P)] \} \quad (4.1.8)$$

where  $U$  is the strain energy in the plate and  $V$  the space of kinematically admissible displacement fields. Now an exchange of the two internal optimization problems in (4.1.8) is performed. This is possible due to a saddle point condition in the space  $[V]^P \times H$  similar to that proved by Lipton (1993b) for the three-dimensional elasticity case (see also Ekeland and Teman, (1976), page 173). The space  $[V]^P$  is the cartesian product (direct sum) of space  $V$ ,  $P$  times, explicitly,  $[V]^P \equiv V \times V \times \dots \times V$ . After exchanging the two internal optimization problems, we obtain

$$\min_{\rho \in X_G} \{ -2 \min_{\{u\} \in [V]^P} \sum_{p=1}^P w_p \max_{m \in H} [U(u^P) - c(u^P)] \} \quad (4.1.9)$$

Finally, since material properties are independent from point to point in the domain, it is possible exchange the maximization over the moments and the strain energy integral to





get

$$\min_{(\rho, m) \in X} C(\{u\}^*) = \min_{\rho \in X_G} -2 \left\{ \min_{\{u\} \in [V]^P} \left\{ \int_{\Omega_0} \max_{m \in H} \sum_{p=1}^P w_p \mu(u^p) d\Omega - C(\{u\}) \right\} \right\} \quad (4.1.10)$$

where  $\mu$  is the strain energy density.

The final arrangement in (4.1.10) suggests an iterative process based on a local problem corresponding to the (point-wise) maximization of the strain energy density for fixed strains, and a global problem in which the amount of material  $\rho(x)$  is updated to minimize the mean compliance for a fixed micro structure.

#### 4.1.2 The Local Problem

For fixed  $\rho(x) \in X_G$ , and kinematically admissible displacement fields  $u^p$ ,  $p=1, \dots, P$ , find  $m = \{m_1, m_2, m_3, m_4\}$  to

$$\max_{m \in H} \sum_{p=1}^P w_p \mu(u^p) = \frac{1}{2} \sum_{p=1}^P w_p (\bar{M}_{ijkl} \varepsilon_{ij}^p \varepsilon_{kl}^p + \bar{B}_{ijkl} \kappa_{ij}^p \kappa_{kl}^p + \bar{S}_{ij} \gamma_i^p \gamma_j^p) \quad (4.1.11a)$$

with

$$H = \{(m_1, m_2, m_3, m_4) : \frac{2m_1^2}{1+m_3} + \frac{2m_2^2}{1-m_3} + \frac{m_4^2}{1-m_3^2} - \frac{4m_1m_2m_4}{1-m_3^2} \leq 1, \\ m_1^2 + m_2^2 \leq 1, \quad -1 \leq m_3 \leq 1\} \quad (4.1.11b)$$

Using definitions from Chapter 3, the weighted sum of the strain energy densities can be written as

$$\sum_{p=1}^P w_p \mu(u^p) = \frac{1}{2} (\bar{M}(m) : e(\{u\}) + \bar{B}(m) : b(\{u\}) + \bar{S}(m) : s(\{u\})) \quad (4.1.12)$$

where formula (3.2.4) was applied to  $\bar{M}$  and  $\bar{B}$ . The following definitions were also used in (4.1.12)

$$\begin{aligned}
e(\{u\}) &\equiv \sum_{p=1}^P w_p E_{\delta\eta}(u^p), \\
b(\{u\}) &\equiv \sum_{p=1}^P w_p K_{\delta\eta}(u^p), \\
s(\{u\}) &\equiv \sum_{p=1}^P w_p \gamma_k(u^p) \gamma_l(u^p).
\end{aligned} \tag{4.1.13}$$

where  $E_{\delta\eta}$  and  $K_{\delta\eta}$  are computed with (3.2.5). Notice that all the information about the different load cases is concentrated in the strains formulas (4.1.13). The solution strategy for this problem will be discussed in section 4.2.

#### 4.1.3 Equilibrium Equations

After solving the local optimization problem, the optimum micro structure for given strain field and resource  $\rho$  at each location of the plate is identified by  $m^*(x)$ . Next, for fixed  $m^*$  the following equilibrium equation is solved. The equilibrium displacements  $\{u\} = \{u^1, \dots, u^P\} \in [V]^P$  satisfy the equation

$$\int_{\Omega_0} \{ \bar{M}(m^*, \rho) : e(\{u\}, \{\hat{u}\}) + \bar{B}(m^*, \rho) : b(\{u\}, \{\hat{u}\}) + \bar{S}(m^*, \rho) : s(\{u\}, \{\hat{u}\}) \} d\Omega = C(\{\hat{u}\}) \quad \forall \{\hat{u}^1, \dots, \hat{u}^P\} \in [V]^P \tag{4.1.14}$$

It is important to realize that the material properties obtained in the solution of the local problem depend upon *all* displacement fields *simultaneously*, that is,  $\bar{M}^* = \bar{M}^*(m^*(\{u\}))$ ,  $\bar{B}^* = \bar{B}^*(m^*(\{u\}))$  and  $\bar{S}^* = \bar{S}^*(m^*(\{u\}))$ . This dependency produces two difficulties. First, the strain energy density is no longer a pure quadratic form of the displacements, and hence the equilibrium equation is non-linear. Second, the strain energy density couples all displacement fields, meaning that the solution of the equilibrium equation should be computed considering all load cases simultaneously. More specifically, the Hessian matrix  $H^*$  of the strain energy density -- which in linear problems represents the stiffness matrix of the equilibrium equation -- consists of sub-matrices  $H_{ij}^*$  ( $i, j=1, \dots, P$ ) given by



$$H_{ij}^* = \frac{\partial^2}{\partial u^i \partial u^j} \left\{ \frac{1}{2} \mu^*(u^1, \dots, u^P) \right\}, \quad (i, j = 1, \dots, P). \quad (4.1.15)$$

In general, these sub-matrices are non-zero causing the coupling between different load cases. In section 4.2 there is a discussion about how to solve this complex problem.

#### 4.1.4 The Global Problem

For fixed  $m^*$  and fixed equilibrium displacement fields  $\{u\}^*$  find  $\rho(x)$  that

$$\min_{\rho \in X_G} (-2 \Pi(\{u^*(\rho, m^*)\})) = \min_{\rho \in X_G} (-2 \min_{\{u\} \in [V]^P} \left( \int_{\Omega_0} \mu^*(\{u\}) d\Omega - C(\{u\}) \right))$$

$$X_G = \{ \rho(x) : x \in \Omega_0, \int_{\Omega_0} \rho d\Omega \leq V_{max}, 0 < \rho_{min} \leq \rho \leq 1 \} \quad (4.1.16)$$

Using Lagrange multiplier techniques, an optimality criterion can be derived to solve (4.1.16). Introduce the Lagrangian function,

$$\begin{aligned} L(\rho, \Phi, \alpha_{min}, \alpha_{max}) = & \int_{\Omega_0} \{ \bar{M}(m^*, \rho) : e(\{u\}^*) + \bar{B}(m^*, \rho) : b(\{u\}^*) + \\ & \bar{S}(m^*, \rho) : s(\{u\}^*) d\Omega - 2C(\{u\}^*) + \\ & \Phi \left( \int_{\Omega_0} \rho d\Omega - V_{max} \right) + \int_{\Omega_0} \alpha_{min}(\rho_{min} - \rho) + \alpha_{max}(\rho - 1) d\Omega \end{aligned} \quad (4.1.17)$$

where  $\Phi$ ,  $\alpha_{min}$  and  $\alpha_{max}$  are non-negative Lagrange multipliers. The first variation of the potential energy  $\Pi^*(\rho)$  with respect to the density  $\rho$  is the sensitivity of an optimum solution (defined by  $m^*$ ) as the ‘parameter’  $\rho$  changes. In this particular case, since the constraints of the local problem do not depend on the density  $\rho$ , this sensitivity is simply the first variation of  $\Pi^*(\rho)$ , leading to,

$$\frac{\partial \bar{M}(m^*)}{\partial \rho} : e(\{u\}^*) + \frac{\partial \bar{B}(m^*)}{\partial \rho} : b(\{u\}^*) + \frac{\partial \bar{S}(m^*)}{\partial \rho} : s(\{u\}^*) - \Phi + \alpha_{min} - \alpha_{max} = 0. \quad (4.1.18)$$



Complementary conditions can be also obtained from (4.1.17), i.e.,

$$\Phi\left(\int_{\Omega_0} \rho d\Omega - V_{max}\right) = 0, \quad \alpha_{min}(\rho_{min} - \rho) = 0, \quad \alpha_{max}(\rho - 1) = 0 \quad (4.1.19)$$

## 4.2 Numerical Implementation of the Optimization Problem

The computational implementation of the hierarchical formulation presented above can be organized in two main steps: the solution of the equilibrium equation and the solution of the optimization problem. Here there is a presentation of these two topics in more detail.

### 4.2.1 Solution of the Equilibrium Equation

It was discussed in section 4.1 that the equilibrium equations that appear in the hierarchical moment formulation of the optimization problem are non-linear and coupled due to the non quadratic form of the strain energy density with respect to the strains. This results in a Hessian matrix of the form

$$H^* \equiv \begin{bmatrix} H_{11}^{e*} & H_{12}^{e*} & \cdots & H_{1P}^{e*} \\ H_{21}^{e*} & H_{22}^{e*} & \ddots & \vdots \\ \vdots & \ddots & \ddots & \\ H_{P1}^{e*} & \cdots & & H_{PP}^{e*} \end{bmatrix} \quad (4.2.1)$$

where the 8x8 sub-matrices  $H_{ij}^{e*}$  ( $i, j=1, \dots, P$ ) are given by

$$H_{ij}^{e*} = \frac{\partial^2}{\partial u^i \partial u^j} \left\{ \frac{1}{2} \mu^*(u^1, \dots, u^P) \right\}, \quad (i, j=1, \dots, P). \quad (4.2.2)$$

where  $u^p$ ,  $p=1, \dots, P$  is the  $p^{th}$  displacement field and  $\mu^*$  is the strain energy density computed for the optimum moments  $m^*=(m_1, m_2, m_3, m_4)^*$ .

In order to decouple the problem and to simplify the analysis the Hessian matrix is approximated setting zero all off-diagonal sub-matrices and using the same sub-matrix in all diagonal entries, that is, setting

$$H^{*approx.} \equiv \begin{bmatrix} \hat{H}^{e*} & 0 & \dots & 0 \\ 0 & \hat{H}^{e*} & \ddots & \vdots \\ \vdots & \ddots & \ddots & \\ 0 & \dots & & \hat{H}^{e*} \end{bmatrix}, \quad \hat{H}^{e*} \equiv \begin{bmatrix} \bar{M}^* & 0 & 0 \\ 0 & \bar{B}^* & 0 \\ 0 & 0 & \bar{S}^* \end{bmatrix} \quad (4.2.3)$$

where  $\bar{M}^*$ ,  $\bar{B}^*$  and  $\bar{S}^*$  are the stiffness properties computed for the optimum solution of the local problem. This approximation is simply a linearization of the original problem where the dependence of the material properties on the displacement fields is neglected. The solution of the approximated problem requires much less computational effort than the solution of the original one. A linear finite element code can be used in order to obtain the solution of the approximated problem. In this work the program Monique™ from RTB Corp. was used to solve the approximated equilibrium problem.

#### 4.2.2 Solution of Optimization Problems

Two types of optimization problems were presented in section 4.1: the global optimization problem on the material resource  $\rho$ , and the local optimization problem on the moments. The optimization problem over the material resource is N-dimensional (N is the number of finite elements in the mesh) and is usually solved using an optimality criterion approach, while the optimization problem over the moments is four-dimensional and can be solved using a non-linear programming optimization algorithm.

##### Optimality Criteria Approach - Global problem

Optimality criteria approaches find the distribution of  $\rho(x)$  such that the optimality conditions given in (4.1.18) are satisfied for every location  $x$  in the domain. This is done using an iterative scheme where at each iteration the resource  $\rho(x)$  is updated according to how far it is from the satisfaction of (4.1.18). If at a given point the optimality conditions are satisfied, the material resource will not be changed, but if the optimality conditions are violated, the material resource will be modified proportionally to some measure of the violation.

After the discretization of the plate domain into  $N$  finite elements, optimality conditions represented by equation (4.1.18) can be written for each element as





$$\frac{\partial \bar{M}_i(m^*)}{\partial \rho_i} : e_i(\{u\}^*) + \frac{\partial \bar{B}_i(m^*)}{\partial \rho_i} : b_i(\{u\}^*) + \frac{\partial \bar{S}_i(m^*)}{\partial \rho_i} : s_i(\{u\}^*) = \Phi + \alpha_{max_i} - \alpha_{min_i},$$

$$i=1, \dots, N \quad (4.2.4)$$

In elements where the material resource has not attained its lower or upper bound, complementary conditions in (4.1.19) result in  $\alpha_{max_i} = \alpha_{min_i} = 0$ . For these elements it is possible to write (4.2.4) in the more convenient form

$$\Xi_i \equiv \frac{(me)_i}{\Phi} = 1, \quad i=1, \dots, N \quad (4.2.5)$$

where the sum of the three left-hand-side terms in (4.2.4) is usually called ‘mutual energies’ and denoted here as  $(me)_i$ . The ratio in (4.2.5) will be called here “optimality condition ratio” which is equal to one (1) only for elements with  $\rho_{min} < \rho < 1$ , and only at a stationary point of the Lagrangian, which we assume corresponds to the optimum solution of the shape optimization problem. Since the global stiffness increases monotonically with the amount of material, the constraint on the total amount of material available is always active and the Lagrange multiplier  $\Phi$  is greater than zero.

Using the optimality condition ratio it is possible to construct an algorithm to update the material resource at each element of the mesh. Notice that  $\Xi_i$  is quadratic in the strains, and therefore, high values of  $\Xi_i$  (values greater than 1) are associated with high strains that can be reduced adding more material. On the other hand, low values of  $\Xi_i$  (values less than 1) are associated with low strains that can be increased subtracting material. This is the basis of the algorithm. Suppose that at certain iteration  $k$  of the optimization algorithm there is an element with material resource  $\rho_i^k$  and  $\Xi_i \neq 1$ . Then the proposed value for the material resource in the next iteration will be

$$\rho_i^{k+1} = \left( \Xi_i^k \right)^\zeta \rho_i^k = \left( \frac{(me)_i^k}{\Phi^k} \right)^\zeta \rho_i^k, \quad i=1, \dots, N \quad (4.2.6)$$

where  $0 < \zeta < 1$  is a “damping” factor that is used to improve the behavior of the algorithm.

To apply (4.2.6), it is required that the Lagrange multiplier  $\Phi^k$  be known. This



multiplier is computed such that the constraint on the total amount of material available is active. This means that it is necessary to iterate in a inner loop using (4.2.6) until the constraint in (4.1.16) is active. A bisection search method is suitable for these task. Clearly, values of  $\rho$  computed using (4.2.6) must be maintained between the bounds of the material resource,  $\rho_{min}$  and 1 (see (4.1.16)). Also, it is convenient to introduce a maximum step size,  $\delta$ , to obtain a stable convergence in the iteration process. A practical implementation of (4.2.6) that takes into account these issues is

$$\rho_i^{k+1} = \begin{cases} \max\{(1-\delta)\rho_i^k, \rho_{min}\} & \text{if } \Xi_i^k \rho_i^k \leq \max\{(1-\delta)\rho_i^k, \rho_{min}\} \\ (\Xi_i^k)^\zeta \rho_i^k & \text{if } \max\{(1-\delta)\rho_i^k, \rho_{min}\} \leq \Xi_i^k \rho_i^k \leq \min\{(1+\delta)\rho_i^k, 1\} \\ \min\{(1+\delta)\rho_i^k, 1\} & \text{if } \min\{(1+\delta)\rho_i^k, 1\} \leq \Xi_i^k \rho_i^k \end{cases}$$

$$i=1, \dots, N \quad (4.2.7)$$

This approach was used in the original paper of Bendsøe and Kikuchi (1988) and has seen to be effective using values of  $\zeta$  between 0.7 and 0.85, and  $\delta$  between 0.45 and 0.55.

#### Nonlinear Programming Approach - Local Problem

In the hierarchical formulation of the optimization problem, the local problem over the moments can be solved using conventional nonlinear programming techniques. In this case we used the algorithm presented in (Schittkowski, (1985/6)) implemented in the subroutine NLPQL and supplied by Professor Schittkowski.

#### 4.2.3 Convergence Criteria

The convergence of the iterative algorithm is checked comparing two consecutive values of the sequence  $\{F\}_0^k$ , where  $F$  is the objective function, and  $k$  is the iteration step. Given a non-negative small tolerance  $t \ll 1$ , the used convergence criterion is:

$$\text{If } \left| \frac{F^{(k)} - F^{(k-1)}}{F^{(k-1)}} \right| < t, \quad \text{then } CONVERGED \quad \text{else } ITERATE \quad (4.2.8)$$

Additional stopping criteria are used to prevent the program from running infinite iterations when the sequence does not satisfy inequality (4.2.8) in a reasonable number of



iterations. A limit in the number of iterations is the easiest way to stop the process in these cases:

*If  $k \geq \text{Limit of Iterations}$ , then STOP,  
else ONE MORE ITERATION. (4.2.9)*

#### 4.2.4 Algorithm Implementation

This is a sketch of the algorithm implemented to solve the layout and shape optimization problem using the hierarchical moment formulation.

```

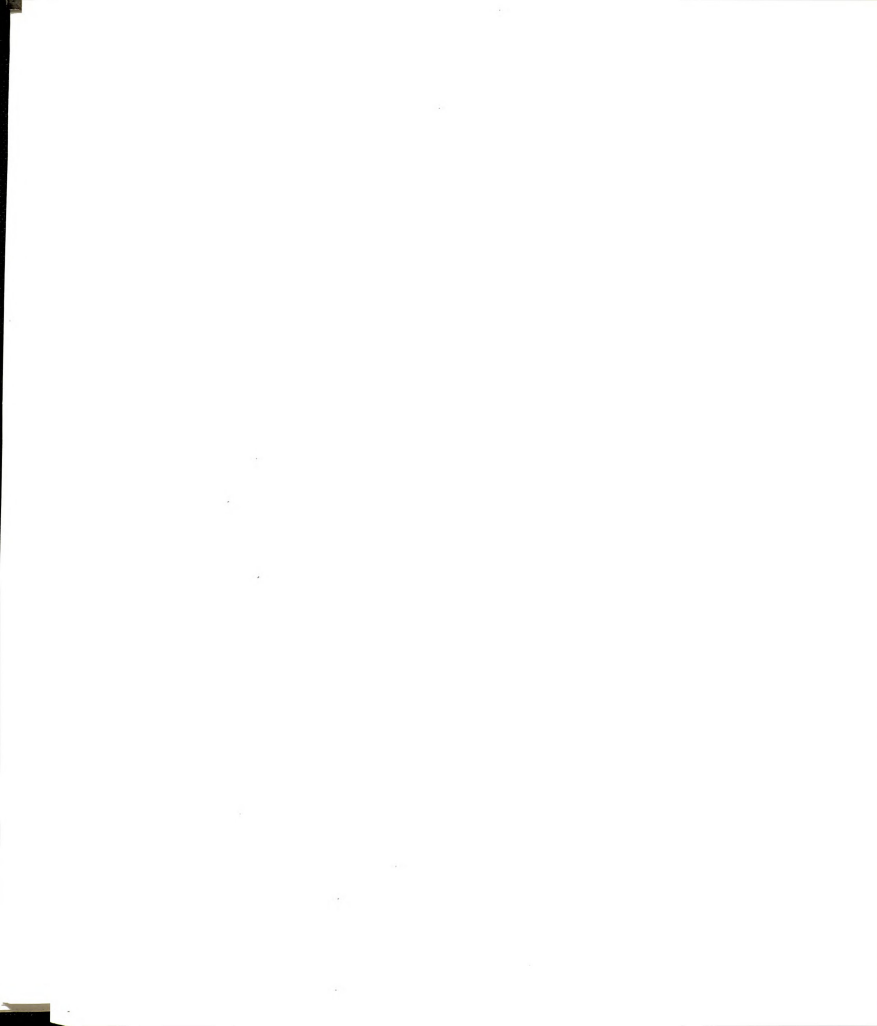
10 Read data: plate geometry, boundary conditions,  $V_{\max}$ ,
    $h_1$ ,  $h_2$ , material properties.
20 Assign uniform distribution of  $\rho$  and moments.
30 Compute effective properties using homogenization.
40 Solve equilibrium equation using finite element
   methods to get the strains.
50 Solve the local problem and obtain optimum values of
    $m_1$ ,  $m_2$ ,  $m_3$  and  $m_4$ .
60 Compute optimality condition ratio for each element.
70 Update distribution of  $\rho$  in the global problem.
80 Check convergence:
   If converged, PRINT RESULTS, else goto 30
90 Stopping criterion:
   If  $k > \text{Limit of Iteration}$ , PRINT RESULTS and STOP,
   else goto 30
100 Post-Processing: Plot optimum shape, and compute the
    geometry of the micro structure.
```

After reading the data (10), a uniform distribution of the design variables is assigned to the whole domain (20). Using explicit formulas developed in Chapter 3, effective properties are computed for each finite element in the mesh (30). Then, the equilibrium equations are solved calling the finite element program (40). Non-linear programming techniques are used to solve the local problem in (50) to obtain  $m_1^*$ ,  $m_2^*$ ,  $m_3^*$  and  $m_4^*$  for



given density  $\rho$  and given strain fields. In (60) the sensitivity of the potential energy with respect to the resource  $\rho$  is computed in order to obtain the optimality condition ratio with (4.2.5). Step (70) corresponds to the updating of the distribution of  $\rho$  in the global optimization problem using the optimality condition approach. Finally, the convergence is checked (80) and the stopping criterion is in (90). Results are revised off-line in a post-processing step (100).





## CHAPTER 5 EXAMPLES

This chapter is devoted to the solution of some layout optimization example problems using the homogenization approach and the stiffness properties for rank-2 and rank-L derived in Chapter 2 and 3, respectively. Optimum shapes will be presented in a gray scale (see Figure 5.1) where areas where the plate is of thickness  $2h_2$  are denoted by black, and the core plate of thickness  $2h_1$  by white. Gray areas indicate the presence of rapidly varying thickness between  $2h_1$  and  $2h_2$ , i.e., a composite material plate. In the iteration histories the mean compliance is normalized using the mean compliance of a uniform thickness plate made with the same amount of material. The isotropic material used in all examples has Young modulus  $E=2 \cdot 10^{11}$  Pa and Poisson ratio  $\nu=0.3$ . The weak material used to model the perforations and gaps between ribs has a Young modulus that is 5% of the strong material.

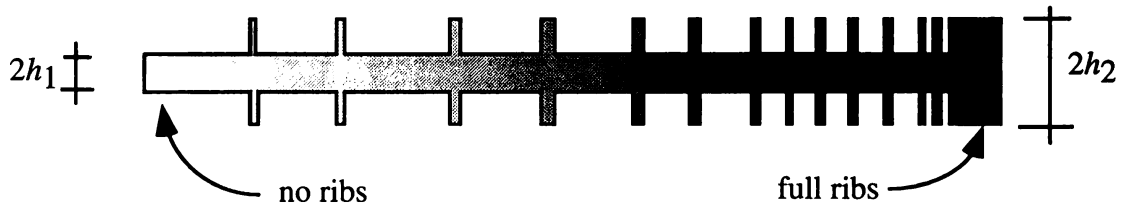


Figure 5.1. Gray scale to identify the cross section of the plate in the optimum shapes.

### Optimality Condition Satisfaction

The simplest way to measure the satisfaction of the optimality conditions is counting the number of ribbed finite elements, i.e., elements with  $\rho_{min} < \rho < 1$ , for each value of the optimality condition ratio (O.C.R.)  $\Xi_i$ . With this information it is possible to construct a histogram of the percentage of ribbed elements for each O.C.R. value as shown in Figure 5.2. Theoretically, when optimality conditions are satisfied, such histograms must show



a single peak of value 1 at  $\Xi_i = 1$ . Figure 5.2 shows an optimality condition histogram from a real problem where the micro structure was modeled using rank-2 materials with rib widths  $a$  and  $b$ . Notice that peaks at  $\Xi_i = 1$  are less than 70% of the total ribbed elements, but between 0.9 and 1.1 in the horizontal axis the percentage of ribbed elements adds up to more than 90%. This can be considered as a good result.

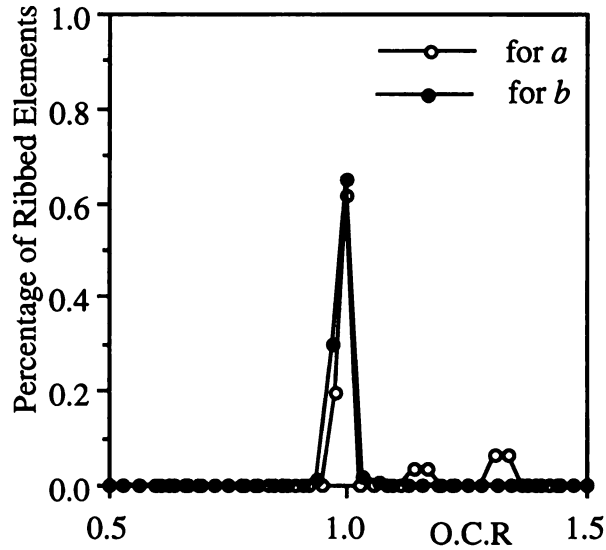


Figure 5.2. Typical histogram for optimality condition.

This chapter is divided in four sections. In section 5.1 the homogenized plate model developed in Chapter 2 is compared with results from a previous work of Cheng and Olhoff, (1981). In section 5.2 a parametric study is performed to show the influence of some parameters involved in the optimization problem. In section 5.3 there is a comparison of optimum shapes computed with the rank-2 and rank-L micro structures, and finally, in section 5.4 some industrial examples are solved, showing the applicability of the approach in mechanical design.

## 5.1 Comparison with Previous Work

In 1981 Cheng and Olhoff used the thickness of the plate as design variables to compute the optimum shape of square plates subject to a uniform transverse load. Their results are compared here with the rank-2 plate model derived in Chapter 2. The rank-L plate model



developed in Chapter 3 gives very similar results to the rank-2 model, therefore, we decided not to include the rank-L results in this example.

Figure 5.3 shows the geometry of the plate. The dimensions are  $L_x=L_y=500$  mm, and thicknesses,  $2h_2=10$  mm,  $2h_1=6.67$  mm. The area fraction prescribed to build the ribs is  $V_{max}=0.5$ , meaning that the ribbed area will cover  $0.5*L_x*L_y=125,000$  mm<sup>2</sup>. The transverse uniform load is of unit magnitude. We study two different boundary conditions, simply supported (pinned) and clamped on all sides. The optimum shapes are: Figures 5.4(a) and (b) for the simply supported and clamped plate, respectively, using rank-2 materials; Cheng and Olhoff's results are presented in a three-dimensional view in Figure 5.5 and 5.6. Iteration histories for the rank-2 material plate are shown in Figure 5.7, and the histogram of the optimality conditions is plotted in Figures 5.8(a) and (b) for simply supported and clamped boundary conditions, respectively.

Optimum shapes computed with the rank-2 model are very similar to the results of Cheng and Olhoff for both boundary conditions. The concentration of material in the corner of simply supported plates is due to the stress concentration produced by the known "corner effect" in plates. For the simply supported plate the normalized compliances computed with both methods, i.e., Cheng-Olhoff and homogenization methods, are practically the same. For the clamped boundary conditions, the rank-L plate model gave a more rigid plate,  $C^*=0.65$ , than the result reported by Cheng and Olhoff,  $C^*=0.71$ ., however, this difference is only of 9%. Optimum shapes computed with thickness as design variable (Cheng and Olhoff's method) attain the same optimum shape obtained using composite material plates because, for these cases, the optimum shape is formed by small areas of composites, therefore, the advantages of using microscopically ribbed plates does not appear. Histograms of the optimality conditions for the rank-2 material plate present single high peaks, which indicates satisfaction of the optimality conditions at the optimum shape computed.



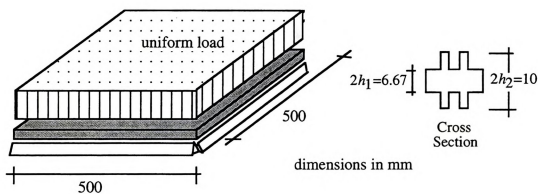
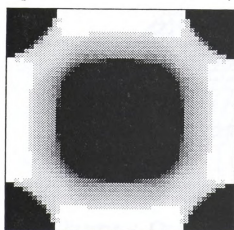
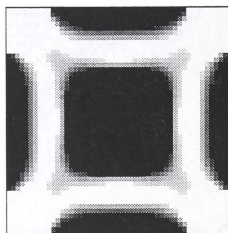


Figure 5.3. Example 1: geometry and loads.



(a) Pinned plate,  $C^* = 0.80$ .



(b) Clamped plate,  $C^* = 0.65$ .

Figure 5.4. Example 1: optimum shapes with rank-2 materials.





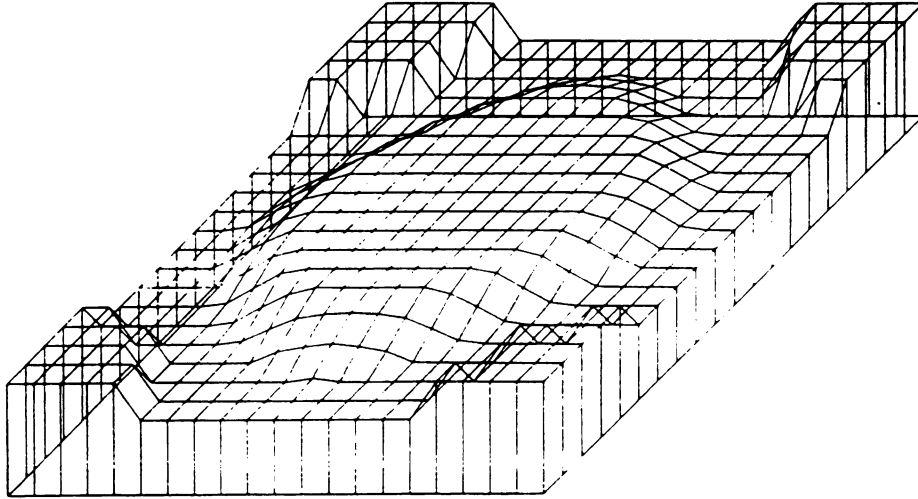


Figure 5.5. Example 1: Cheng and Olhoff (1981) result for the pinned plate,  $C^*=0.82$ .

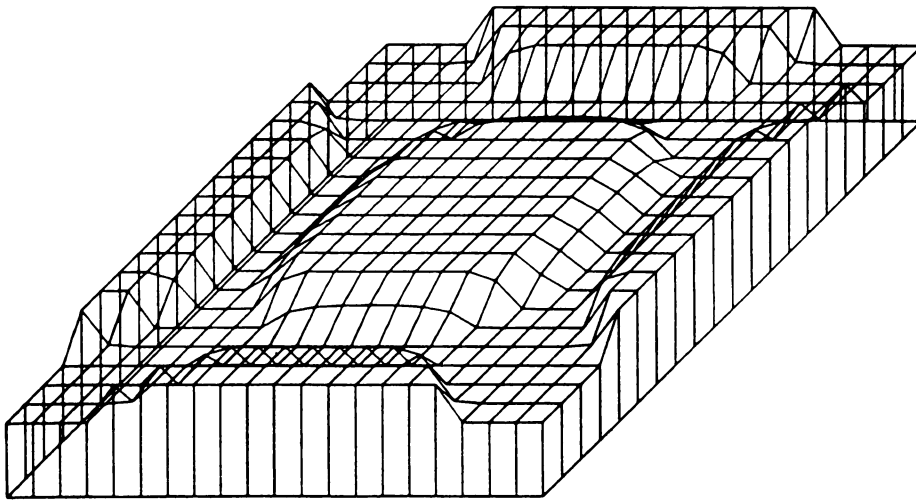


Figure 5.6. Example 1: Cheng and Olhoff (1981) result for the clamped plate,  $C^*=0.71$ .

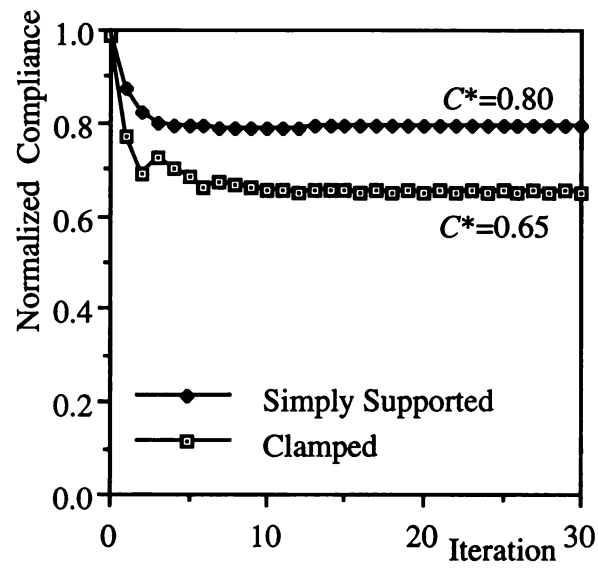


Figure 5.7. Example 1: iteration histories.

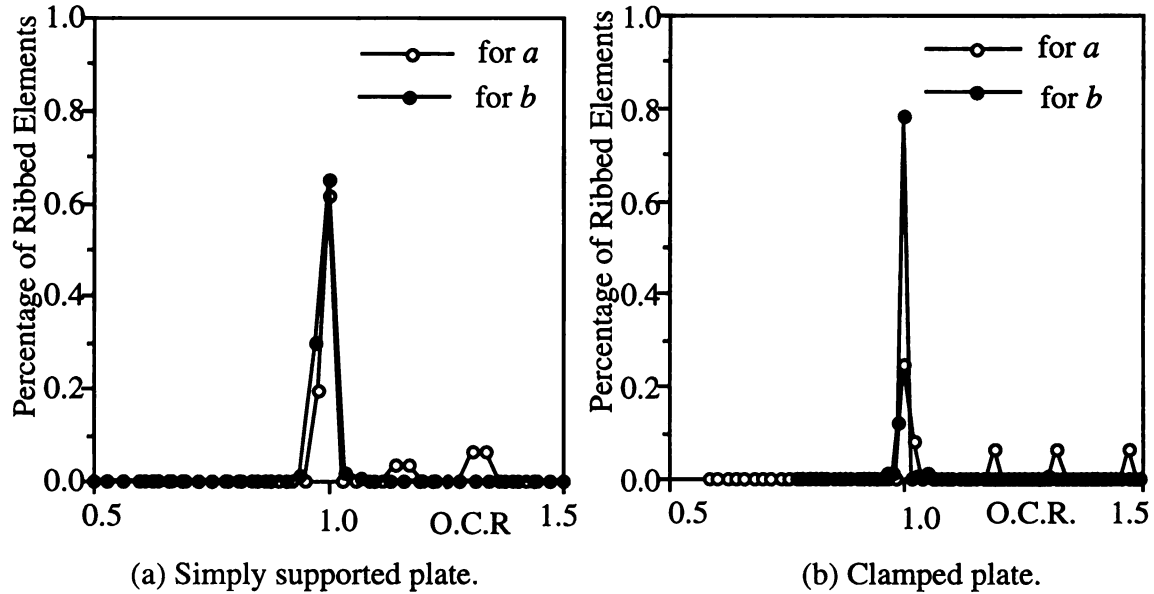


Figure 5.8. Example 1: optimality condition ratio histograms.

## 5.2 Comparison of Micro Structure Models

In this section we solve two example problems and compare the optimum shapes given by the homogenized plate models presented in chapters 2 and 3.

### 5.2.1 Uniform Transverse Load

A simply supported square plate subject to a uniform transverse load is studied (see Figure 5.9). The thicknesses are  $2h_2=10$  mm and  $2h_1=2$  mm, and the prescribed area fraction to build ribs is 50% of the plate area. Figures 5.10(a) and (b) show the optimum shape for the rank-2 material plate and rank-L models, respectively.

The distribution of the number of layers that is obtained for each micro structure model is shown in Figures 5.11-5.13. In these figures the black areas denote locations where the material has the number of layers indicated, and white areas denote locations where the material is isotropic of thickness  $2h_1$  or  $2h_2$ , or where the material has a different number of layers. Notice, for example, that the distribution of materials with only one layer of ribs (see Figures 5.11(a) and (b)) is very similar for both micro structure models. Materials with two layers (see Figures 5.12(a) and (b)) appear at the corners of the plate for both models, but near the center of the plate the rank-2 model produces more materials with two layers than the rank-L model. This difference is caused by the third layer that can be used by the rank-L model (see Figure 5.13). If Figures 5.12(b) and 5.13 are combined, which correspond to the two-layer and three-layer materials obtained with the rank-L model, respectively, we obtain a picture similar to that shown in Figure 5.12(a), which corresponds to the two-layer material obtained with the rank-2 model. In other words, at locations where the rank-L model assigns three-layer materials, the rank-2 model assigns the stiffest ribbed material that it can create, i.e., a two-layer material.

It can be seen that the two optimum shapes are very similar although the rank-L model allows us to use stiffer micro structures with three layers. Also notice that there is little use of three-layer materials in the rank-L solution. These two observations indicate that in this problem the difference in stiffness between the rank-2 and rank-3 materials may be small, therefore, the rank-2 model is able to produce results as good as the rank-L model.

The iteration histories for both models (see Figure 5.14) are very similar and the optimum normalized compliance is  $C^*=0.41$ . The optimality condition histograms (see Figure 5.15) show that both models satisfy the optimality conditions quite well.

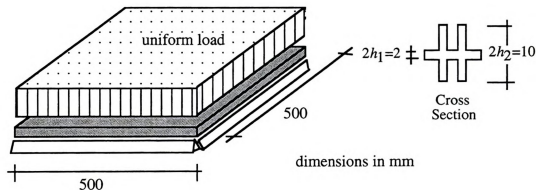
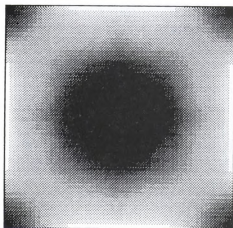
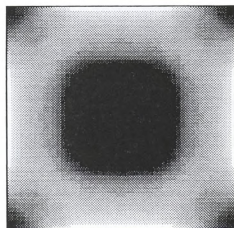


Figure 5.9. Example 2: geometry and loads.



(a) Using rank-2 micro structure.



(b) Using rank-L micro structure.

Figure 5.10. Example 2: optimum shapes.



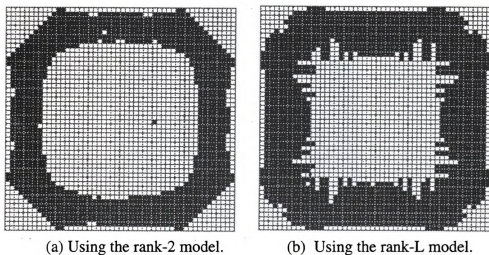


Figure 5.11. Example 2: distribution of one-layer materials in the plate.

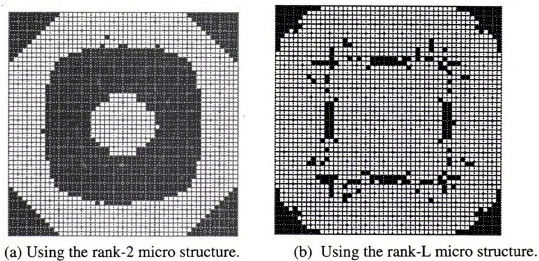


Figure 5.12. Example 2: distribution of two-layer materials in the plate.

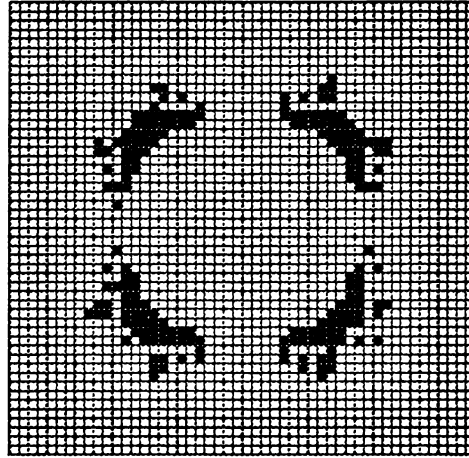


Figure 5.13. Example 2: distribution of three-layer materials using the rank-L micro structure.

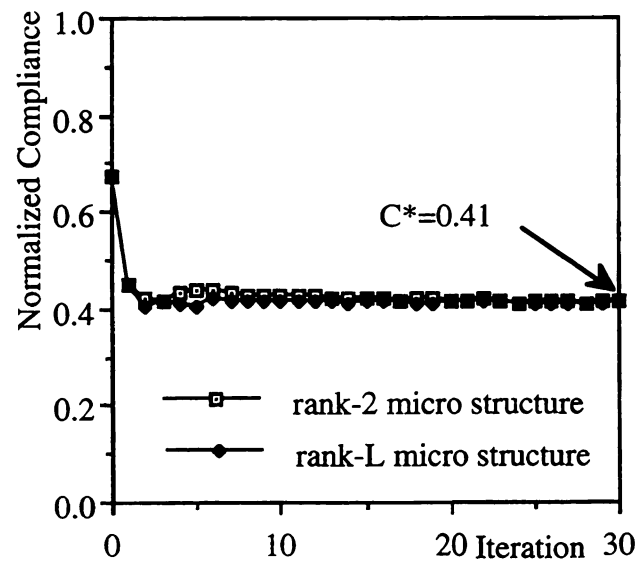


Figure 5.14. Example 2: iteration histories.



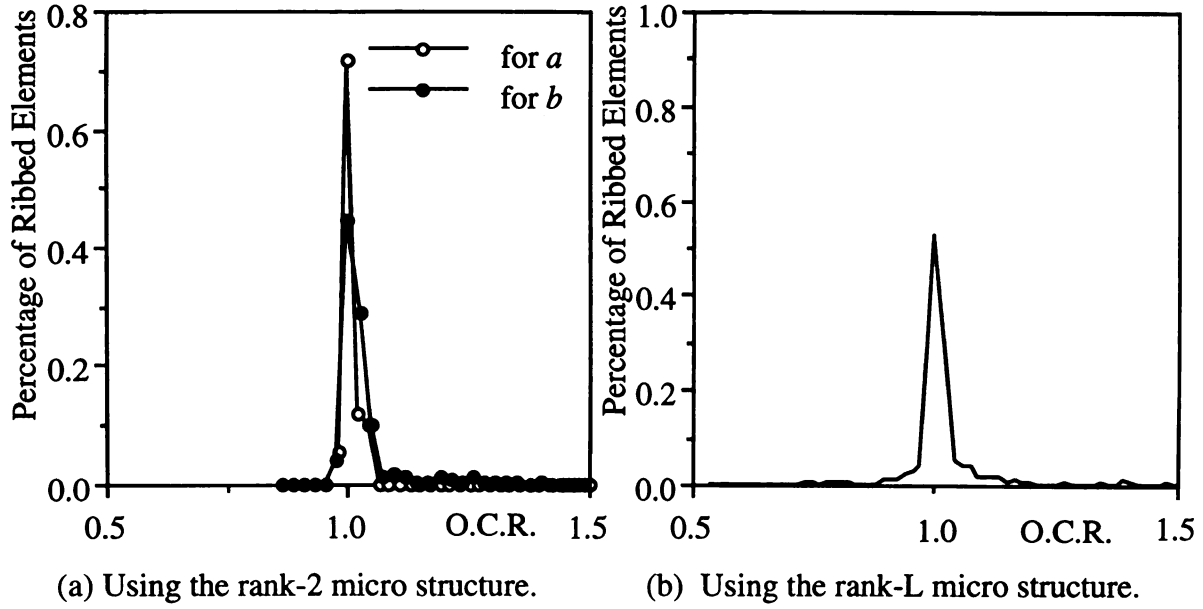


Figure 5.15. Example 2: optimality condition ratio histograms.

### 5.2.2 Point Loads on the Diagonals

In this example we study a simply supported square plate subject to four independent load cases as shown in Figure 5.16. The thicknesses are  $2h_2=10$  mm and  $2h_1=2$  mm, and the prescribed area fraction to build ribs is 50% of the plate area. Optimum shapes are shown in Figures 5.17(a) and (b) for the rank-2 and rank-L models, respectively. Notice that both optimum shapes are again very similar and the presence of three-layer materials is not significant (see Figure 5.20). Distributions of one-layer and two-layer materials are shown in Figures 5.18 and 5.19. The same conclusions drawn from the previous example can also be applied in this case, namely, the rank-2 micro structure is stiff enough to attain an optimum ( $C^*=0.32$ ) very close to the optimum attained when a rank-L micro structure is used ( $C^*=0.31$ ) (see Figure 5.21). Again, optimality condition ratio histograms (see Figures 5.22(a) and (b)) show that at the optimum solution both models satisfy the optimality conditions very well.

From this example and the previous one may say that the availability of three-layer materials in the rank-L micro structure did not make a substantial difference in the optimum solution obtained.

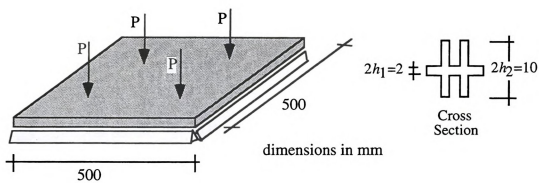
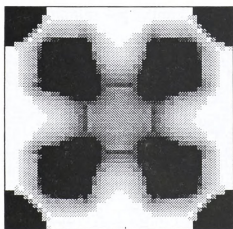
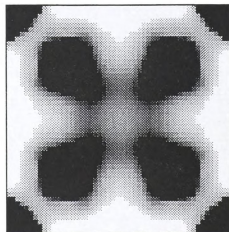


Figure 5.16. Example 2: geometry and loads.

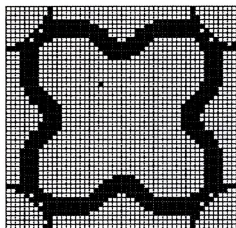


(a) Using rank-2 micro structures.

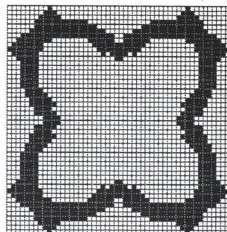


(b) Using rank-L micro structures.

Figure 5.17. Example 2: optimum shapes.

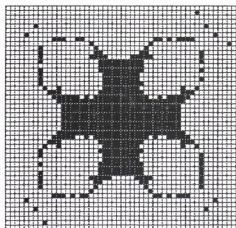


(a) Using the rank-2 micro structure.

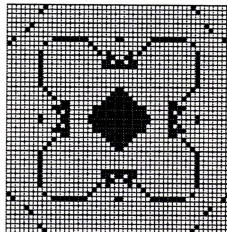


(b) Using the rank-L micro structure.

Figure 5.18. Example 2: distribution of one-layer materials in the plate.



(a) Using the rank-2 micro structure.



(b) Using the rank-L micro structure.

Figure 5.19. Example 2: distribution of two-layer materials in the plate.

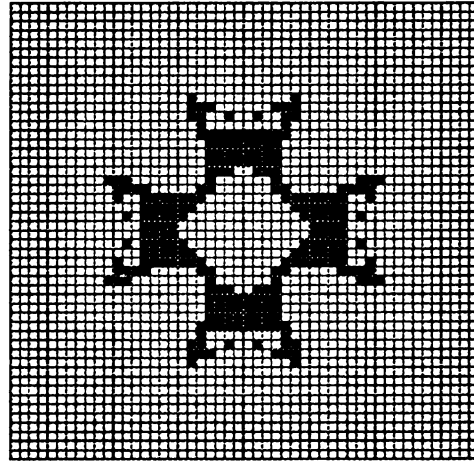


Figure 5.20. Example 2: distribution of three-layer materials using the rank-L micro structure.

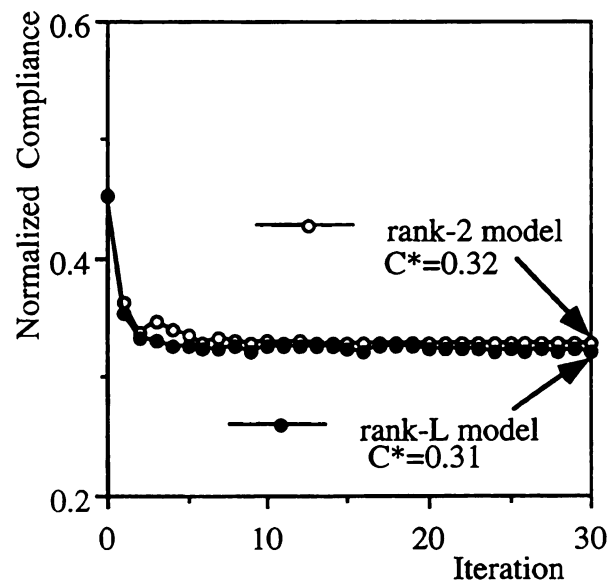


Figure 5.21. Example 2: iteration histories.



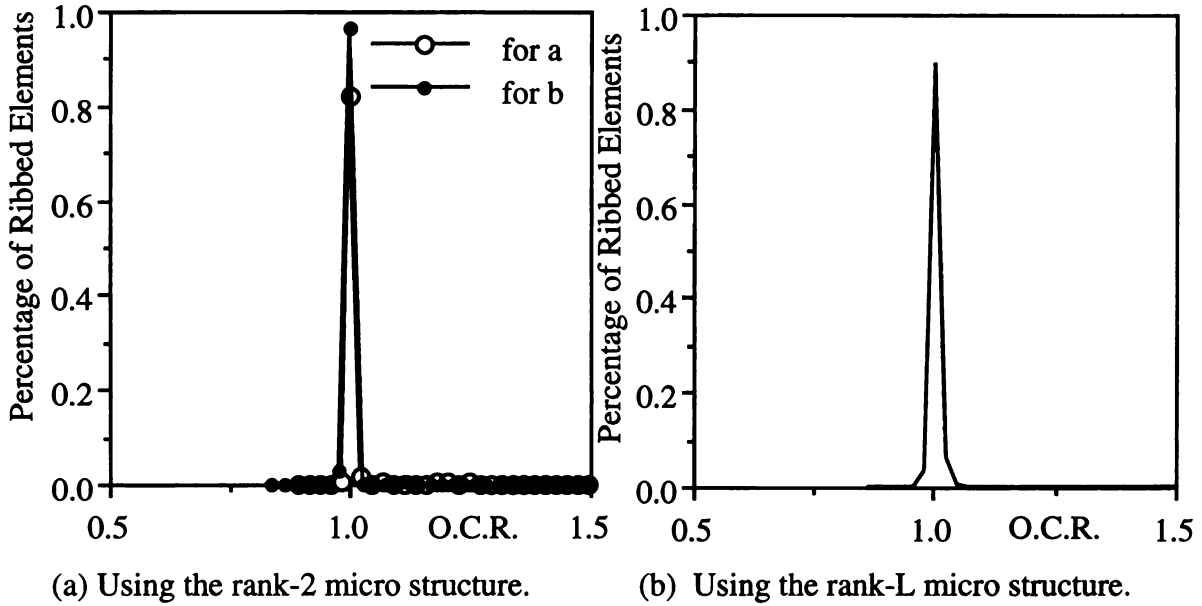


Figure 5.22. Example 2: optimality condition ratio histograms.

### 5.3 Parametric Study

In these examples we perform a parametric study of variables that appear in the formulation of the layout optimization problem. The effect of the thickness ratio  $r=h_2/h_1$ , the amount of material  $V_{max}$  and the type of cross section (ribbed, honeycomb or perforated) on the optimum shape is studied.

#### 5.3.1 Influence of the Thickness Ratio $r=h_2/h_1$

In this example a simply supported rectangular plate (Figure 5.23) is considered to study the effect of the thickness ratio on the optimum shape of the plate. The total thickness is fixed at  $2h_2=25$  mm and the core plate thickness  $2h_1$  is computed such that three values of the thickness ratio are considered, namely,  $r=h_2/h_1=1.5, 3$  and  $6$ . The prescribed amount of material used to build ribs is 20%.

Optimum shapes using the rank-2 material plate are shown in Figure 5.24. Notice that for high values of  $r=h_2/h_1$ , the optimum shape presents more areas with ribs (gray areas)

in comparison with the optimum shapes for low values of  $r$ . This happens because a required level of stiffness can be obtained with less material when the ribs are higher. In other words, when the ratio between the stiffness of the strong plate and the stiffness of the weak plate is high more gray areas are expected in the optimum shape. Iteration histories in Figure 5.25 show that tall ribs ( $r=6$ ) can achieve a reduction of 83% of the compliance of a uniform thickness plate, while short ribs ( $r=1.5$ ) can only reduce 21%.

The three optimum shapes shown in Figures 5.24 produce important reductions in the compliances and have good iteration histories (see Figure 5.25). When the histograms of the optimality condition ratio are computed (see Figure 5.26) one can see that for the rib width “ $a$ ” there are always several peaks far from the main peak. A closer look at the results showed that the number of elements satisfying  $a_{min} < a < 1$  was less than 10% of the total number of elements in the mesh, meaning that the poor satisfaction of the optimality conditions for “ $a$ ” is not so important. Additionally, it was found that the number of elements satisfying  $a > a_{min}$  was the same as before, that is, about 90% of the elements had  $a = a_{min}$ , meaning that the width “ $b$ ” was giving the optimum shape and “ $a$ ” did not participate much in the optimum solution.

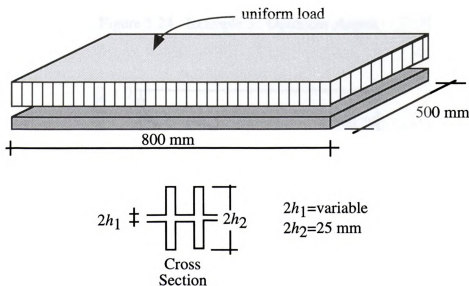


Figure 5.23. Example 3: geometry and loads.

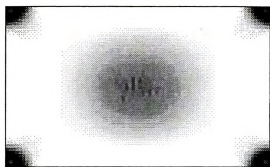
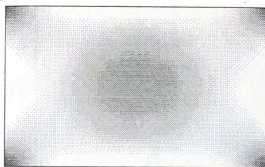
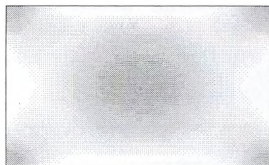
(a) For  $h_2/h_1=1.5$ (b) For  $h_2/h_1=3.0$ (c) For  $h_2/h_1=6.0$ 

Figure 5.24. Example 3: Optimum shapes.

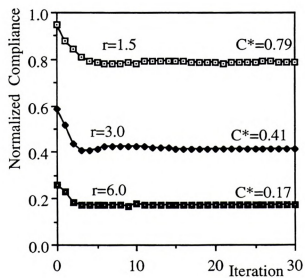
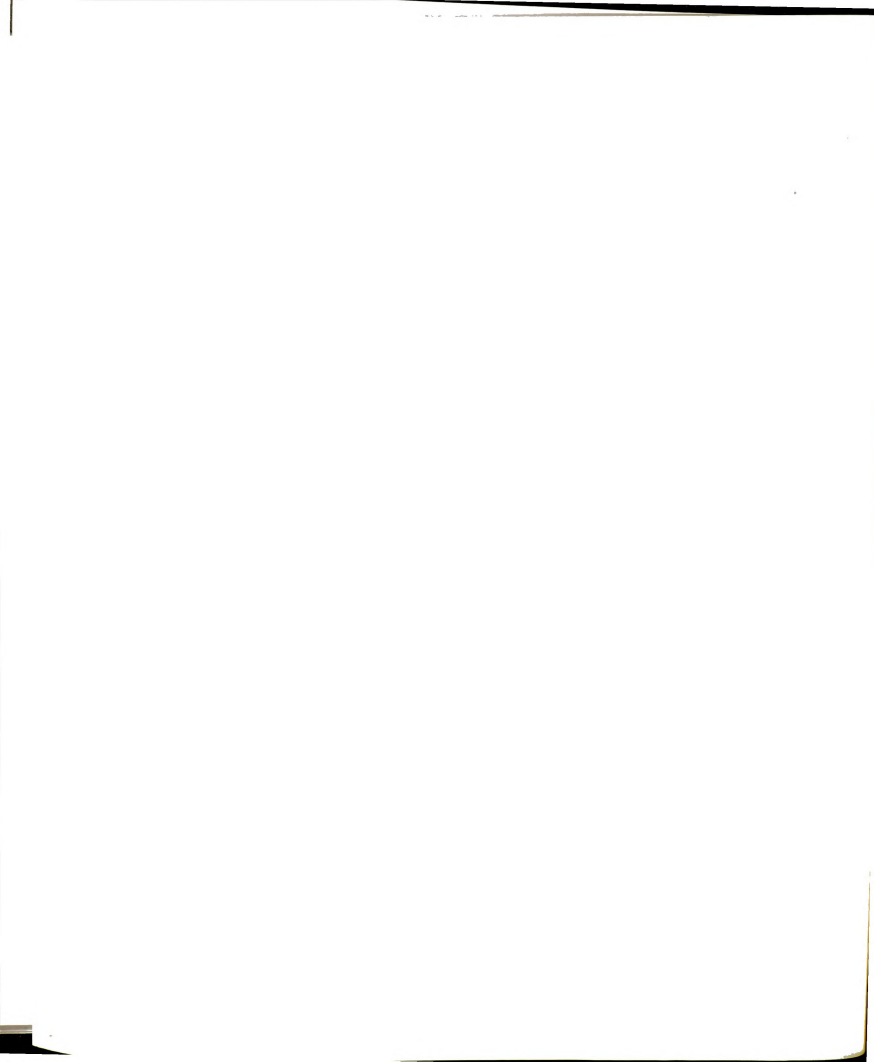


Figure 5.25. Example 3: Iteration histories.





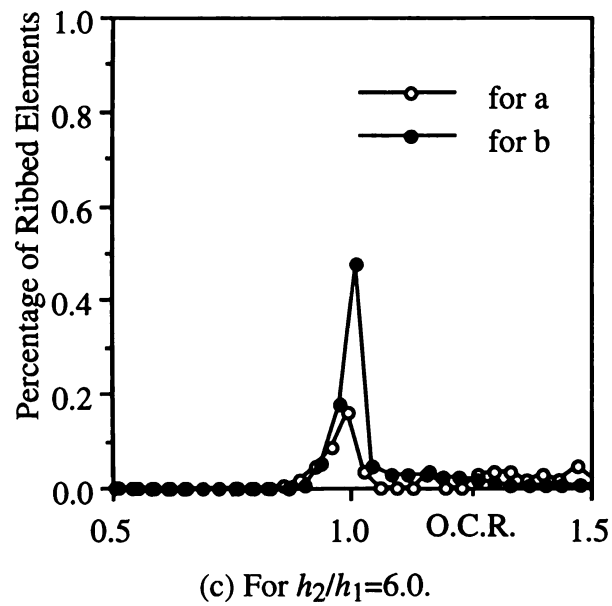
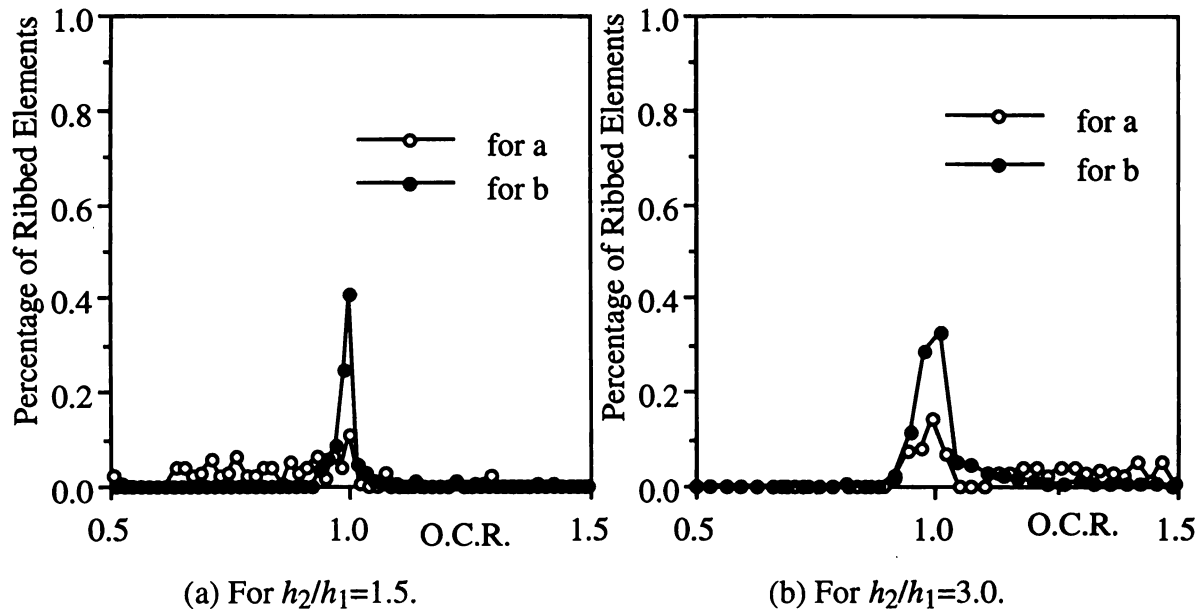
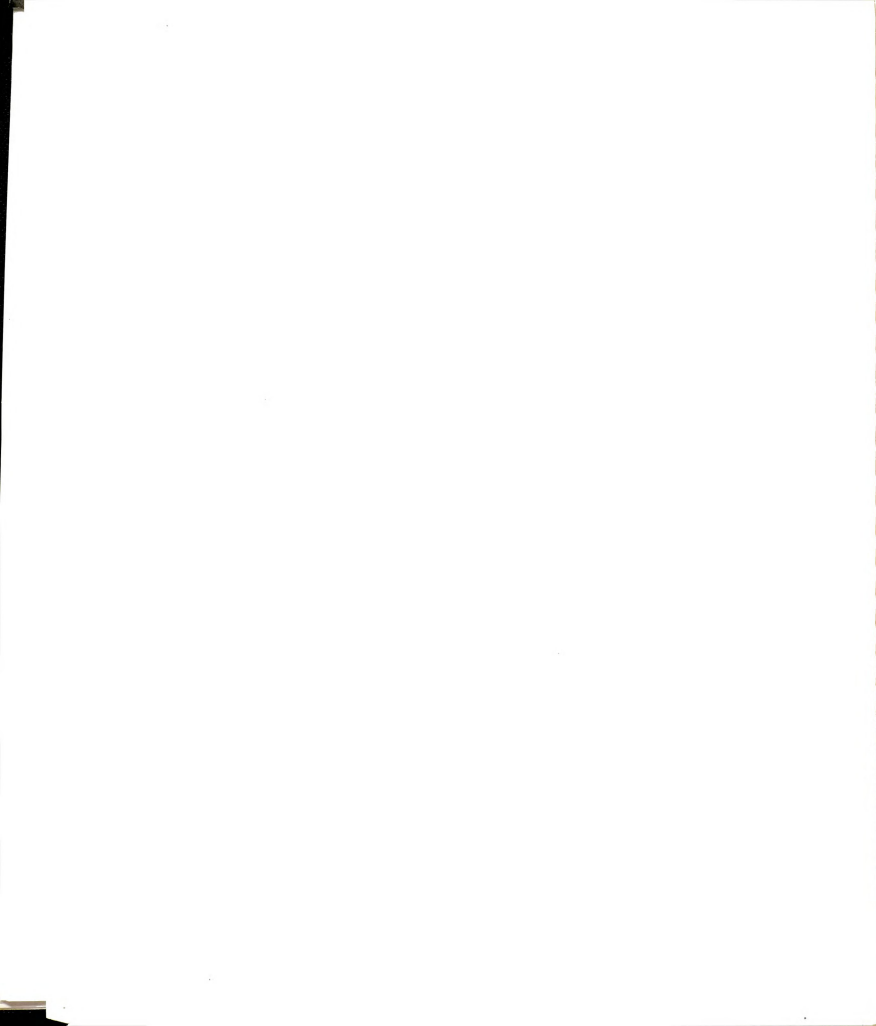


Figure 5.26. Example 3: optimality condition ratio histograms.



### 5.3.2 Influence of the Amount of Material $V_{max}$

In this example we study the variation of the optimum shape with changes in the prescribed area fraction of ribs,  $V_{max}$ . A clamped rectangular plate (Figure 5.27) of dimensions 800mm x 500mm subject to a uniform transverse load is studied for four different amounts of material,  $V_{max}=5\%$ , 10%, 20% and 40% of the plate area. The thicknesses are fixed at  $2h_2=5\text{mm}$  and  $2h_1=1\text{mm}$ . Optimum shapes are given in Figure 5.28.

It is important to realize that each time more material is added, this material is not only used to reinforce areas that already had ribs -- which would imply that the topology does not change --, but is also used to reinforce new areas that did not have ribs previously. This produces new topologies as the material is added to the plate. More black areas with thickness  $2h_2$  appear as more material is available to allocate ribs. The concentration of material on the sides of the plate is a characteristic of the clamped plates that also was seen in the example of comparison with Cheng and Olhoff results above. The iteration histories (see Figure 5.29) indicate that the more material is used, the less improvement on the minimization of the compliance is achieved. This is consistent with the limit case of  $V_{max}=100\%$  that corresponds to  $C^*=1$ . Notice that a reduction of almost 90% in the compliance is achieved when the amount of material is less or equal to 10%. Optimality condition histograms showed in Figure 5.30 indicate a good satisfaction of the optimality conditions. Notice that when  $V_{max} \leq 10\%$  there are no plots for the optimality conditions for  $a$ . This is because the optimum shape only uses one-layer materials of width  $b$ , and  $a=0$ , therefore, there are no points to plot for the rib width  $a$ .

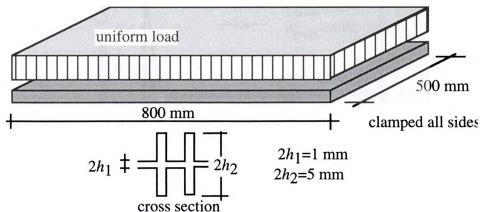


Figure 5.27. Example 3: geometry and loads.



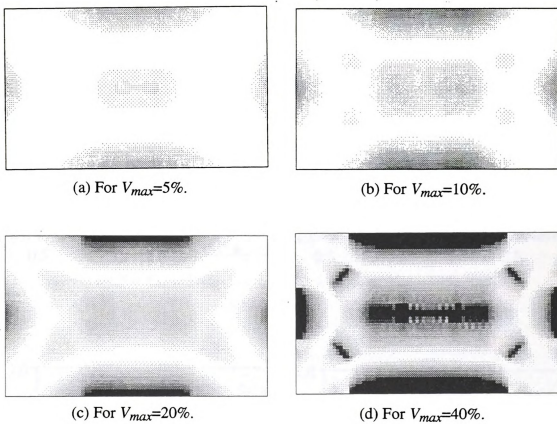


Figure 5.28. Example 3: optimum shapes.

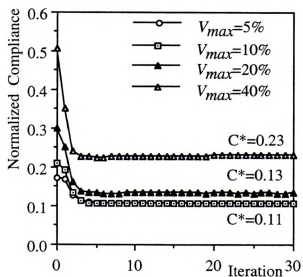


Figure 5.29. Example 3: iteration histories.

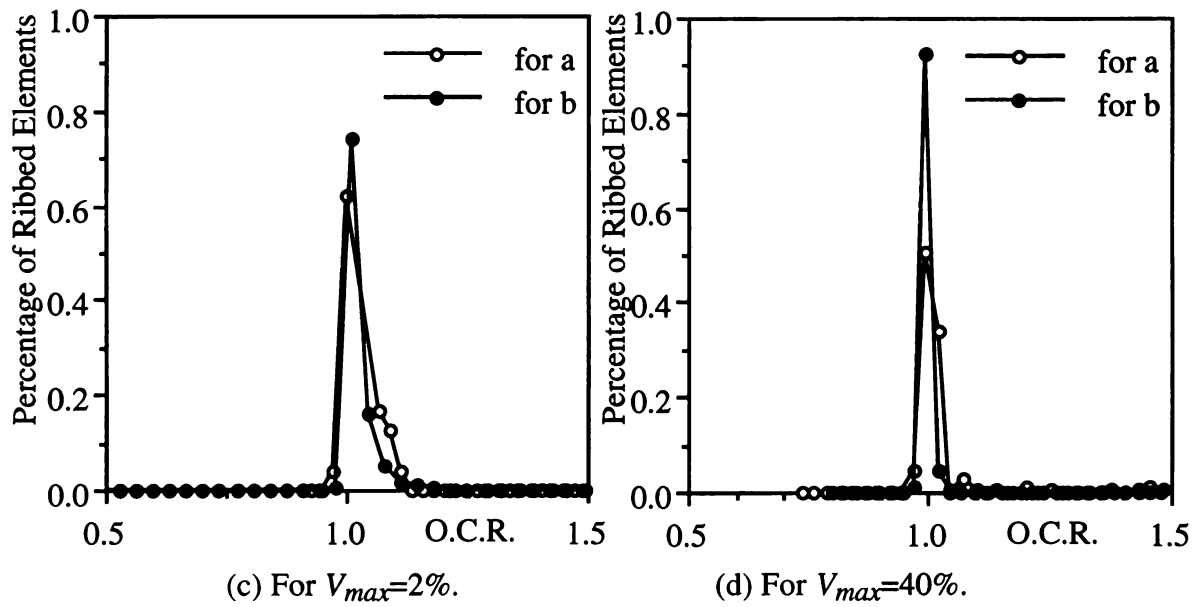
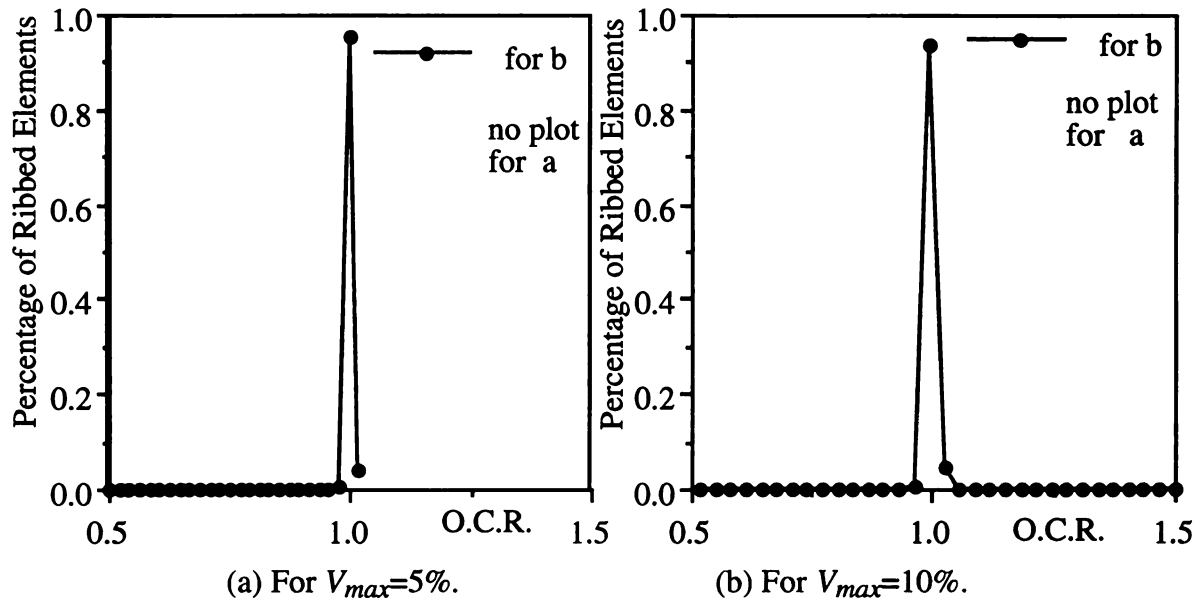


Figure 5.30. Example 3: optimality condition ratio histograms.

### 5.3.3 Comparison of Cross Sections

In this example, the effect of the cross section on the optimum shape is studied. A simply supported plate subject to five simultaneous point loads (see Figure 5.31) is considered for the experiment. The area fraction of ribs is  $V_{max}=50\%$  and the dimensions of the ribbed cross section are  $2h_2=15$  mm and  $2h_1=5$  mm. The honeycomb cross section has the same external thickness  $2h_2$  and the height of the internal ribs is such that the amount of material is the same as in the ribbed plate. The perforated cross section has a thickness of  $2h_2=20$ mm to preserve the amount of material for the three cross sections studied.

When the ratios between the bending stiffness of the strong plate and the stiffness of the weak plate are computed for each cross section, the results are, 1.4 for the honeycomb, 27.0 for the ribbed, and  $\infty$  for the perforated cross section. Therefore we can see this experiment as if we were studying three different thickness ratios  $r=h_2/h_1$  such that the thicknesses produce the three stiffness ratios computed above. The optimum shapes in Figure 5.32 are consistent with the results obtained when we studied the effect of the ratio  $h_2/h_1$ , namely, large areas of rapidly varying thickness for the relatively stiffer cross section (the perforated one) and small areas of rapidly varying thickness for the relatively less stiff cross section (the honeycomb one). The ribbed cross section gives an intermediate result between the perforated and the honeycomb cross sections. Iteration histories and optimality condition histograms are shown in Figures 5.33 and 5.34, showing a good convergence and satisfaction of the optimality conditions. For the honeycomb cross section, Figure 5.34(c), peaks far away from the main peak (for the width "a") are not important since only 5% of the elements of the mesh satisfy  $a_{min} < a < 1$  and only few of them do not satisfy optimality conditions.

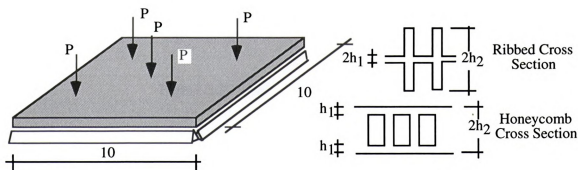
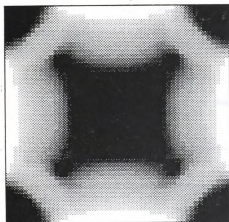


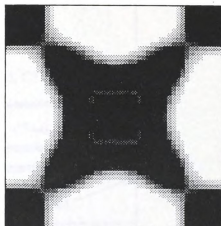
Figure 5.31. Example 3: geometry and loads.



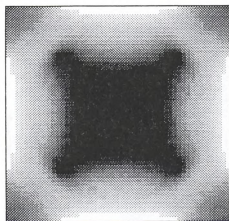




(a) For the ribbed cross section.



(b) For the honeycomb cross section.



(c) For the perforated cross section.

Figure 5.32. Example 3: optimum shapes.

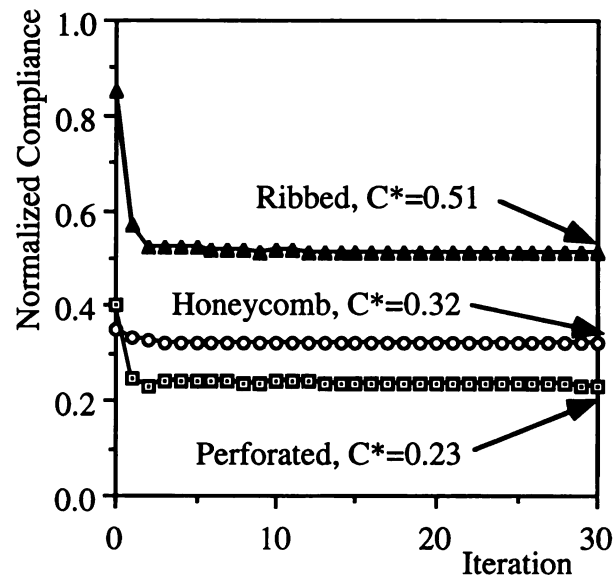


Figure 5.33. Example 3: iteration histories.

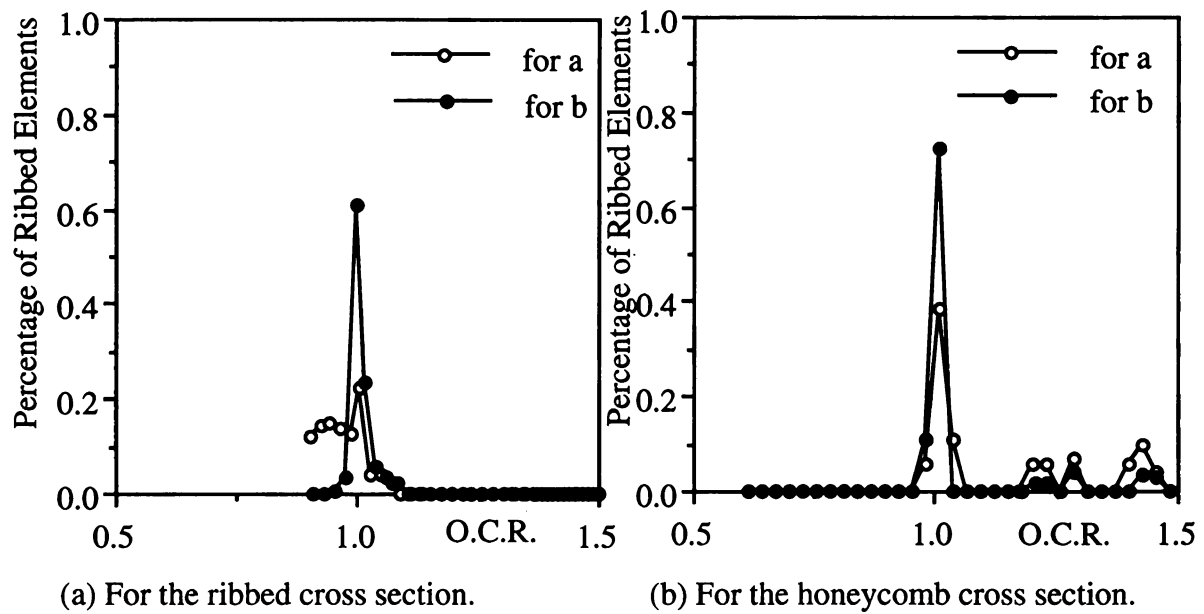
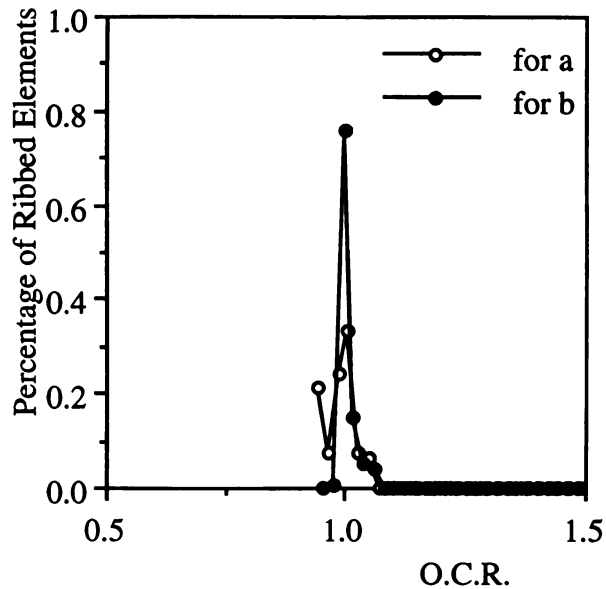


Figure 5.34. Example 3: optimality condition ratio histograms.





(c) For the perforated cross section.

Figure 5.34. (cont.) Example 3: optimality condition ratio histograms.

## 5.4 Industrial Examples

### 5.4.1 A Car Hood

In this example we compute the optimum reinforcement of a car hood subject to three independent load cases, a frontal load and two lateral loads as shown in Figure 5.35. The two lateral loads are applied independently but always together such that the resulting optimum shape is symmetric. These loads simulate the crash of the car from the front and from the sides. The weighted compliance is computed using equal weights. In this case we use a perforated cross section with total thickness  $2h_2=1$  mm and the prescribed amount of material covers 30% of the area of the hood shell.

When the frontal and lateral loads are studied separately we obtain the two optimum shapes shown in Figures 5.36(a) and (b), respectively. Notice that more material is allocated where the loads are applied.

When the three load cases are considered, the optimum shape obtained is that shown in Figure 5.36(c). Since we are using a perforated cross section, large gray areas (rapidly



varying thickness plate areas) appear in the optimum shape. The iteration histories of the normalized compliance (Figure 5.37) show that the reduction in compliance for the three load cases (the frontal and the two lateral loads) is almost 70% of the uniform thickness plate compliance. If we were to build the hood, we could interpret the optimum reinforcement in Figure 5.36(c) as is shown in Figure 5.38. The prescribed amount of material is violated in Figure 5.38, but the essence of the optimum shape is preserved.

This problem was also studied using the rank-L micro structure model of Chapter 3. In this case, we only studied the situation when the three loads were applied. The optimum shape is shown in Figure 5.39 and the iteration history in Figure 5.40. Both micro structures, the rank-2 and the rank-L, give basically the same optimum shape and the same final normalized compliance. Again, the use of a stiffer micro structure did not improve the optimum shape or the normalized compliance. Optimality condition histograms are shown in Figure 5.41.

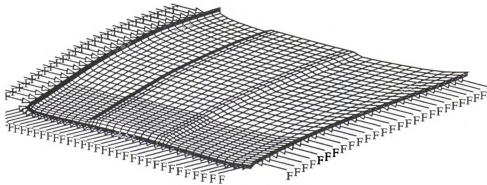
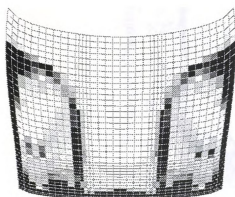


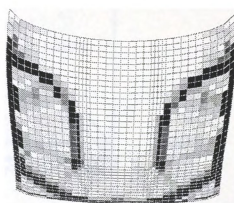
Figure 5.35. Example 4: geometry and loads.



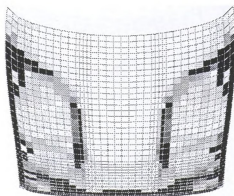




(a) Frontal load.



(b) Two lateral loads.



(c) Frontal and lateral loads.

Figure 5.36. Example 4: optimum shapes.



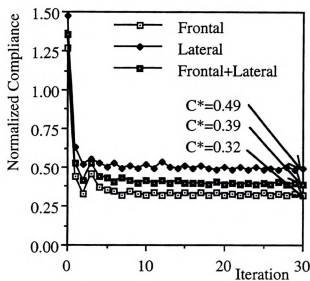


Figure 5.37. Example 4: iteration histories.



Figure 5.38. Example 4: Interpretation of the optimum shape of the car hood.



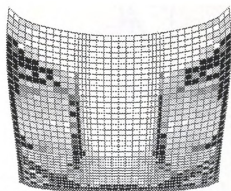


Figure 5.39. Example 4: optimum shape obtained using the rank-L micro structure.

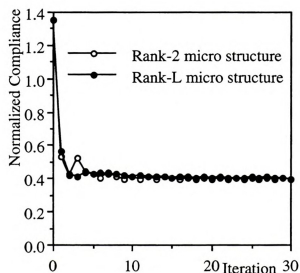


Figure 5.40. Example 4: iteration histories.



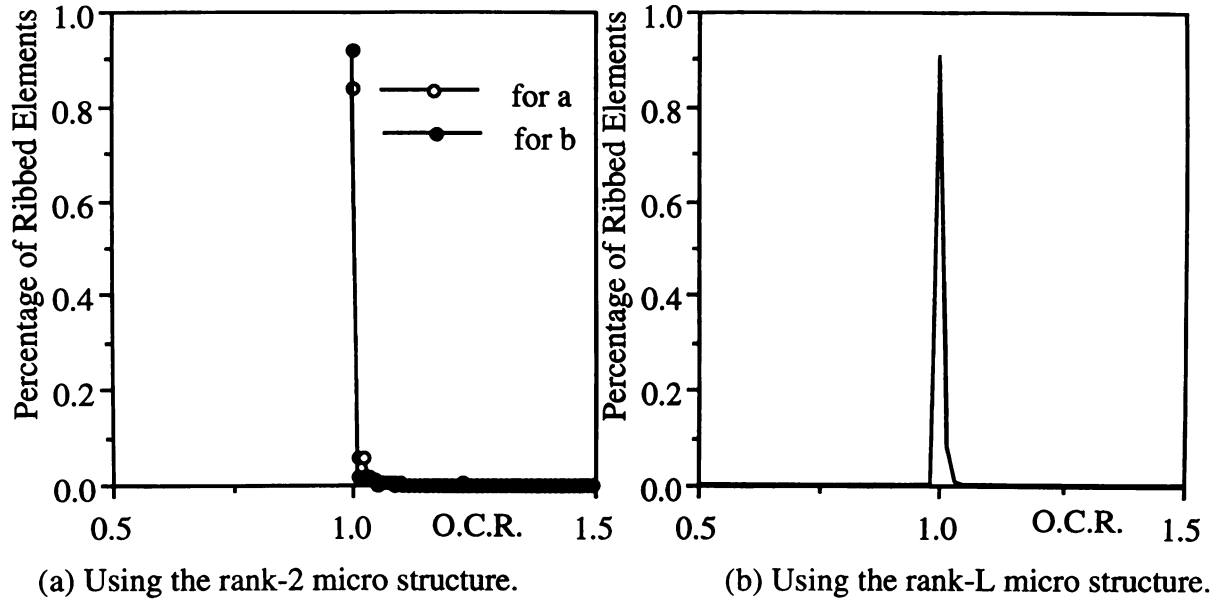


Figure 5.41. Example 4: optimality condition ratio histograms.

#### 5.4.2 A Car Door

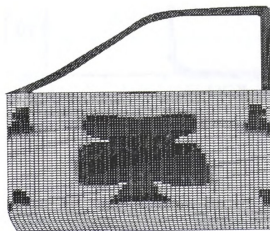
Figure 5.42 shows the geometry of a car door that is subject to a point load at the center of the main panel and is supported at four points. The thicknesses are  $2h_2=1$  mm and  $2h_1=0.67$  mm, and the prescribed amount of material is  $V_{max}=35\%$ . The frame of the window has fixed thickness equal to  $2h_2$  and is not considered in the optimization problem. The problem was solved using the rank-2 and the rank-L micro structures. The optimum shapes obtained are shown in Figures 5.43(a) and (b). One more time, optimum shapes computed with both micro structures are very similar. The optimum normalized compliance is  $C^*=0.64$  for both shapes. Histograms in Figures 5.45 indicate that optimum shapes satisfy optimality conditions satisfactorily.



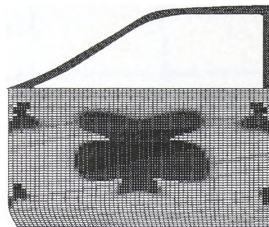




Figure 5.42. Example 5: geometry and loads.

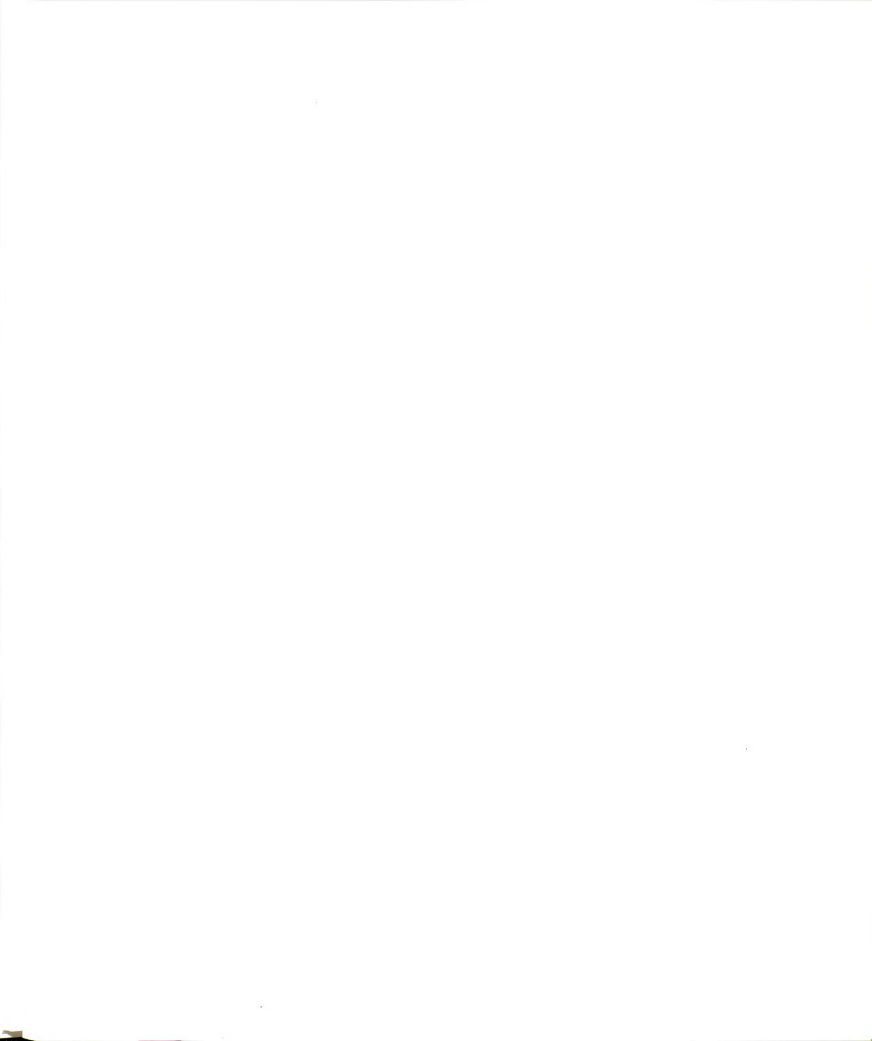


(a) Using rank-2 micro structure.



(b) Using rank-L micro structure.

Figure 5.43. Example 5: optimum shapes.



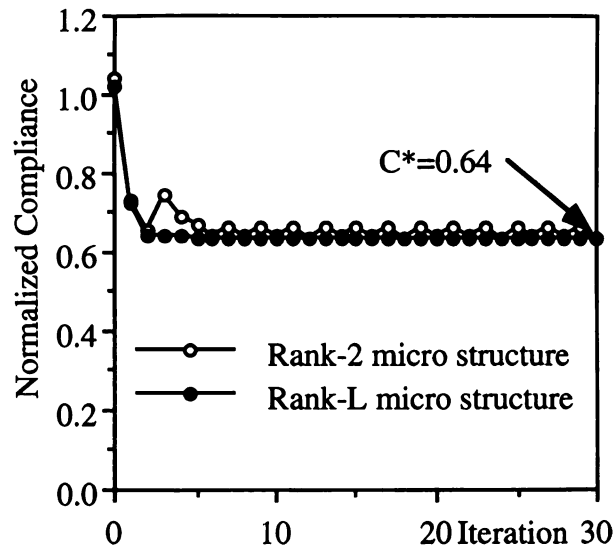


Figure 5.44. Example 5: iteration histories.

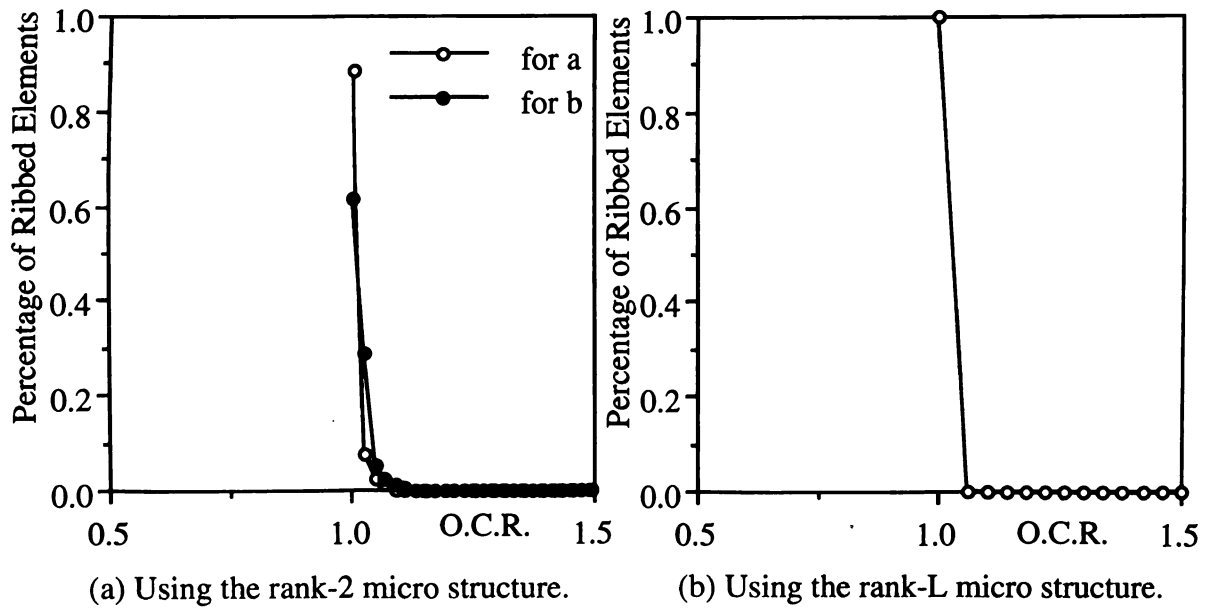


Figure 5.45. Example 5: Optimality condition ratio histograms.



## CONCLUDING REMARKS

### General

As in most dissertations, a significant portion of the work presented here is an extension of previous research. In this case, the effort -- often independent -- of M. Bendsøe, A. Díaz, N. Kikuchi, R. Lipton and K. Suzuki was the starting point of our research. A substantial amount of time was spent collecting diverse knowledge on the subject and putting it together to clarify many aspects that were not fully understood when this research began. There were also other aspects in the subject of shape optimization of plates that had not been addressed in the literature and were developed in our investigation. Conclusions about specific topics studied in this research were given in Chapters 2, 3, 4 and 5. Here we only present general conclusions emphasizing the new results introduced in this work.

In Chapter 2 we presented the mathematical derivation of the effective properties for bending and transverse shear deformations of plates made of *two orthogonal* layers of ribs (rank-2 material plates) using the method of asymptotic expansions on the Mindlin's plate equations. An extension of this work to plates with other cross sections (honeycomb and transversely perforated) was also described.

The use of rank-2 material to solve shape optimization problems in plates is one of the main contributions of Chapter 2. Previous work used other micro structures whose effective properties were computed using approximate numerical procedures. The formulas developed in Chapter 2 represent an important improvement in the computation of effective properties of plates in topology optimization algorithms based on homogenization techniques.

The difference between homogenized plate models based on two-dimensional elasticity and plate equations was also addressed in this work. We concluded that effective plate properties computed when the homogenization techniques are applied to the two-

dimensional elasticity equations are in general less stiff than those obtained when the homogenization techniques are applied directly to plate equations. The implication of this difference from the shape optimization viewpoint is that when we use homogenization techniques in the plate equation, optimum topologies prescribe more composite areas.

A comparison of several micro structures discussed in the literature was presented to show the influence of different geometric parameters on individual bending stiffness coefficients. The comparison helps understand relations among popular models used in the literature. Such study was not available in the open literature.

In Chapter 3 we presented a mathematical derivation of the effective properties for bending and transverse shear deformations of plates made of materials with a finite number of layers of ribs oriented in  $L$  arbitrary directions. These properties were then presented in a compact form called the “moment representation”, which uses only four variables (moments) to describe the effective properties of rank-L material plates once an amount of material is prescribed. The important characteristic of these plates is that they attain optimal bounds for multiple energy conditions, i.e., under prescribed strain fields, they are the stiffest plates. This allowed us to solve the layout and shape optimization problem using the stiffest micro structure at each location of the plate.

The derivation of bending and transverse shear effective stiffness properties of rank-L material plates is the main contribution of Chapter 3. The moment representation of these effective properties is new for Mindlin plates. This representation allowed us to solve the shape optimization problem using the stiffest micro structure with only five design variables, namely, the material resource  $\rho$ , and four moments  $m_1, m_2, m_3, m_4$ .

In Chapter 4 we presented the formulation of the layout and shape optimization problem in plate structures using homogenization techniques. The stiffest distribution of the reinforcing material was obtained using the weighted sum of the compliances as the objective function. The optimization problem was split into two problems taking advantage of the moment representation of the effective properties developed in Chapter 3 and using known variational principles. This formulation was called “hierarchical moment formulation” and allowed us to solve the shape optimization problem using optimal micro structures at every location in the plate. Implementation of the hierarchical moment formulation for multiple load cases using the moment representation of the effective properties is new for Mindlin plates.

Implementation issues of the optimization problem using the hierarchical moment formulation were also discussed. From the results obtained in the problem examples we conclude that the proposed strategy to solve the nonlinear equilibrium problem works very well.

In Chapter 5 several example problems were solved in order to show the capabilities of the homogenization approach to solve layout and shape optimization problems. Optimum shapes obtained with the rank-L model showed that, for the problems studied, materials with three layers of ribs are seldom prescribed. This indicates that even though rank-3 materials are, in general, stiffer than rank-2 materials, the difference between them in terms of stiffness may be small. Because of this small difference, optimum shapes and compliances computed with the rank-2 model are very similar to those computed with the rank-L model.

Examples in the automobile industry showed that the optimization algorithm using homogenization works well in practical engineering situations which makes very attractive this approach.

### **Future Research**

It is clear from the examples that the homogenization approach is a very powerful method to solve the layout and shape optimization problem in plate structures. Some improvements are still necessary, and they are cited here as future research directions.

From the examples solved with both the rank-2 and rank-L micro structures, we observed that there is not much difference in the results obtained using these two models. More research should be done to know the reasons of this observation and to understand the behavior of rank-L materials.

One of the drawbacks of the homogenization method applied to shape optimization is the lack of smoothness of the boundaries of the optimum shape due to the discretization of the domain. This can be addressed, in part, using finer meshes, but the cost of the solution of the equilibrium equation increases. Better strategies to solve this problem should be investigated.

For practical applications it is important to consider more realistic constraints in the optimization problem. Local stresses and displacements, buckling and manufacturing constraints should be incorporated in the formulation of the problem.

There is always the question about the quality of the optimum found using optimality criterion methods. These methods use first order conditions that do not guarantee that the minimum is a global one. Some research is required in this subject.

This work intended to contribute to the enrichment of the scientific knowledge in the field of optimum structural design. We hope that this work will help future students and researchers to find new routes to expand the knowledge frontier that we reach in this research.



## **APPENDIX**



## APPENDIX

Matrices of the stiffness coefficients in (2.1.3a)

$$W^{11} = \begin{bmatrix} D_0(1,1) & D_0(1,3) & 0 \\ D_0(1,3) & D_0(1,2) & 0 \\ 0 & 0 & 0 \\ 0 & 0 & 0 \\ 0 & 0 & 0 \end{bmatrix}$$

$$W^{21} = \begin{bmatrix} D_0(1,3) & D_0(3,3) & 0 \\ D_0(3,3) & D_0(2,3) & 0 \\ 0 & 0 & 0 \\ 0 & 0 & 0 \\ 0 & 0 & 0 \end{bmatrix}$$

$$W^{41} = \begin{bmatrix} 0 & 0 & 0 \\ 0 & 0 & 0 \\ 0 & 0 & 0 \\ D_2(3,3) & D_2(2,3) & 0 \\ -D_2(1,3) & -D_2(3,3) & 0 \end{bmatrix}$$

$$W^{51} = \begin{bmatrix} 0 & 0 & 0 \\ 0 & 0 & 0 \\ 0 & 0 & 0 \\ -D_2(1,3) & -D_2(1,2) & 0 \\ D_2(1,1) & D_2(1,3) & 0 \end{bmatrix}$$

$$W^{12} = \begin{bmatrix} D_0(1,3) & D_0(3,3) & 0 \\ D_0(3,3) & D_0(2,3) & 0 \\ 0 & 0 & 0 \\ 0 & 0 & 0 \\ 0 & 0 & 0 \end{bmatrix}$$

$$W^{22} = \begin{bmatrix} D_0(1,2) & D_0(2,3) & 0 \\ D_0(2,3) & D_0(2,2) & 0 \\ 0 & 0 & 0 \\ 0 & 0 & 0 \\ 0 & 0 & 0 \end{bmatrix}$$

$$W^{42} = \begin{bmatrix} 0 & 0 & 0 \\ 0 & 0 & 0 \\ 0 & 0 & 0 \\ D_2(2,3) & D_2(2,2) & 0 \\ -D_2(1,2) & -D_2(2,3) & 0 \end{bmatrix}$$

$$W^{52} = \begin{bmatrix} 0 & 0 & 0 \\ 0 & 0 & 0 \\ 0 & 0 & 0 \\ -D_2(3,3) & -D_2(2,3) & 0 \\ D_2(1,3) & D_2(3,3) & 0 \end{bmatrix}$$

$$\begin{aligned}
 W^{43} &= \begin{bmatrix} 0 & 0 & 0 \\ 0 & 0 & 0 \\ -S(1,2) & -S(2,2) & 0 \\ 0 & 0 & S(2,2) \\ 0 & 0 & -S(1,2) \end{bmatrix} & W^{53} &= \begin{bmatrix} 0 & 0 & 0 \\ 0 & 0 & 0 \\ S(1,1) & S(1,2) & 0 \\ 0 & 0 & -S(1,2) \\ 0 & 0 & S(1,1) \end{bmatrix} \\
 W^{31} &= \begin{bmatrix} 0 & 0 & 0 \\ 0 & 0 & 0 \\ S(1,1) & S(1,2) & 0 \\ 0 & 0 & -S(1,2) \\ 0 & 0 & S(1,1) \end{bmatrix} & W^{32} &= \begin{bmatrix} 0 & 0 & 0 \\ 0 & 0 & 0 \\ S(1,2) & S(2,2) & 0 \\ 0 & 0 & -S(2,2) \\ 0 & 0 & S(1,2) \end{bmatrix}
 \end{aligned}$$

$$W^{13} = W^{23} = W^{33} = [0]_{(5 \times 3)}$$

The major symmetry is present in these matrices, i.e.,

$$W_{ij}^{k\ell} = W_{k\ell}^{ij}$$

but the minor one is not since

$$W_{ij}^{k\ell} \neq W_{ij}^{\ell k} \neq W_{ji}^{k\ell}$$

This results from grouping together all terms from membrane, bending and transverse shear deformations into a single array  $W_{ij}^{k\ell}$ .

## REFERENCES

## LIST OF REFERENCES

- Armand, J-L. (1974), "Numerical Solutions in Optimization of Structural Elements," *First International Conference on Computational Methods in Nonlinear Mechanics*, Austin, Texas.
- Armand, J-L. (1982), "Non Homogeneity and Anisotropy in Structural Design," *Optimization Methods in Structural Design*, eds. H Eschenauer and N. Olhoff, pp. 256-263.
- Allaire, G. and Kohn, R.V. (1993), "Optimal Design for Minimum Weight and Compliance in Plane Stress Using Extremal Microstructures," *European Journal of Mechanics (A/Solids)*, to appear.
- Avellaneda, M. and Milton, G. (1989), "Bounds on the Effective Elasticity Tensor of Composites Based on Two-Point Correlations," *Proceedings ASME the 5-th Energy-Technology Conference and Exhibition*, Houston, TX.
- Babuska, I., (1976), "Homogenization and its Applications. Mathematical and Computational Problems," *Numerical Solution of Partial Differential Equations-III*, ed. B. Hubbard, Academic Press, New York, 9, 89-116.
- Banichuk, N.V. (1980), "Optimality Conditions and Analytical Methods of Shape Optimization," *Optimization of Distributed Parameter Structures*, eds. E.J. Haug and J. Cea, Sijthoff & Noordhoff, Alphen aan den Rijn, Netherlands, pp. 973-1004.
- Bendsøe, M.P. (1982a), "G-Closure and Homogenization Problems in Plate Optimization," *Optimization Methods in Structural Design*, eds. H. Eschenauer and N. Olhoff, pp. 270-275.
- Bendsøe, M.P. (1982b), "Some Smear-Out Models for Integrally Stiffened Plates with Applications to Optimal Design". In *Proc. Int. Symp. Optimum Structural Design*, Univ. Ariz., Tucson, Arizona, 13-29 - 13-34.
- Bendsøe, M.P. (1989), "Optimal Shape Design as a Material Distribution Problem", *Structural Optimization*, 1, 193-202.

- Bendsøe, M.P. and Kikuchi, N. (1988), "Generating Optimal Topologies in Structural Design using a Homogenization Method", *Comp. Meth. in Applied Mech and Engin.*, **71**, 197-224.
- Bendsøe, M., Díaz, A., Kikuchi, N., (1992) "Topology and Generalized Layout Optimization of Elastic Structures," *Proceedings of the NATO Advanced Research Workshop on Topology Design of Structures*, eds. M. Bendsøe and C.A. Mota Soares, Sesimbra, Portugal, June 20-26.
- Bensoussan, A.; Lions, J.-L.; Papanicolaou, G. (1978), *Asymptotic Analysis for Periodic Structures*. Amsterdam: North-Holland.
- Bourgat, J.F. (1977), "Numerical Experiments of the Homogenization Method for Operators with Periodic Coefficients.", *Lecture Notes in Mathematics*, Springer Verlag, Berlin, **704**, 330-356.
- Bourgeat, A.; Tapiero, R. (1983), "Homogenization of a Transversely Perforated Plate in the Frame of Hencky Mindlin's Theory, in the Thermoelastic Case with non Uniform Oscillating Coefficients." *C.R. Acad. Sci. Paris, Serie I*, **297**, 213-216.
- Caillerie, D. (1984), "Thin Elastic and Periodic Plates", *Math. Meth. Appl. Sci.*, **6**, 159-191.
- Cea, J. (1980), "Problems of Shape optimal Design," *Optimization of Distributed Parameter Structures*, ed. E.J. Haug and J. Cea, Sijthoff & Noordhoff, Alphen aan den Rijn, Netherlands, pp. 1005-1048.
- Cheng, K-T. and Olhoff, N. (1981), "An Investigation Concerning Optimal Design of Solid Elastic Plates", *Int. J. Solids Structures*, **17**, 305-323.
- De Giorgi, E. and Spagnolo, S. (1973), "Sulla Convergenza Degli Integrali Dell'energia per Operatori Ellittici del Secondo Ordine". *Boll. U.M.I.*, **8**, 391-411.
- Dems, K. and Mroz, Z. (1978), "Multiparameter Structural Shape Optimization by the Finite Element Method," *International Journal of Numerical Methods in Engineering*, **13**, 247-263.
- Díaz, A. and Belding, B. (1993), "On Optimum Truss Layout by a Homogenization Method," *Transactions of the ASME Journal of Mechanical Design*, **115**, pp. 367-373.
- Díaz, A. and Bendsøe, M. (1992), "Shape Optimization of Structures for Multiple Loading Conditions using a Homogenization Method," *Structural Optimization*, **4**, 17-22.

- Díaz, A. and Kikuchi, N. (1992), "Solutions to Shape and Topology Eigenvalue Optimization Problems Using a Homogenization Method," preprint, Dept. of Mech. Engng., Michigan State University, East Lansing, MI, USA.
- Duvaut, G. (1976), "Analyse Fonctionnelle et Mécanique des Milieux Continus. Application à L'étude des Matériaux Composites Élastiques à Structure Périodique - Homogénéisation". In W.T. Koiter, (ed) *Theoretical and Applied Mechanics*, p.119. Amsterdam: North-Holland.
- Ekeland, I. and Teman, R. (1976), "Convex Analysis and Variational Problems," North-Holland Pub. Co., pp. 402.
- Francfort, G.A. and Murat, F. (1986), "Foundations of Solid Mechanics," Prentice-Hall, Inc., New Jersey, 525 p.
- Fung, Y.C. (1965), "Homogenization and Optimal Bounds in Linear Elasticity." *Arch. Rat. Mech. Anal.*, **94**, 307-334.
- Guedes, J. M. (1990), Nonlinear Computational Models for Composite Materials using Homogenization, Ph.D. Thesis, University of Michigan, Ann Arbor.
- Guedes, J. M. and Kikuchi, N. (1990), "Preprocessing and Post processing for Materials Based on the Homogenization Method with Adaptive Finite Element Methods". *Comp. Meth. in Applied Mech and Engin*, **83**, 143-198.
- Hashin, Z., and Shtrikman, S.A. (1963), "A Variational Approach to the Theory of the Elastic Behavior of Multiphase Materials," *J. Mech. Phys. Solids*, **11**, p. 127.
- Jog, C.S., Haber, R.B., Bendsøe, M.P. (1992), "Topology Design Using a Material with Self-Optimizing Microstructure," in *IUTAM Symposium on Optimal Design with Advanced Materials*, Lyngby, Denmark, August 18-20.
- Jones, R. (1975) *Mechanics of Composite Materials*, New York: McGraw Hill.
- Kohn, R.V. and Strang, G. (1982), "Structural Design Optimization, Homogenization and Relaxation of Variational Problems," *Proceeding of the Conference on Disordered Media*, New York University, June.
- Kohn, R.V. and Strang, G. (1986a,b,c), "Optimal Design and Relaxation of Variational Problems," *Comm Pure Appl Math*, **39**, 1-25 (Part I), 139-182 (Part II), 353-377 (Part III).
- Kohn, R.V. and Vogelius, M. (1984) "A New Model for Thin Plates with Rapidly Varying Thickness," *Int. J. Solid Structures*, **20**, 333-350.



- Krein, M.G. and Nudel'man, A.A. (1977) "The Markov Moment Problem and Extremal Problems," *Translation of Mathematical Monographs*, Volume 50, American Mathematical Society, Providence, Rhode Island.
- Kristensen, E.S., Madsen, N.F. (1976), "On the Optimum Shape of Fillet in Plates Subjected to Multiple In-Plane Loading Cases," *International Journal of Numerical Methods in Engineering*, **10**, 1007-1019.
- Lewinski, T.; Telega, J.J. (1988), "Asymptotic Method of Homogenization of Two Models of Elastic Shells". *Arch Mech.*, **40**, 705-723.
- Lewinski, T. (1991), "Effective Models of Composite Periodic Plates - III. Two-Dimensional Approaches". *Int. J. Solids Structures*, **27**, 1185-1203.
- Lipton, R. (1993a) "Optimal Design and Relaxation for Reinforced Plates Subject to Random Transverse Loads", *J. of Probabilistic Engineering Mechanics*, to appear.
- Lipton, R. (1993b) "On the Relaxation for Optimal Structural Compliance Problems," *J. of Optimization Theory and Applications*, to appear.
- Lipton, R. (1993c) "Identification of Microstructures that Extremize Sums of Energies," *SIAM Journal on Applied Mathematics*, to appear.
- Lipton, R. (1993d). Personal communication.
- Lipton, R. (1994) "On Optimal Reinforcement of Plates and Choice of Design Parameter," to appear in *Control and Cybernetics*, Systems Research Institute, Polish Academy of Sciences, Warsaw, Poland, **7**.
- Lurie, K.A. and Cherkhev, A.V. (1976), "Prager Theorem Application to Optimal Design of Thin Plates," *MTT (Mechanics of Solids)*, **11**, 157-159.
- Lurie, K. and Cherkhev, A. (1986), *Uspekhi Mekhaniki*, **9**, 1-81 (in Russian).
- Michell, A.G.M. (1904), "The Limits of Economy of Material in Frame Structures," *Philosophical Magazine*, Series 6, **8**, 589-579.
- Olhoff, N. (1975), "On Singularities, Local Optima and Formation of Stiffeners in Optimal Design of Plates," *Optimization in Structural Design*, eds. A. Sawczuk and Z. Mroz, Springer-Verlag, N.Y., 82-103.
- Olhoff, N., Lurie, K.A., Cherkhev, A.V., Fedorov, A.V. (1980), "Sliding Regimes and Anisotropy in Optimal Design of Vibrating Axisymmetric Plates," *DCAMM-Rept.*, The Danish Center for Applied Mathematics and Mechanics.

- Pedersen, P. (1970), "On the Minimum Mass Layout of Trusses," AGARD Conf. Proc. No. 36, *Symposium on Structural Optimization*, AGARD-CP-36-70.
- Pedersen, P. (1989), "On Optimal Orientation of Orthotropic Materials". *Structural Optimization*, **1**, 101-106.
- Prager, W. , Taylor, J. (1968), "Problems of Optimal Structural Design," *J. of Applied Mechanics*, **35**, 102-106.
- Prager, W., Rozvany, G.I.N. (1977), "Optimal Layout of Grillages," *J. Struct Mech*, **5**, 1-18.
- Rousselet, B., Haug, E.J. (1980), "Design Sensitivity Analysis in Structural Mechanics III: Shape Variation," *Optimization of Distributed Parameter Structures*, ed. E.J. Haug and J. Cea, Sijthoff & Noordhoff, Alphen aan den Rijn, Netherlands, pp. 1397-1442, .
- Rozvany, G.I.N.; Olhoff, N.; Bendsøe, M.P.; Ong, T.G., Sandler, R., Szeto, W.T. (1987) "Least-Weight Design of Perforated Elastic Plates", *Int. J. Solids Struct.*, **35**, 521-536 (I); 537-550 (II).
- Schittkowski, K. (1985/6), "NLPQL: A Fortran Subroutine Solving Constrained Nonlinear Programming Problems." *Annals of Operations Research*, **5**, pp. 485-500.
- Suzuki, K.; Kikuchi, N. (1991a), "A Homogenization Method for Shape and Topology Optimization," *Comp. Meth. in Applied Mech and Engin*, **93**, 291-318.
- Suzuki, K. and Kikuchi, N. (1991b) "Generalized Layout Optimization of Shape and Topology in Three-Dimensional Shell Structures." In *Geometric Aspects of Industrial Design*. ed. V. Komkov, SIAM, Philadelphia.
- Tvergaard, V. (1975), "On the Optimum Shape of a Fillet in a Flat Bar with Restrictions," *Optimization in Structural Design*, ed. A. Sawczuk and Z. Mroz, Springer-Verlag, N.Y., 181-195.
- Zienkiewicz, O.C., Campbell, J.S. (1973), "Shape Optimization and Sequential Linear Programming," *Optimum Structural Design*, ed. R.H. Gallagher and O.C. Zienkiewicz, Wiley, N.Y., 109-126.





MICHIGAN STATE UNIV. LIBRARIES



31293010256471